Alma Mater Studiorum – Università di Bologna

DOTTORATO DI RICERCA IN

BIOLOGIA CELLULARE E MOLECOLARE

Ciclo XXXIV

Settore Concorsuale: 05/E2 – BIOLOGIA MOLECOLARE

Settore Scientifico Disciplinare: BIO/11 – BIOLOGIA MOLECOLARE

Mapping new non-genetic dependencies in Malignant Pleural Mesothelioma

Presentata da: Eugenia Lorenzini

Coordinatore Dottorato
Vincenzo Scarlato

Supervisore
Alessia Ciarrocchi

Co-supervisore
Davide Carlo Ambrosetti

Esame finale anno 2022

ABSTRACT

Malignant Pleural Mesothelioma (MPM) is a very aggressive cancer whose incidence is growing in many industrialized countries and developing areas. MPM escapes the classical models of carcinogenesis and lacks a distinctive genetic fingerprint, keeping obscure the molecular events that lead to tumorigenesis. This severely impacts on the limited therapeutic options and on the lack of specific biomarkers for early diagnosis that concur to make MPM one of the deadliest forms of cancer.

Despite many genetic studies performed in recent years to identify driver mutations, MPM still remains a therapy orphan disease. To overcome the limitations of purely descriptive omics profiling, here we performed an integrated analysis by combining a functional genome-wide loss of function CRISPR/Cas9 screening with patients' transcriptomic and clinical data, to identify protein-coding genes essential for MPM cells' survival. Also, in light of the massive contribution of the non-coding genome to cancer, we explored the role of non-coding RNAs to MPM progression by analysing gene expression profiles and clinical data from the MESO-TCGA dataset.

We identified the epigenetic keeper TRIM28 and the long non-coding RNA (lncRNA) LINC00941 as new vulnerabilities of MPM, associated with disease aggressiveness and bad outcome of patients. Tripartite Motif Containing 28 (TRIM28), also known as KAP1, is a large multi-domain protein that, modifying chromatin structure, is involved in many cellular processes, including transcription regulation. As a transcriptional cofactor, TRIM28 is able to work as either repressor or activator of gene expression. We showed that loss of TRIM28 in MPM cells impairs cell growth and clonogenicity by blocking cells in mitosis. Mechanistically, we showed that TRIM28 is required for the correct timing of mitosis genes expression. In particular, RNA-seq profiling showed that loss of TRIM28 dramatically abolished the expression of major mitotic players including AURKA, AURKB, FOXM1 and B-MYB. Analysis of ChIP-Seq data and Co-IP experiments showed that TRIM28 is part of the B-MYB/FOXM1-MuvB complex that specifically drives the activation of mitotic genes.

In parallel, we found LINC00941 as the top scoring non-coding transcript correlating with reduced survival probability in MPM patients. LINC00941 KD profoundly reduced MPM cells' growth, migration and invasion. This is accompanied by profound changes in morphology, cytoskeleton organization and cell-cell adhesion properties. RNA-seq profiling showed that LINC00941 affect the overall transcriptional program of MPM, hitting many crucial functions of MPM, including the HIF1α-mediated hypoxia response.

Collectively these data provided new insights into MPM biology and demonstrated that the integration of functional screening with patients' clinical data is a powerful tool to highlight new non-genetic cancer dependencies that associate to a bad outcome *in vivo*, paving the way to new MPM-oriented targeted strategies and prognostic tools to improve patients risk-based stratification.

INDEX

INTRODUCTION 6
Malignant Pleural Mesothelioma 6
Genomic Landscape of MPM 7
Epigenetic Events in MPM 9
Asbestos-mediated epigenetic changes 11
Genome-wide knock-out screening as functional approach to define new non-genetic cancer vulnerabilities 12
Tripartite Motif Containing 28 (TRIM28) 14
TRIM28 Protein Structure 14
TRIM28 and Cancer 15
TRIM28 as Negative Regulator of Transcription 16
TRIM28 as Positive Regulator of Transcription 17
TRIM28 as Repressor of Endogenous Retroviruses (ERVs) 18
The non-coding genome 20
Long non-coding RNAs (lncRNAs) 21
lncRNAs in MPM 22
LINC00941 and Cancer 23
AIM OF THE STUDY 24
RESULTS 25
Integration of genome-wide screening and clinical data identified a core of chromatin-associated genes essential for MPM progression 25
Loss of TRIM28 strongly impairs proliferation and induces apoptosis of MPM cells 30
TRIM28 controls the expression of mitotic genes and is required for correct mitosis execution 34
TRIM28 cooperates with the B-MYB/FOXM1-MuvB complex to mediate CDK9-dependent RNA-PolII proficient transcription of mitotic genes 39
The CDK9 inhibitor AZD4573 mimics TRIM28 KD effects in MPM cells 42
Model validation in a separate cohort of MPM patients 44
TRIM28 controls Innate Immune Response 48
Analysis of TCGA clinical data revealed several lncRNAs associated with MPM patients' survival 51
LINC00941 promotes proliferation, migration and invasion of MPM cells 55
LINC00941 mediates HIF1α signalling in MPM cells 62
DISCUSSION 64
MATERIAL AND METHODS 70
Cell Culture 70
Lentiviral Infection 70

Generation of MSTO-211H clones stably expressing Cas9 70
Genome-wide screening 71
TCGA Data Analysis 72
Knockout cell lines generation and Competition Assays 72
Alt-R Genome Editing Detection Kit 73
siRNA Transfections 74
Proliferation and Colony Forming Assays 74
RNA Extraction, Reverse Transcription and quantitative real-time PCR (qRT-PCR) 75
Western Blot 76
Apoptosis Analysis 78
Cell Cycle Analysis 78
Immunofluorescence 78
RNA-Seq and Bioinformatics Analysis 79
ChIP-seq analysis 80
Co-Immunoprecipitation (Co-IP) 80
ChIP-qPCR 81
Patients Selection and Nanostring Analysis 82
CDKs inhibitors 83
Scratch Wound Healing Assay 83
Invasion Chamber Assay 83
$CoCl_2$ treatment 84
Statistical Analysis 84
REFERENCES 85
ACKNOWLEDGEMENTS 98

INTRODUCTION

Malignant Pleural Mesothelioma

Malignant Mesothelioma (MM) is a solid tumor that arises from the thin monolayer of mesothelial cells that lines body cavities and organs' surfaces (C. Bianchi & Bianchi, 2007; Carbone et al., 2012). It can develop in the pleural space, peritoneum, tunica vaginalis testis and ovarian epithelium. According to the histological features, MM can be classified in 3 different histotypes, based on cells' degree of differentiation: epithelioid, sarcomatoid and biphasic or mixed, that contains both epithelioid and sarcomatoid cells. The clinical behavior among them is different, being the sarcomatoid the most aggressive and the one with the worst prognosis histotype (Carbone et al., 2012; Ismail-Khan et al., 2006).

Malignant Pleural Mesothelioma (MPM) develops in the lung's pleura and is the most common subtype of MM, representing 83% of all MM cases. It is characterized by high mortality rate and dismal prognosis due to the limited treatment options available. The majority (about 80%) of MPM cases are associated to asbestos exposure, either professional or environmental (Figure 1) (C. Bianchi & Bianchi, 2007; Carbone et al., 2012; Ismail-Khan et al., 2006). The discovery that asbestos fibers are the causative agent of MPM dates back to 1960s (Wagner et al., 1960). Surprisingly, several studies demonstrated that a longer exposure time does not modify the risk of developing MPM (Remon et al., 2015). MPM is characterized by a long latency period between asbestos exposure and tumor development, spanning from 20 to 50 years. This explain why, despite asbestos limitations in industrialized countries, incidence and mortality rates of MPM continued to increase in the last decades and are expected to still grow in the next one (C. Bianchi & Bianchi, 2007; Carbone et al., 2012). Besides, emerging economies like China and India are still largely using asbestos, representing a plausible scenario of many MPM cases in the next decades. Accurate diagnosis of MPM is difficult due to the lack of specific and sensitive biomarkers (Ahmadzada et al., 2018). This is the reason why MPM is usually diagnosed at advanced stages, being the

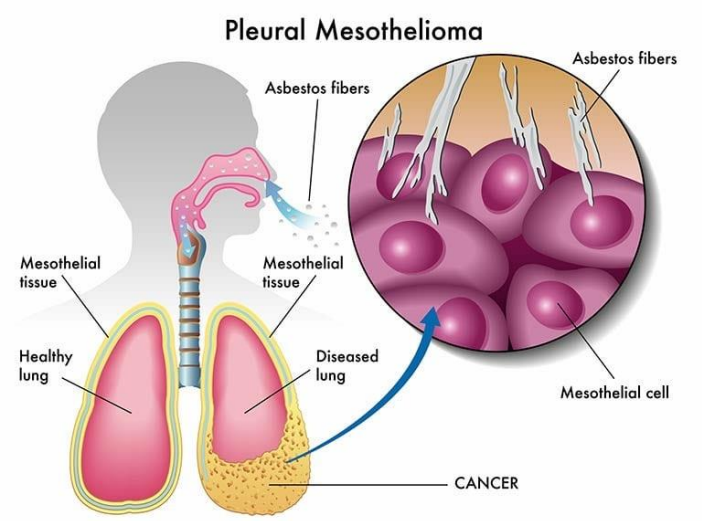

Figure 1. Representation of asbestos fibers inhalation and deposition in the mesothelial cells of the lungs pleura, causing MPM. From https://iscc-charity.org/mesothelioma-children/

cause of the extremely low overall survival (OS) of MPM patients (8-36 months). In particular, patients with sarcomatoid MPM have a very poor outcome compared to epithelioid MPM (Christoph & Eberhardt, 2014). Moreover, surgery is effective and practicable only in early stages of the disease, when the tumor size is limited, while for the majority of patients standard chemotherapy is often ineffective (Remon et al., 2015). First line therapy for unresectable MPMs consists of a combination of Cisplatin and Pemetrexed, an anti-folate compound. However, there is no defined second line therapy following this treatment (Haas & Sterman, 2013). For these reasons, new diagnostic and treatment approaches are urgently needed. Although recent advances in MPM biology, its management still remains a clinical challenge. Despite many efforts, several clinical trials undertaken in recent years did not improve the standard approved chemotherapy regimen for this tumor (Yap et al., 2017).

Genomic Landscape of MPM

Deep sequencing of MPM revealed that this tumor is characterized by a low mutational burden, with a mean of <2 somatic non-synonymous mutations per megabase and few recurrent gene mutations (Bueno et al., 2016; Guo et al., 2015; Hmeljak et al., 2018; Hylebos et al., 2016). Despite the low number of point mutations, MPM is characterized by frequent tumor suppressor genes (TSGs) inactivation by different mechanisms: copy number losses, gene fusions and promoters' hypermethylation. These mechanisms often affect epigenetic keepers and proteins involved in chromatin organization (Lorenzini et al., 2021; Sage et al., 2018). The most frequently mutated genes in MPM are *BAP1*, *NF2*, *TP53*, *CDKN2A*, *CDKN2B*, *SETD2* and to a lesser extent *SETDB1* (Figure 2) (Bueno et al., 2016; Guo et al., 2015; Hmeljak et al., 2018; Sage et al., 2018).

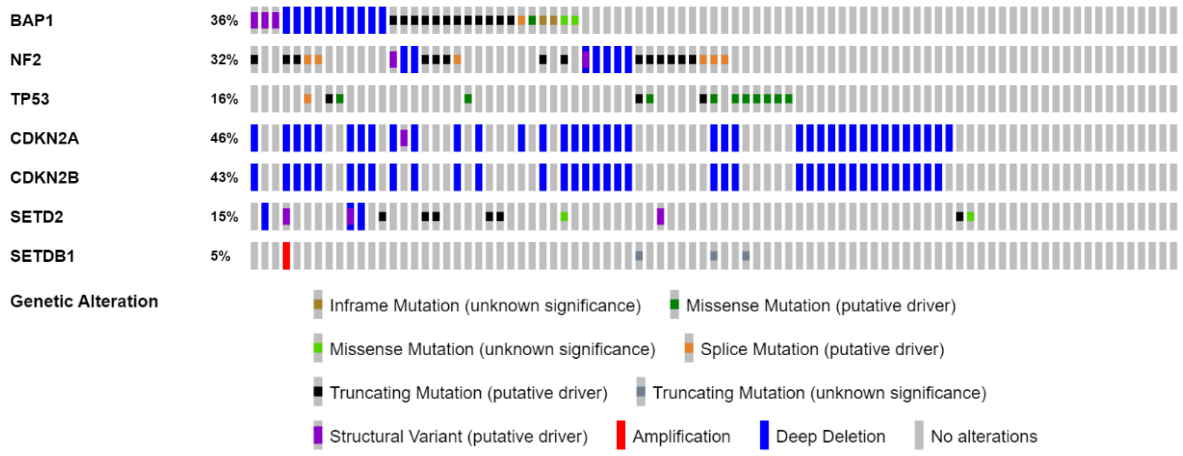

Figure 2. Most represented genetic alterations in the MESO-TCGA dataset (N=87). Data are from https://www.cbioportal.org/

Besides alterations affecting single genes, different mutational signatures have been identified in mesothelioma, however, these are not different in the cases with or without known asbestos exposure (Sage et al., 2018).

BAP1, being inactivated by either copy number alterations (CNA) or point mutations in >50% of cases, is the most frequently mutated gene in MPM (Bueno et al., 2016; Guo et al., 2015; Hmeljak et al., 2018). BAP1 is a deubiquitinase involved in DNA repair, cell cycle checkpoints, heterochromatin formation and centrosome amplification, affecting genome stability (Masclef et al., 2021). Recently, BAP1 has been described as a putative epigenetic regulator and its inactivation induced global methylation through the activation of Polycomb repressive complex 2 (PRC2) (LaFave et al., 2015). Moreover, by deubiquitinating histones and transcription factors (TFs) it's plausible that BAP1 is involved in transcription regulation. *BAP1* acts as a tumor suppressor gene and mutations disrupting its deubiquitinase activity or its nuclear localization concur to tumor progression (Ventii et al., 2008). Besides, germline mutations in *BAP1* are associated with an increased risk of developing MPM as well as other types of cancer (Cheung et al., 2013; Yoshikawa et al., 2012). Consistently, BAP1 germline mutations were found in families with a high percentage of MPM cases as well as other types of cancer, primarily melanoma (Betti et al., 2016; Ohar et al., 2016; Testa et al., 2011).

The Neurofibromatosis 2 (***NF2***) gene is a tumor suppressor gene that encodes the moesin-ezrin-radixin like protein (Merlin), associated with the actin filaments. It is inactivated in 40-50% of MPM cases (A. B. Bianchi et al., 1995; Guo et al., 2015; Sekido, 2011). When dephosphorylated, Merlin accumulates in the nucleus where it inhibits the pro-oncogenic function of the E3 ubiquitin ligase CRL4 (DCAF1), thus preventing the expression of several oncogenes (W. Li et al., 2010). In a small number of patients bearing *LATS2* loss of function mutations, Merlin loss is believed to contribute to tumorigenesis via Hippo Pathway inactivation (Sekido, 2011; Tranchant et al., 2017). *LATS2* is inactivated in about 11% of MPM patients by either point mutations or deletions and its loss correlates with a bad prognosis (Hmeljak et al., 2018; Tranchant et al., 2017). Both *NF2* and *LATS2* inactivation hyper-activate YAP, the effector TF of the Hippo Pathway, whose disruption is crucial in MPM tumorigenesis (Miyanaga et al., 2015).

Tumor Suppressor ***TP53*** was found mutated in 8-9% of MPMs (Bueno et al., 2016; Guo et al., 2015), a smaller percentage compared to other tumor types. Importantly, *TP53* mutations were absent from the epithelioid subtype, and patients harboring *TP53* mutations

had a lower OS than patients with wild-type (WT) *TP53*, suggesting the aggressiveness of tumors bearing TP53 mutations (Bueno et al., 2016).

CDKN2A and ***CDKN2B*** are tumor suppressor genes located in region 9p21 that in MPM is affected by frequent copy number losses, resulting in their inactivation. Coherently, about 45% of MPM patients show deletions of region 9p21 (Bueno et al., 2016; Guo et al., 2015; Hmeljak et al., 2018). *CDKN2A* and *CDKN2B* encode for CDK inhibitors, thus their inactivation causes the disruption of cell cycle regulation. *CDKN2A* loss is associated to reduced OS of MPM patients (Dacic et al., 2008) and with non-epithelioid histology (De Rienzo et al., 2016), highlighting its association with aggressive tumors .

SETD2 is a histone lysine methyltransferase that, specifically, trimethylates histone H3K36, a mark associated to transcriptional elongation that peaks at 3'end of genes. SETD2-dependent H3K36 trimethylation is involved in several processes within the cell, including chromatin accessibility and ensures genome stability (Pfister et al., 2014). *SETD2* is mutated majorly by truncating mutations in 8% of cases in the study performed by Bueno et al. (Bueno et al., 2016).

SETDB1, as SETD2, is a histone lysine methyltransferase that methylates H3K9, generating H3K9-me2 and –me3 histone marks that are associated to silent chromatin. *SETDB1* is usually overexpressed in cancer, instead in MPM frequent loss of function mutations are reported (Hmeljak et al., 2018; Kang et al., 2016; Strepkos et al., 2021), affecting 3% of MPM patients in the Bueno cohort (Bueno et al., 2016), suggesting a different role of SETDB1 in this context, still to be elucidated (Kang et al., 2016).

Epigenetic Events in MPM

Epigenetic modifications include DNA methylation, histone modifications and chromatin remodeling. These modifications heavily affect gene expression without altering DNA sequence and are involved in many biological processes, including tumorigenesis (L. Zhang et al., 2020). Also several microRNAs (miRNAs) and long non-coding RNAs (lncRNAs) act as epigenetic regulators (Lorenzini et al., 2021). Epigenetic alterations are being extensively studied in recent years in MPM since they are emerging as potential tools for an improved diagnosis and prognosis of MPM.

DNA methylation is catalyzed by DNA methyltransferases (DNMTs) and consists in the addition of a methyl group to the fifth carbon of a cytosine, usually within CpG islands. DNA methylation leads to chromatin compaction, inhibiting the binding of the transcriptional

machinery that thus results in gene silencing (Edwards et al., 2017). Hypermethylation of TSGs is a common mechanism in many cancers, including MPM (Christensen et al., 2008). Christensen et al. for the first time compared the methylation profile of MPMs to normal pleura, finding a global higher methylation status in the tumors compared to normal tissues. They also found a positive correlation between higher methylation status and shorter OS and between higher methylation and asbestos exposure (Christensen et al., 2009). Indeed, analysis of asbestos-associated MPM cell lines revealed an overexpression of all the DNA methylases DNMT1, DNMT3A and DNMT3B and of the epigenetic regulators EZH2 and SUZ12. Moreover, the overexpression of these epigenetic keepers correlates with a reduced OS of patients (McLoughlin et al., 2017). DNMTs expression is affected by cytokine signaling, largely produced as a consequence of the chronic inflammation status caused by asbestos' fibers inhalation (McLoughlin et al., 2017; Yang et al., 2010).

Histone modifications, influencing chromatin structure and accessibility also affect gene expression. Being many enzymes involved in histone post-translational modifications (BAP1, SETD2 and SETDB1) frequently mutated in MPM, it is plausible that these modifications have a role in disease progression. There are evidence supporting global chromatin hypoacetylation in MPM. Decreased acetylation of H3 and H4 is reported in MPM as well as in other cancer types (Chi et al., 2010). Histones' acetylation causes chromatin relaxation and gene transcription activation. Histone acetylation is catalyzed by histone acetyltransferases (HATs), while deacetylation is performed by histone deacetylases (HDACs) (Hassig & Schreiber, 1997). Several HDAC inhibitors have been developed since HDAC1 and HDAC2 are often deregulated in cancer and showed promising results for the treatment of many cancers (Eckschlager et al., 2017). BAP1 has been reported to regulate *HDAC2* expression, indeed reduced *HDAC2* levels are reported in *BAP1* mutated tumors. *BAP1* or *HDAC2* loss caused an increased sensitivity to HDAC inhibitors, differently from HDAC1 inhibition, suggesting a non-redundant role for the two deacetylases (Sacco et al., 2015).

Inactivation of TSGs by promoter hypermethylation together with chromatin hypoacetylation paved the way for the use of DNMT inhibitors (DNMTi) and HDAC inhibitors (HDACi) in MPM. The use of single-agent epigenetic drugs have shown poor results, but their combination with other classes of epigenetic drugs or chemotherapy are showing promising effects. Several preclinical trials are on the way and the combination of different HDACi and

DNMTi results in tumor growth inhibition as well as induction of the immunogenic response (Lorenzini et al., 2021).

Asbestos-mediated epigenetic changes

Asbestos consists of a group of naturally occurring silicate minerals that were largely used until a few decades ago in the sectors of industry and construction. Asbestos is known to cause genotoxicity through DNA breaks and oxidative DNA damage, however an association between asbestos exposure and a precise mutational signature could not be identified (C. Bianchi & Bianchi, 2007; Chew & Toyokuni, 2015; Hmeljak et al., 2018; Mossman et al., 1996). On the other hand, there are evidence supporting a role of asbestos in inducing epigenetic changes, even if the molecular mechanisms involved are not completely clear (Bueno et al., 2016; Hmeljak et al., 2018). Asbestos fibers, when inhaled, set down in the lungs triggering the inflammatory response that involves the continue production of free radicals, reactive oxygen (ROS) and nitrogen (RNS) species (Carbone et al., 2012; Mossman et al., 1996). These molecules are potent mutagens that damage cellular components, promoting DNA mutation and triggering transformation (Chew & Toyokuni, 2015). The majority of asbestos fibers contain iron or are able to induce hemolysis and release iron ions in the extracellular space (Harington et al., 1971). Free iron is the catalyst of the Fenton reaction that generates hydroxyl radicals (OH), able to damage biomolecules, including DNA. In particular, OH can hydroxylate deoxiguanosine on C8, forming 8-hydroxy-2'-deoxyguanosine (8-OHdG), generating DNA base mispairing and G-to-T transversions (Figure 3) (Cheng et al., 1992). ROS are produced not only by mesothelial cells but also by macrophages. Failing to engulf long asbestos fibers, macrophages die releasing a massive amount of ROS, in a phenomenon described as "frustrated phagocytosis" (Donaldson et al., 2010). Besides ROS production, mesothelial cells exposed to asbestos release high-mobility group box 1 protein (HMGB1) in the extracellular space, where it stimulates the production of TNF-α and IL-1β, key factors in mesothelial cells malignant transformation. HMGB1, together with TNF-α and other inflammatory cytokines, stimulates macrophages activation. All these pro-inflammatory molecules converge on the activation of NF-kB, which promotes survival of damaged mesenchymal cells, supporting tumor establishment and progression (Yang et al., 2006, 2010). Moreover, asbestos fibers can cause genetic damage directly, being able to induce DNA double strand breaks or mechanical disruption of the mitotic spindle during cell division (Msiska et al., 2010). The chronic production of ROS imposed by asbestos fibers implantation in the lungs, creates a

dangerous stressed microenvironment which consequences are hard to overcome (Figure 3) (Sage et al., 2018). This chronic inflammation also impacts on the overall epigenetic landscape of mesothelial cells, in particular through the hypermethylation of TSGs (Shames et al., 2007). Evidence report an association between oncosuppressors' hypermethylation and a poor outcome (Christensen et al., 2009).

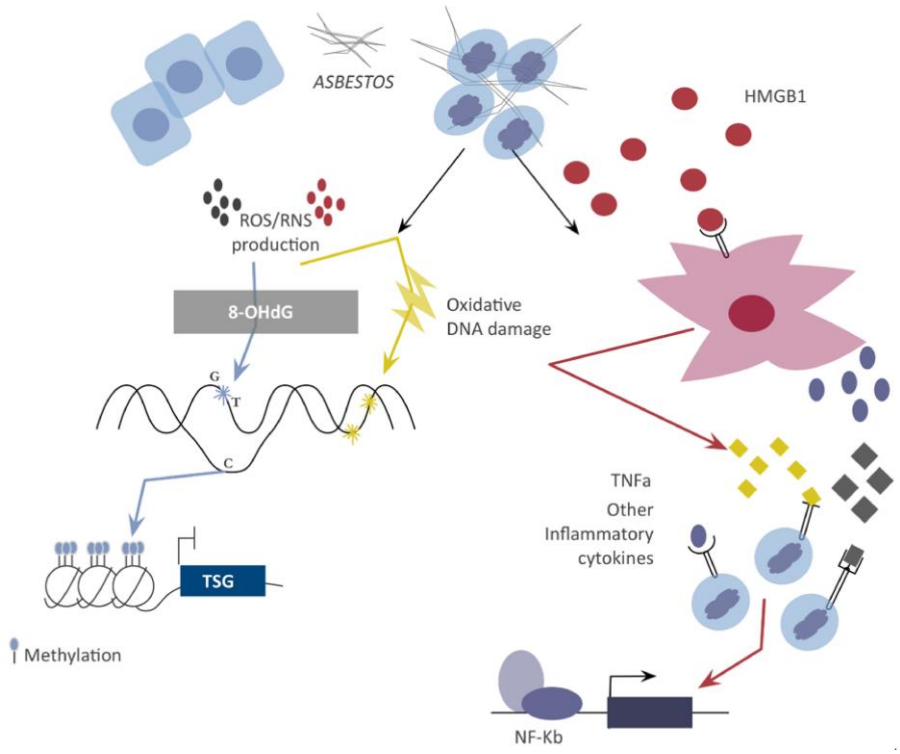

Figure 3. Inhalation of asbestos fibers causes an inflammatory response in the lungs that results in the chronic production of ROS and RNS. 8-OhdG can generate DNA base mispairing, resulting in G-to-T transversions. Asbestos fibers increase methylation status of mesothelial cells, in particular of TSGs. Moreover, mesothelial cells exposed to asbestos undergo necrosis, releasing HMGB1 in the extracellular space and recruiting macrophages and stimulating the chronic inflammation response. From *Lorenzini et al., 2021*

Genome-wide knock-out screening as functional approach to define new non-genetic cancer vulnerabilities

In the latest 10 years the massive application of omics profiling technologies has elucidated the complicated network of genomic and genetic alterations that characterize cancer and identified many driver mutations that helped the definition of new therapeutic opportunities for cancer patients (Nakagawa & Fujita, 2018). However, the great expectation raised by the idea that through this approach it would be possible to assign each patient to a precise target drug was disregarded by the enormous structural and temporal complexity of cancer lesions, by the purely descriptive nature of profiling studies and, above all, by the fact that cancer additions are not only of a genetic nature (Tsherniak et al., 2017). Indeed, mounting evidence point to transcriptional or epigenetic processes as crucial dependencies for cancer cells, highlighting the need of moving towards functional approaches to search new candidates to hit cancer. This is particularly true for a cancer that, like MPM, escapes to the classical model of cancer evolution, lacks a distinctive genetic signature and is characterized

by a great heterogeneity and few and scattered gene mutations (Hmeljak et al., 2018; Oehl et al., 2018).

To overcome these limitations, one approach is to perform genome-wide loss of function screening in order to highlight essential genes for survival of a given cell line (Sanjana et al., 2014). The combination of different cell lines, representing tumor heterogeneity, allows to identify genes essential for the progression of specific malignancies. To this aim, Tsherniak and colleagues analyzed 501 genome-wide loss of function screening performed in many human cancer cell lines to define cancer-specific non-genetic dependencies (Tsherniak et al., 2017), paving the way for the development of new specific targeted therapies. This approach allowed the discovery of new oncogenes not recognizable by purely descriptive profiling studies (Cowley et al., 2014; Tsherniak et al., 2017). Indeed oncogenes, differently from TSGs that usually bear loss of function mutations to be inactivated in cancer, promote tumorigenesis mainly by being overexpressed from cancer cells to sustain their expansion.

The last decade has been characterized by a great progress in the field of genome-wide screening, that took advantage of RNA Interference (RNAi), short-hairpin RNAs (shRNAs) and ultimately of the CRISPR/Cas9 (clustered regularly interspaced short palindromic repeats/CRISPR associated) genome editing system (Sanjana et al., 2014; Shalem et al., 2014). The latest is the most used today for genome-scale screening, being easy to use and owing higher specificity than the other technologies (Shalem et al., 2014)

Integration of functional screening with patients' clinical and transcriptomic data permits to identify genes that not only are essential for proliferation of cancer cells, but that are also associated to an aggressive disease. The Cancer Genome Atlas (TCGA) Pan-Cancer project has profiled and analyzed a great number of human tumors to provide insights into aberrations at the DNA, RNA, protein and epigenetic levels (Cancer Genome Atlas Research Network et al., 2013). Combination of these data with the results of a genome-wide screening, allows to stratify the identified cancer dependencies according to the clinical features of the tumor, such as aggressiveness, patients' survival and tumor histotype. Thus, integration of these two approaches represent a powerful tool to identify the cancer-specific dependencies that *in vivo* are associated to tumor aggressiveness and to a bad outcome of patients. This approach, besides opening the door for the development of cancer-specific targeted therapies, can be used by clinicians as a prognostic tool to define cancers' aggressiveness.

Tripartite Motif Containing 28 (TRIM28)

Tripartite Motif Containing 28 (TRIM28) – also known as KAP1 (KRAB-associated protein 1) and TIF1β (transcription intermediary factor 1-beta) - is a member of the Tripartite motif-containing (TRIM) family, comprising almost 60 human genes (Ozato et al., 2008). TRIM28 is highly related to three other TRIM proteins, TRIM24 (TIF1α), TRIM33 (TIF1γ) and TRIM66 (TIF1δ), and together they constitute the Transcriptional Intermediary Factor 1 (TIF1) family (Iyengar & Farnham, 2011). Although the TIF1 proteins share many structural characteristics, they have little functional overlap and their expression pattern is different (H. Peng et al., 2002). TRIM28 was firstly described as an interacting partner of the family of Kruppel-Associated Box Zinc Finger Proteins (KRAB-ZFPs) TFs (Friedman et al., 1996; Iyengar & Farnham, 2011). Today it is known that TRIM28 is involved in many cellular processes, such as development, gene transcription regulation, DNA damage response (DDR) and regulation of retrotransposons, thus being involved in genome stability (Czerwińska et al., 2017). Participating in such many biological processes, it is not surprising that TRIM28 is implicated in tumor development, since high levels of this protein are reported in many cancers. Moreover, its overexpression in cancer is correlated to a reduced OS of patients (Addison et al., 2015; Yokoe et al., 2010). However, evidence reporting tumor-inhibiting roles of TRIM28 have emerged (Chen et al., 2012) and still its tumor activating or inhibiting role are under debate.

TRIM28 Protein Structure

TRIM28 is constituted by an N-terminal RBCC or TRIM domain that comprises a RING finger, two B-box zinc fingers and a coiled coil (CC) domain. RBCC domain is the responsible for the interaction with other proteins, and in particular with the KRAB module of KRAB-ZFPs (Friedman et al., 1996; Iyengar & Farnham, 2011). Next to the RBCC domain is the TIF1 short signature (TSS), essential for gene repression. Consistently, its deletion in TIF1γ abolishes its repressive function (Venturini et al., 1999). The central region of KAP1 consists of a hydrophobic PxVxL pentapeptide that mediates the interaction with Heterochromatin Protein 1 (HP1) (Lechner et al., 2000). The C-terminal PHD (Plant Homeo Domain) and bromodomain constitute a unit for transcriptional repression by recruiting components of the Nucleosome Remodeling Deacetylase (Mi2/NuRD) and the histone H3K9 methyltransferase SETDB1 that are involved in chromatin condensation (Schultz et al., 2001) (Figure 4). Thus, the HP1-binding domain (HP1BD), PHD and bromodomain cooperate to condense chromatin, characterizing the repressive activity of TRIM28. The

PHD domain has E3 ligase activity and directs SUMOylation of the adjacent bromodomain on 3 lysine residues (K554, K779 and K804). The SUMOylated state of these 3 residues is crucial for the recruitment of the Mi2/NuRD complex, SETDB1 and interaction with HP1 protein (Ivanov et al., 2007; Zeng et al., 2008). Usually, bromodomains are a feature of transcriptional activators, being them involved in the recognition of acetylated histone tails (Zeng & Zhou, 2002), while TRIM28's bromodomain has lost its ability to bind to acetyl-lysine residues (Schultz et al., 2001).

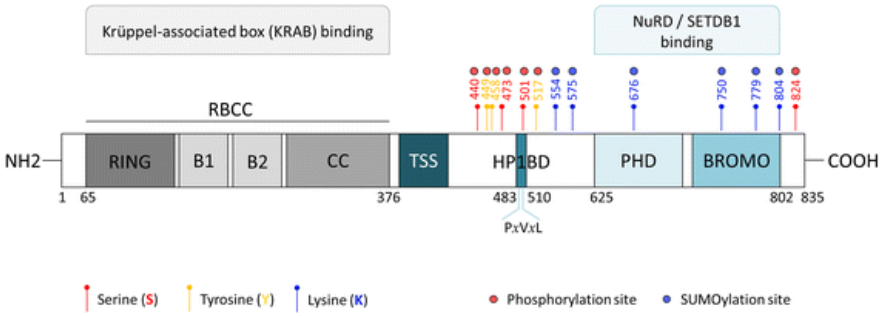

Figure 4. Schematic representation of TRIM28 protein structure and functional domains. The image is from *Czerwińska et al., 2017. (http://creativecommons.org/licenses/by/4.0/)*

TRIM28 and Cancer

TRIM28 upregulation has been reported in several cancer tissues, as well as its association to a bad prognosis, suggesting a role for this protein in cancer progression. Being associated either to induction of cells' proliferation (Addison et al., 2015) or to growth inhibition (Chen et al., 2012), its role as oncogene or as tumor suppressor is still subject of discussion. High TRIM28 levels have been associated to pro-metastatic cervical cancer (Lin et al., 2013). TRIM28 overexpression has been reported also in glioma (Qi et al., 2016), gastric (Yokoe et al., 2010) and ovarian (M. Hu et al., 2015) cancer, where it is associated to a bad prognosis. In hepatocellular carcinoma, high TRIM28 expression was reported as compared to adjacent normal tissue, and its expression correlated with tumor size, tumor stage and reduced OS of patients (Y. Wang et al., 2016). Moreover, several studies reported overexpression of TRIM28 in breast cancer and breast cancer metastases and it was associated to tumor aggressiveness (Addison et al., 2015; Wei et al., 2016). According to these data, TRIM28 overexpression and association to clinical aggressiveness is a common feature of many solid cancers. TRIM28 has been described to promote Epithelial to Mesenchymal Transition (EMT) in several cancers, including cervical (Lin et al., 2013) and pancreatic cancer (Yu et al., 2014). Moreover, in Non-small cell lung cancer (NSCLC), TRIM28 expression is induced upon TGF-β treatment, leading to increased cell migration and invasion (Chen et al., 2014). In breast cancer, TRIM28 participates to EMT by regulating the TF TWIST1 and knockdown (KD) of TRIM28 resulted in decreased migration and invasion of breast cancer cells (Wei et al., 2016). However, opposite results have also been

reported: in early stage lung cancer, high levels of TRIM28 are associated to a better OS (Chen et al., 2012), suggesting a different role in different settings.

TRIM28 as Negative Regulator of Transcription

As a transcriptional corepressor, TRIM28 exerts its function by helping KRAB-ZFPs in their repressive activity. KRAB-ZFP family comprises 400 human genes that encode for more than 700 different proteins (Huntley et al., 2006). This huge family of TFs is involved in many processes, such as embryonic development and cancer progression (Urrutia, 2003). TRIM28 helps the repressive activity of KRAB-ZFPs by acting as a platform for the recruitment of heterochromatin inducing factors. Upon binding their sequence specific DNA elements, KRAB-ZFPs recruit TRIM28 by binding to its RBCC domain (Friedman et al., 1996). Following this interaction, TRIM28 bromodomain is SUMOylated by the adjacent PHD domain, stimulating the recruitment of SETDB1 and the NuRD complex (Figure 5). These proteins are responsible for H3K9me3 mark deposition and histones' deacetylation. H3K9me3 further recruits HP1 that, binding the HP1BD of TRIM28, stabilizes the complex formation. H3K9me3 and histones' deacetylation are silent heterochromatin marks that lead to chromatin condensation in correspondence of KRAB-ZFPs-TRIM28 binding, resulting in transcriptional repression (Ivanov et al., 2007; Schultz et al., 2001). Acting as a scaffold for heterochromatin inducing complexes, TRIM28 exerts its repressive function as an epigenetic regulator, by mediating chromatin remodeling.

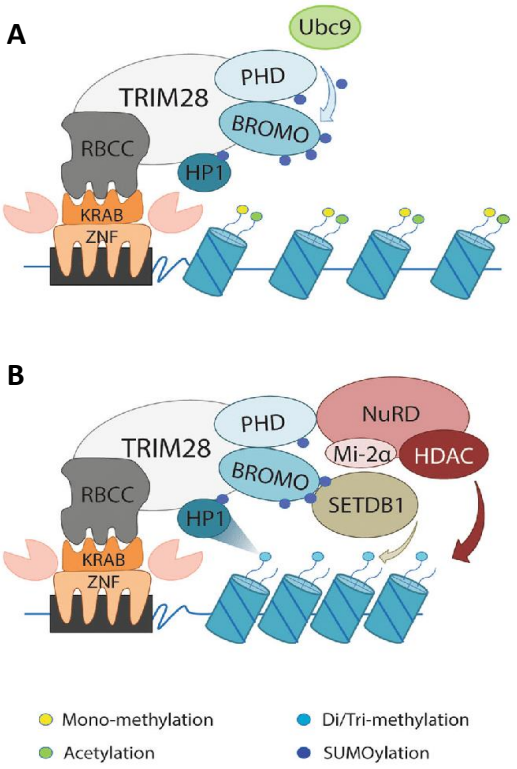

Figure 5. **A)** TRIM28 is recruited to target genes by KRAB-ZFPs that bind specific DNA sequences. This interaction stimulates TRIM28 auto-SUMOylation of Bromodomain. **B)** SUMOylated TRIM28 recruits SETDB1 and the NuRD complex that create H3K9me3 histone mark and deacetylation of adjacent nucleosomes. The image is from *Czerwińska et al., 2017*; *(http://creativecommons.org/licenses/by/4.0/)*

Besides heterochromatin formation, TRIM28 can also induce chromatin relaxation. Being phosphorylated on S824 by ATM kinase following DNA damage, TRIM28 mediates DDR facilitating chromatin accessibility. Phosphorylation of S824 is mutually exclusive with SUMOylation of the bromodomain, thus resulting in SETDB1 and NuRD release and consequent chromatin relaxation (Czerwińska et al., 2017). This modification has been reported to mediate also TRIM28 role in positive regulation of transcription (Bunch et al., 2014; X. Li et al., 2007).

TRIM28 as Positive Regulator of Transcription

Besides its well established role as corepressor, TRIM28 has been recently identified as a regulator of the elongation step of RNA Polymerase II (RNA-PolII) during transcription. TRIM28 was identified in a screening looking for proteins bound close to the Transcription Starting Site (TSS) of the human *HSPA1B* gene to regulate RNA-PolII pausing (Bunch et al., 2014). Transcription is initiated by RNA-PolII recruitment at promoters and formation of the transcription preinitiation complex (PIC), composed by general TFs (TFII-X) (Grünberg & Hahn, 2013). TFIIH is the subunit responsible for RNA-PolII phosphorylation of S5 on its C-terminal domain (CTD) that allows transcription initiation. About 20-65 nucleotides (nt) downstream of the transcription start site (TSS), RNA-PolII often pauses due to the action of the Negative Elongation Factor (NELF) and DRB Sensitivity-Inducing Factor (DSIF) (Peterlin & Price, 2006). RNA-PolII release into productive elongation is stimulated by the recruitment of the positive transcription elongation factor (P-TEFb), composed by a heterodimer of Cyclin T1 or T2 (Cyc T1/T2) and Cyclin-dependent kinase 9 (CDK9) (Gomes et al., 2006). P-TEFb, once recruited, phosphorylates NELF, DSIF and S2 on CTD of RNA-PolII, facilitating RNA-PolII pause release and entry into productive elongation (Zhou et al., 2012). P-TEFb is usually found in its inactive form, bound to the 7SK-snRNP complex (He et al., 2008). Recent studies found TRIM28 as an interacting partner of the 7SK-snRNP complex and as a crucial factor for its delivery to signal-regulated gene promoters. TRIM28 facilitates the recruitment of the 7SK-snRNP complex to promoters containing paused RNA-PolII, enabling P-TEFb activation and pause release (McNamara et al., 2016). TRIM28 loss resulted in reduced 7SK-snRNP complex at promoters, while no alterations in RNA-PolII binding were reported. Thus, upon TRIM28 KD, reduced RNA-PolII elongation and consequent gene activation was observed (D'Orso, 2016; McNamara et al., 2016). This cycle of RNA-PolII pause and pause release is a key step in timing the activation of transcriptional programs dependent on signal transduction cascades. Thus, TRIM28, by

stabilizing paused RNA-PolII at the TSS of inactivated genes, permits its readily activation upon induction (Figure 6). Bacon et al. showed that TRIM28 by directly binding to histone 4 hypo-acetylated tails, orchestrates the interactions between RNA-PolII, CDK9 and pathway-specific TFs to activate transcriptional programs that sustain cancer cells (Bacon et al., 2020). This function of TRIM28 is dependent on the phosphorylation of Ser824 that induces chromatin relaxation allowing RNA-PolII elongation (Bunch et al., 2014; X. Li et al., 2007)

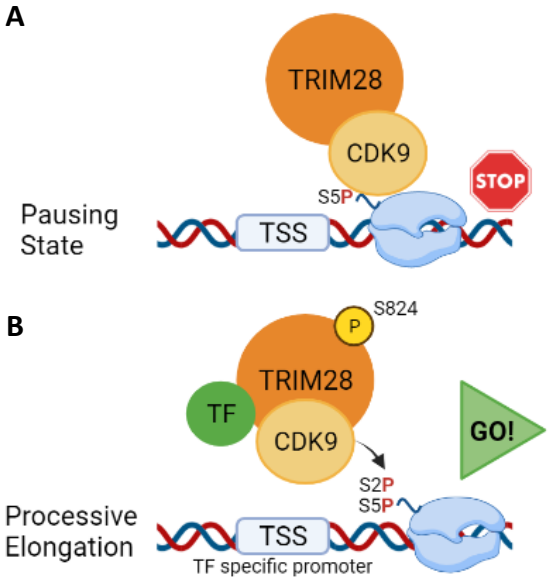

Figure 6. A) RNA-PolII paused downstream the TSS of a target gene. **B)** Upon specific stimuli, TRIM28 recruits pathway-specific TFs to their target genes' promoters together with active CDK9, that phosphorylates RNA-PolII on Ser2. Meanwhile, TRIM28 is phosphorylated on S824 causing chromatin relaxation and allowing RNA-PolII elongation. Created with *Biorender.com*

TRIM28 as Repressor of Endogenous Retroviruses (ERVs)

Transposable Elements (TEs) are mobile DNA elements that, constituting more than a half of the human genome, are the major representatives of the non-coding genome (de Koning et al., 2011; Lander et al., 2001). TEs can be subdivided in two classes: DNA transposons and retrotransposons. Retrotransposons, being still capable of retrotransposition, are harmful elements for genome stability and can heavily influence gene expression profiles. They are divided in two macro-categories, depending on the presence of Long Terminal Repeats (LTR) or not (non-LTR). Non-LTR retrotransposons are further divided in Long Interspersed Elements (LINEs) and Short Interspersed Elements (SINEs) (de Koning et al., 2011). LTR retrotransposons are also known as Endogenous Retroviruses (ERVs) and constitute up to 8% of the human genome (Figure 7) (Geis & Goff, 2020). These elements are the remnants of ancient retroviruses infection (Stoye, 2012). ERVs transcription has a fine regulation through multiple levels in human stem cells (HSCs) and different mechanisms are specific of different cell types, indicating an important role of these elements during

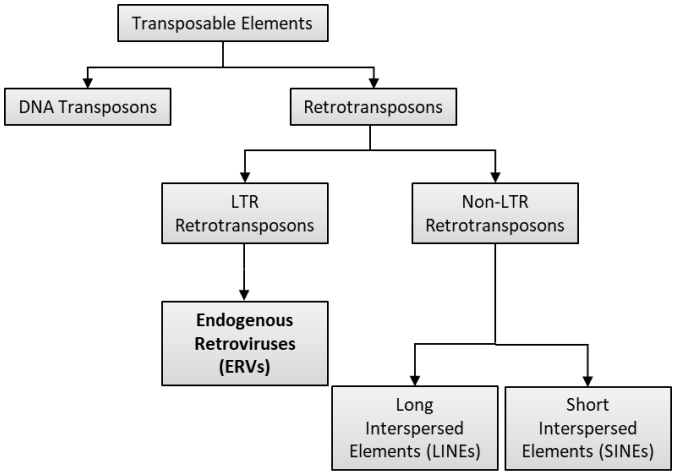

Figure 7. Schematic representation of Transposable Elements (TEs) classification.

development (Geis & Goff, 2020). The mechanisms of ERVs regulation in differentiated cells are still to be elucidated, however it is clear that they are usually repressed through DNA methylation to avoid an autoimmune response (Gautam et al., 2017). Resembling retroviruses, ERVs transcripts are sensed by viral RNA sensors, such as Toll-like receptors (TLRs) and RIG-I-like receptors. Their activation triggers IRF signaling pathway and induces Interferon-I response that, ultimately, leads to cell death (Chiappinelli et al., 2015; Mu et al., 2016). Coherently, treatment of cancer cells with DNA demethylating agents such as 5-azacytidine (5-AZA) induces ERVs reactivation and the expression of interferon-stimulated genes (ISGs) (Chiappinelli et al., 2015; Roulois et al., 2015). A microarray study was performed in 19 different human healthy tissues and revealed that ERVs are actively transcribed with a different signature based on cell-type. They also found a correlation between ERVs transcription and the proliferative rate of a cell (Seifarth et al., 2005).

It is consolidated that TRIM28 together with KRAB-ZFPs, SETDB1 and DNA methyltransferases, is responsible for ERVs epigenetic silencing during development (Rowe et al., 2010; Turelli et al., 2014) (Figure 8). Rowe and colleagues demonstrated that TRIM28 silencing caused the re-expression of several ERVs, in particular of Intracisternal A-type Particles (IAP) in mouse embryonic stem cells and early embryos. They observed loss of H3K9me3 mark at 5'UTR of IAP elements following TRIM28 silencing, resulting in their overexpression (Rowe et al., 2010). Recently, a role for TRIM28 in keeping repressed ERVs also in differentiated cells has been reported. Turelli et al. showed that TRIM28 regulates ERVs in human CD4+ T cells (Turelli et al., 2014) and the same observation was reported in neural progenitor cells (Brattås et al., 2017). DNA binding analyses revealed that two thirds of KRAB-ZFPs are specifically bound to transposable elements (Imbeault et al., 2017). Moreover, TRIM28 KD upregulated ISGs, promoting innate immune response likely as a consequence of ERVs reactivation (Tie et al., 2018).

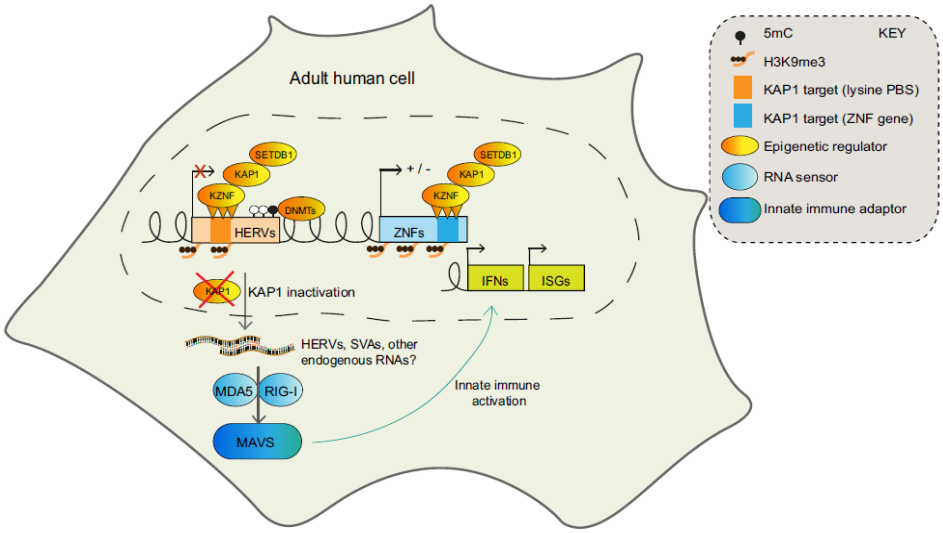

Figure 8. TRIM28 (KAP1) and SETDB1 are recruited to human ERVs (HERVs) promoter by KRAB-ZFPs. TRIM28 by recruiting heterochromatin inducing factors, mediates H3K9-me3 that primes chromatin condensation and HERVs repression. TRIM28 inactivation leads to demethylation of HERVs, inducing their transcription. dsRNAs activate Interferon type I response through MAVS. The figure is from *Tie et al. 2018.*

The non-coding genome

From the release of the human genome project (Green et al., 2015) it appeared evident that what we had imagined about the organization and functioning of the genome was over-simplified and far from the truth, with coding regions insufficient to explain life and the complexity of human diseases. Over 98% of our genome is occupied by non-coding elements, that greatly outnumber coding elements (Alexander et al., 2010; Djebali et al., 2012; ENCODE Project Consortium et al., 2007). Far from being just “junk” DNA, the systematic functional annotation of the non-coding genome has revealed that more than 80% of it is engaged in gene expression regulation (Engreitz et al., 2016; Gil & Ulitsky, 2020) and that SNPs associated with diseases by Genome Wide Association Studies (GWAS) are enriched within non-coding functional elements (F. Zhang & Lupski, 2015). This indicates that sequence alterations in key elements within non-coding regions may alter their functionality and lead to aberrant programs, affecting cell behavior. Surprisingly, up to 90% of non-coding regions are transcribed in an impressive number of non-coding RNAs (ncRNAs) (Djebali et al., 2012; Iyer et al., 2015). Based on their size, ncRNAs are classified in two categories:

1) Small non-coding RNAs (<200 bp) that comprises microRNAs (miRNAs), PIWI-interacting RNAs (piRNAs), small nucleolar RNAs (snoRNAs) and small interfering RNAs (siRNAs) (Esteller, 2011; Quinn & Chang, 2016).

2) Long non-coding RNAs (lncRNAs) (>200 bp) that are divided in long intergenic non-coding RNAs (LINCRNAs), pseudogenes, circular RNAs (circRNAs) and antisense transcripts (Esteller, 2011; Quinn & Chang, 2016).

Among these, lncRNAs have been reported to control several biological processes affecting gene expression at multiple levels, from transcription to protein localization and stability (Quinn & Chang, 2016). Over 60000 lncRNAs have been identified in human (Iyer et al., 2015) and more than 8000 were discovered as selectively expressed in cancer cells. Their elevated number and high expression specificity candidate these molecules as a valuable source of biomarkers and potential therapeutic targets (Chandra Gupta & Nandan Tripathi, 2017; Iaccarino & Klapper, 2021).

Long non-coding RNAs (lncRNAs)

LncRNAs are transcripts of >200 nt in length transcribed by RNA-PolII that lack the ability to encode proteins. However, they share many biological features with mRNAs (Kondo et al., 2017). They comprise a heterogeneous class of intragenic and intergenic transcripts and sense or antisense transcripts. LncRNAs are implicated in many biological processes, such as: 1) regulation of transcription *in cis* or *in trans*; 2) modulation of mRNA processing; 3) regulation of miRNAs activities; 4) regulation of protein localization and functions; 5) regulation of chromatin dynamics (Quinn & Chang, 2016). Their function is mainly associated to their localization into the cell, with the majority of lncRNAs being located in the nucleus (Bridges et al., 2021). Nuclear lncRNAs act as scaffold molecules for the recruitment of different proteins to form 3D structures that impact on genes' transcription by directly interacting with the transcriptional machinery or DNA regulatory elements or by affecting chromatin organization and mRNA splicing. Besides, cytoplasmic lncRNAs exert their function primarily by interacting with other types of RNAs. They can directly bind mRNAs, affecting their translation and stability or can act as miRNA "sponge", inhibiting their downregulation of target mRNAs (Bridges et al., 2021; Kondo et al., 2017). By regulating gene expression, lncRNAs are involved in a wide variety of biological processes, such as cell cycle, growth, apoptosis, metastasis and drug resistance. Having a great specificity of expression compared to coding transcripts and being easily detectable in tissues and biological fluids, in recent years there is a mounting interest in using lncRNAs as possible disease biomarkers (Chandra Gupta & Nandan Tripathi, 2017; Iaccarino & Klapper, 2021). It is by now consolidated that dysregulation of lncRNAs is associated with cancer pathogenesis, suggesting that lncRNAs are a new emerging class of oncogenes and tumor

suppressor genes. They participate to tumor progression by epigenetic regulation, both at the transcriptional and post-transcriptional level. For example, overexpression of metastasis associated lung adenocarcinoma transcript 1 (*MALAT1*), is associated with metastasis and poor outcome of patients with NCSLC (Schmidt et al., 2011). The Hox transcript antisense intergenic RNA (*HOTAIR*) is upregulated in several cancers and it is associated to metastasis. By recruiting the Polycomb repressor complex, it mediates transcriptional silencing of the *HOXD* locus (Gupta et al., 2010).

lncRNAs in MPM

In order to identify lncRNAs that could be involved in MPM pathogenesis, Wright et al. analyzed their expression in 4 MPM cell lines and compared to a normal pleura cell line, finding 33 lncRNAs that were significantly differentially expressed. The upregulation of six lncRNAs have been validated in both MPM cell lines and tissues, compared to normal pleura cell lines and tissues. This signature was able to discriminate tumor from normal tissue with high specificity and sensitivity. Two candidates were associated with metastases and OS of MPM patients: ***NEAT1*** and ***SNHG7*** (Wright et al., 2013). *NEAT1* is a lncRNA located on 11q13.1, a region reported to be amplified in MPM. It is involved in mRNA transport regulation and it is a structural component of paraspeckles (Clemson et al., 2009). The small nucleolar RNA host gene 7 (*SNHG7*) is a bidirectional lncRNA and is thought to encode the snoRNAs *SNORA43* and *SNORA17*. snoRNAs are implicated in ribosome biogenesis, critical for protein synthesis during cell growth. Interestingly, inhibition of this pathway in mesothelioma decreased cell invasion and motility (Iadevaia et al., 2012). This study lay the basis for the employment of lncRNAs as potential biomarkers for MPM.

Plasmacytoma variant translocation 1 (***PVT1***) is a lncRNA initially identified in Burkitt's Lymphoma (Graham & Adams, 1986) that acts as an oncogene in various human cancers (Guan et al., 2007; J. Hu et al., 2018; D. Wang & Hu, 2019). It is located in the same region of *C-MYC* (8q24) and amplifications of this region have been described in MPM (Riquelme et al., 2014). KD of *PVT1* but not of *C-MYC* in 8q24 amplified cell lines showed an increase in apoptosis, a decrease in cells' proliferation and an improved sensitivity to cisplatin (Riquelme et al., 2014). Fujii and colleagues found PVT1 expression to be upregulated in several MPM cell lines and its KD decreased proliferation and migration of MPM cells (Fujii et al., 2022). Interestingly, *PVT1* KD caused a downregulation of *FOXM1*, and the inactivation of both enhanced the effect of each KD alone (Fujii et al., 2022), suggesting a functional interplay between the two factors.

Growth arrest-specific 5 (***GAS5***) is a lncRNA that encode for several snoRNAs and has been proposed to act as a tumor suppressor gene. Coherently, its expression was found downregulated in MPMs compared to healthy mesothelial cells (Renganathan et al., 2014).

LINC00941 and Cancer

Long Intergenic non-protein Coding RNA 941 (LINC00941), also known as MSC-upregulated factor (MUF), is a lncRNA located in 12p11.21 region of the human genome. *LINC00941* has been found as associated with development and progression of several cancers, like gastric cancer (Luo et al., 2018), head and neck squamous cell carcinoma (Y. Hu et al., 2020), papillary thyroid cancer (Gugnoni et al., 2021), non-small cell lung cancer (Ren et al., 2021), pancreatic cancer (J. Wang et al., 2021) and colon cancer (Chang et al., 2021). Several studies demonstrated that *LINC00941* is associated to growth and metastasis of different tumors. *LINC00941* is overexpressed in oral squamous cell carcinoma, where it promotes tumor progression by activating the WNT/β-Catenin signalling pathway (Ai et al., 2020). The same mechanism is observed in hepatocellular carcinoma, where it promotes EMT (Yan et al., 2017). In lung adenocarcinoma, *LINC00941* takes part to the PI3K-AKT signaling pathway and its high expression is associated to a reduced survival of patients (L. Wang et al., 2019). In colorectal cancer, high *LINC00941* expression correlates with poor prognosis and promotes EMT by activating the TGF-β-SMAD2/3 axis, increasing cell invasion and metastasis (Wu et al., 2021). High *LINC00941* expression in pancreatic cancer is associated to a larger tumor size, lymph node metastasis and poor prognosis. Coherently, *LINC00941* KD significantly decrease pancreatic cancer cells' growth, metastasis and EMT (J. Wang et al., 2021). In gastric cancer (GC) the expression of *LINC00941* is associated with tumor depth and distant metastasis. Its inactivation decreased GC cells' proliferation, migration and invasion *in vitro* and modulates tumor growth *in vivo* (H. Liu et al., 2019). High levels of *LINC00941* were found also in colon cancer (CC) tissues and cell lines, where it promotes proliferation, migration and invasion of CC cells. In this model, *LINC00941* regulates the expression of MYC by sponging miR-205-5p (Chang et al., 2021). Overexpression of *LINC00941* in NSCLC promoted angiogenesis and tumor progression by regulating VEGFA through miR-877-3p (Ren et al., 2021).

AIM OF THE STUDY

MPM is a current clinical emergency. Its incidence is rapidly growing in both industrialized and developing countries and the lack of MPM specific targeting strategies alongside with the poor efficacy of standard chemotherapy, are the major causes of the poor life expectancy of MPM patients. At the basis of such emergency are the peculiar features of MPM that, escaping classical models of carcinogenesis, is characterized by an insufficient knowledge of the molecular mechanisms leading to MPM development and progression, limiting the therapeutic opportunities. Also, in light of the massive contribution of ncRNAs to cancer, genome structure and function is currently regarded as the epicentre of many cancer supporting functions, in particular through the control of gene expression and chromatin organization.

In this work, we explored the contribution of both coding and non-coding genome to the growth and survival mechanisms that sustain MPM cells, with the aim of identifying new non-genetic vulnerabilities using two separated approaches:

1. A CRISPR-Cas9 based knockout genome-wide loss of function screening was performed looking for protein-coding genes that are essential for MPM cells' survival and proliferation.
2. The analysis of gene expression profiles and clinical data from the TCGA-MPM dataset was undertaken to explore the contribution of lncRNAs to MPM survival and progression.

The integration of the results with clinical data of patients allowed us to link gene perturbations with their functional consequences *in vivo*. This approach should overcome the limitation of purely descriptive genetic omics profiling, identifying true addictions and shedding lights on the molecular mechanisms driving MPM development, thus opening the doors to the design of new MPM-oriented therapies.

RESULTS

Integration of genome-wide screening and clinical data identified a core of chromatin-associated genes essential for MPM progression

With the purpose of identifying new vulnerabilities essential for MPM progression, we performed a CRISPR/Cas9 genome-wide knockout (KO) screening in the MPM MSTO-211H cell line, previously engineered to express Cas9 (Figure 9A, B). Clone G12 was the one with the highest Cas9 activity and selected to perform the screening and further experiments (Figure 9A, B). To this aim, we used the GecKOv2 library (Shalem et al., 2014) that targets over 19000 genes in the human genome to infect MSTO-211H/Cas9 cells (Figure 9C-E). Cells were harvested at day 0 (T0), day 16 (T16) and day 23 (T23) after selection. We assessed library composition by Next Generation Sequencing (NGS) and compared single-guide RNAs (sgRNAs) frequencies to day 0, to identify sgRNAs that were depleted or enriched over cell growth. Considering only sgRNAs that were consistently depleted or enriched at both time points and in both bio-replicates, we identified sgRNAs targeting 1228 genes that were depleted and sgRNAs targeting 183 genes that were enriched (Figure 9E). The sgRNAs depleted over cell growth are expected to target genes that are essential for MPM cells' proliferation and survival, thus we called these genes "essential genes"; on the other hand, the sgRNAs enriched over cell growth likely target genes that restrain MPM cells' proliferation and we refer to these genes as "suppressor genes".

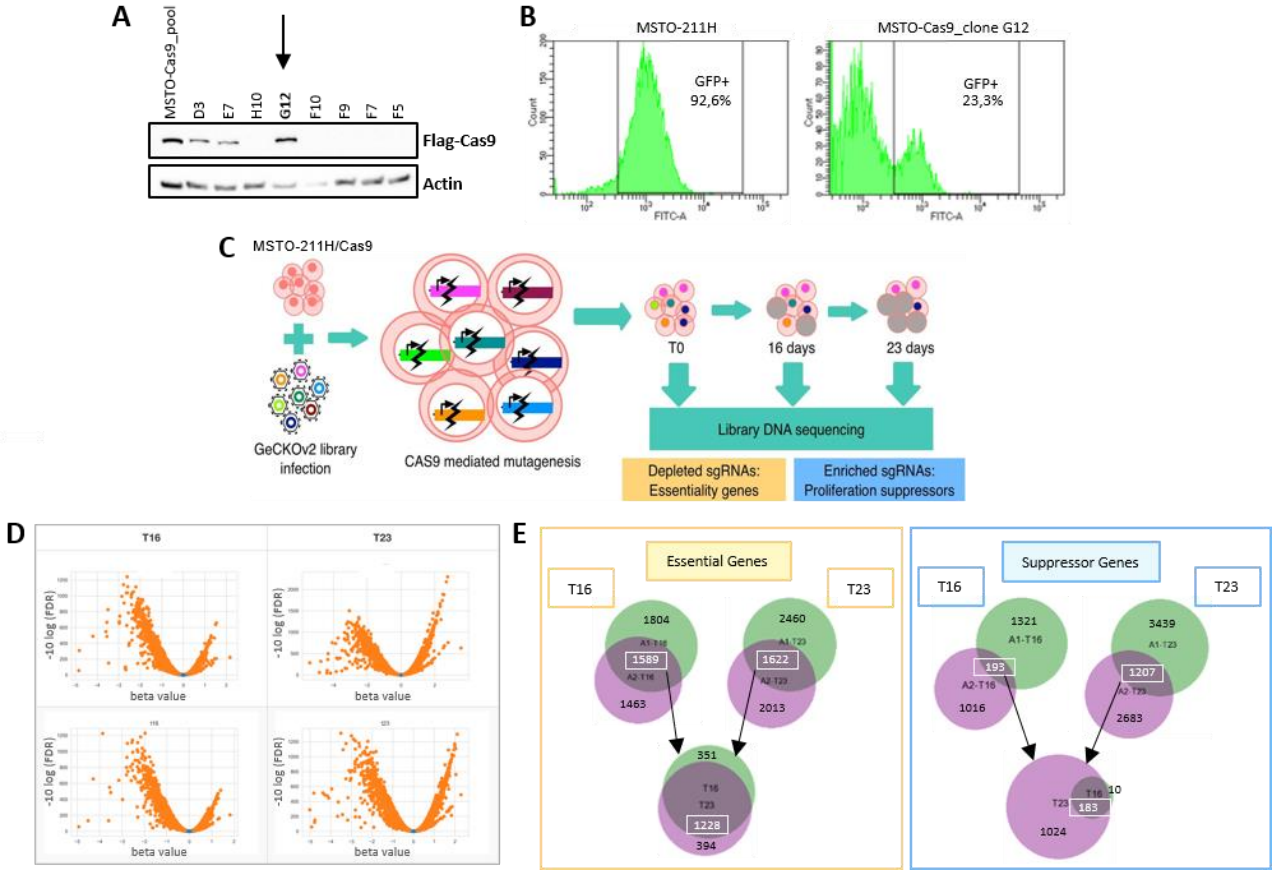

Figure 9. A) Western Blot showing the levels of expression of Flag-Cas9 in MSTO-211H/Cas9 pool and in the selected clones. Clone G12 was chosen for following experiments. **B)** FACS plots indicating the percentage of GFP positive cells in MSTO-211H vs MSTO-211H/Cas9-clone G12 cells transduced with pXPR_011 plasmid. Cas9 expression causes GFP decadence (see Material and Methods for further details). **C)** Graphic overview of the genome-wide CRISPR/Cas9 screening performed in MSTO-211H/Cas9-clone G12 cells; time points are relative to the end of the selection. **D)** Volcano Plots showing beta value and FDR adjusted p-value distributions of each sgRNA at both time points and in each bio-replicate. **E)** Venn diagrams reporting the number of genes identified in the two replicates at each time point and final merge for both essential (left) and suppressor (right) genes.

From these gene lists, we removed genes coding for miRNAs and common essential genes (common to all cell lines) (Figure 10A). Then, to validate our results, we investigated the Cancer Dependency Map Project (DEPMAP) (Tsherniak et al., 2017) that systematically identifies essential genes across over 500 cancer cell lines using either RNA Interference (RNAi) or CRISPR/Cas9 genome-wide loss of function screening. Essential genes are defined based on the “dependency score”: the lower the dependency score is and the higher is the probability that a given cell line is strongly dependent on that gene. Data from CRISPR/Cas9 perturbations were available for 7 MPM cell lines; genes from our screening were considered validated only if showing concordant trend in at least 6 of the 7 MPM cell lines available. 51% (N=233) and 26% (N=45) of the identified essential and suppressor genes, respectively, were confirmed by this approach supporting the validity of our analysis

and underlining a certain homogeneity in survival mechanisms across MPM cell lines (Figure 10A-B). Gene Ontology (GO) analysis performed on the list of essential genes revealed that they were largely involved in cell cycle regulation, chromatin and chromosome organization (Figure 10C). Instead, GO analysis performed on the list of suppressor genes did not identify any significant enriched pathway. Since our goal was to identify new non-genetic vulnerabilities that drive MPM progression, we focused on the 233 essential genes for further validation.

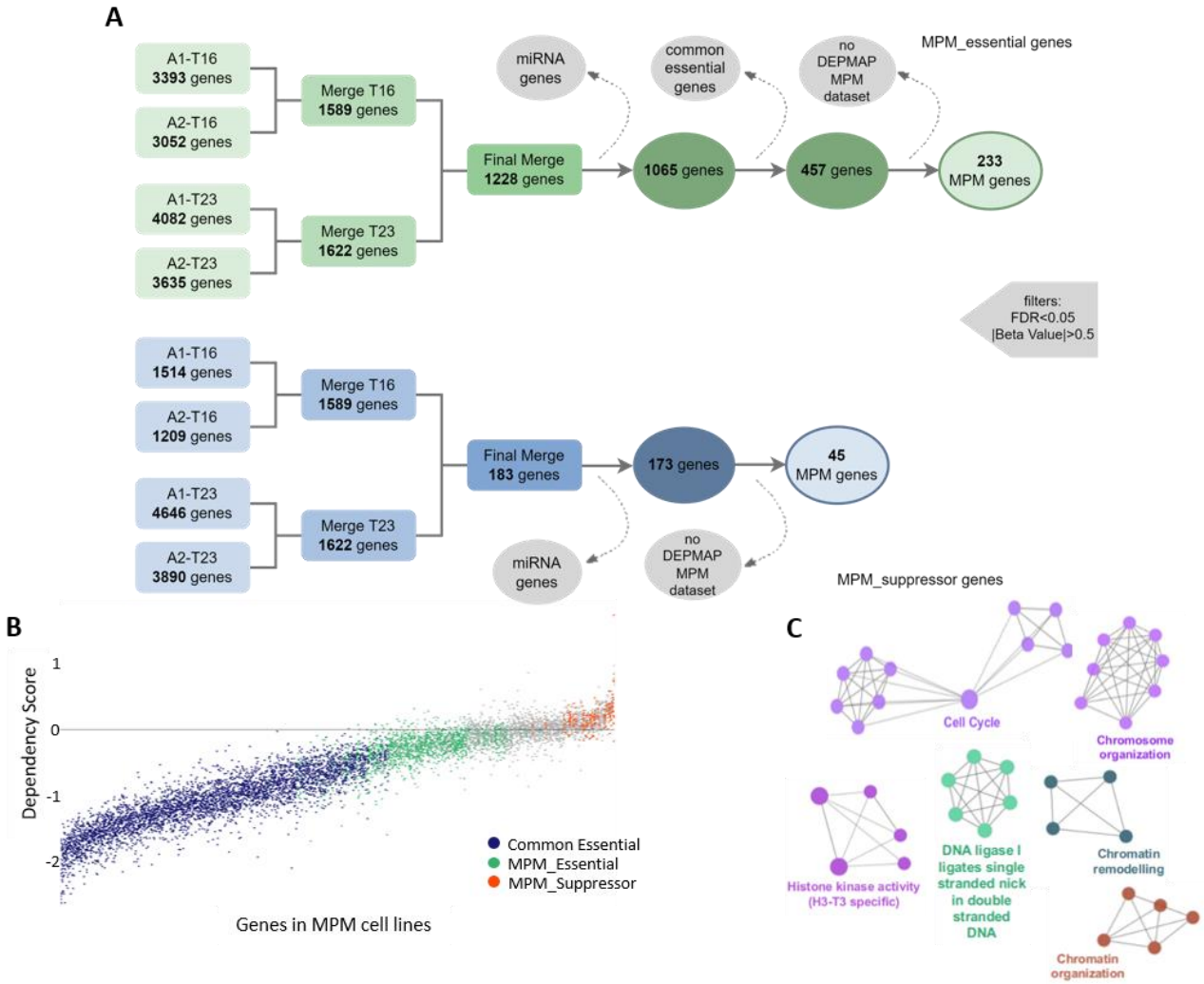

Figure 10. A) Schematic representation of the flowchart that we adopted to analyze the screening results. **B)** Graphic representation of the distribution of common essential, MPM essential and MPM suppressor genes (X axis) in 7 MPM cell lines (Y axis) according to DEPMAP database, ordered for dependency score. **C)** Network representation of the most significant enriched pathways for the 233 MPM essential genes.

To choose the best candidates and select the ones with clinical relevance, we correlated the expression of the 233 MPM essential genes with patients' survival probability in the TCGA-MESO repository (N=87). 22% of these genes (N=51) showed a significant correlation with reduced survival probability of MPM patients ($p \leq 0.05$), among which 18

showed the strongest association (q≤0.1). Patients' survival curves for these 18 genes are shown in Figure 11A. To confirm the essential role of some of these genes for MPM cells growth, we performed a competition assay in MSTO-211H/Cas9 cells. We infected the cells with two different sgRNAs targeting each gene (*VRK1*, *SMURF2*, *HASPIN*) with an efficiency of 60-70%, to obtain two populations of infected (GFP+) and non-infected (GFP-) cells. We followed the competition between the two populations by measuring the GFP% over time (Figure 11B-C). Thus, considering the decrease of GFP positive cells over time, which effect was not observed for NT1 infected cells (negative control), we confirmed the essential role of *SMURF2*, *VRK1* and *HASPIN* for MSTO-211H/Cas9 cells proliferation. The efficiency of the KO was assessed using the Alt-R kit (Figure 11D).

The epigenetic keeper TRIM28 is the one with the strongest effect in terms of patients' survival: low-TRIM28 patients have a median survival of 43 months, while high-TRIM28 patients have a 11-month median survival (HR 6.3) (Figure 11A). The 18 epigenetic keepers identified were functionally interconnected as shown by protein-protein network analysis of Figure 11E. Moreover, in the TCGA-MESO cohort their expression is positively correlated (Figure 12A, B). We then correlated their expression with the most common MPM genetic alterations and we found that, except for *ATG101* and *P2Ry2*, these genes are positively associated with Copy Number Alterations (CNA) in the cell cycle inhibitors *CDKN2A*, *CDKN2B* and the methylthioadenosine phosphorylase (*MTAP*), that are often co-deleted together in cancer (Figure 12C) (Krasinskas et al., 2010). Moreover, *WDR76*, *VRK1*, *LIG1*, *UBE2S*, *SMURF2*, *CENPL*, *ATG101*, *FOSL1*, *HASPIN* and *CKS2* displayed a positive correlation with mutations in *LATS2* (Figure 12C). LATS2, together with LATS1, is a kinase responsible for the phosphorylation and activation of YAP and TAZ, the downstream effectors of the Hippo pathway (Ma et al., 2019). Interestingly, FOSL1 has been described as a target gene of YAP. Moreover, FOSL1 together with JUN constitute the TF complex AP-1 that has been reported to synergize with YAP, stimulating its activity (Rozengurt et al., 2018).

Collectively these data, besides confirming the validity of our analysis, indicate that the 18-genes identified in our screening may represent a MPM-specific essential functional core.

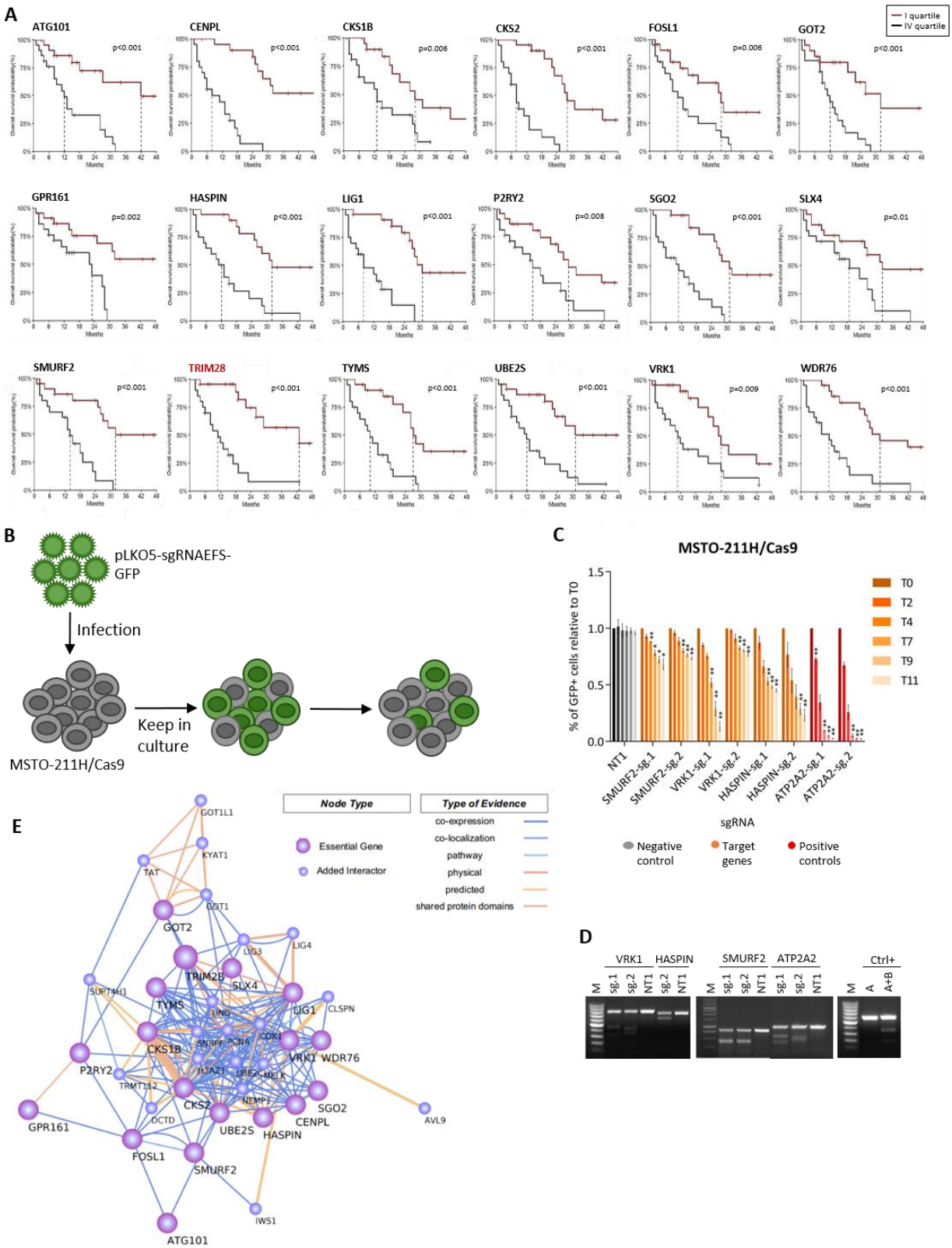

Figure 11. A) Kaplan Meyer plots showing correlation of the 18 epigenetic keepers with MPM patients' survival based on TCGA-MESO data (N=87). Patients were divided in quartiles of expression for each gene and patients in the 1st quartile (red, low expression) were compared to patients in the 4th quartile (black, high expression). **B)** Schematic representation of the procedure used for competition assays. **C)** Validation assay of the effect of the reported MPM essential genes using a competition assay. For each time point the ratio between GFP-positive (infected) and GFP-negative (uninfected) cells has been calculated and normalized on T0. Statistical significance has been calculated by comparing the normalized ratio for each sample to T0.

ATP2A2 is a common essential gene used as a positive control. Data are mean ± SEM; *≤0.05, **≤0.01, ***≤0.001; N=2. **D)** Agarose gel showing Alt-R mismatch analysis in MSTO-211H/Cas9 cells infected with the respective sgRNAs. As control, the cells were infected with a non-targeting sgRNA (NT1). Positive control to check nuclease activity (Ctrl+) was provided in the kit. M is the molecular weight marker in the range between 100 bp and 1000 bp. **E)** Protein-protein interaction network of the 18 epigenetic keepers essential for MPM survival and added interactors by STRING (v11). The type of evidence linked to each edge is represented by a color scale.

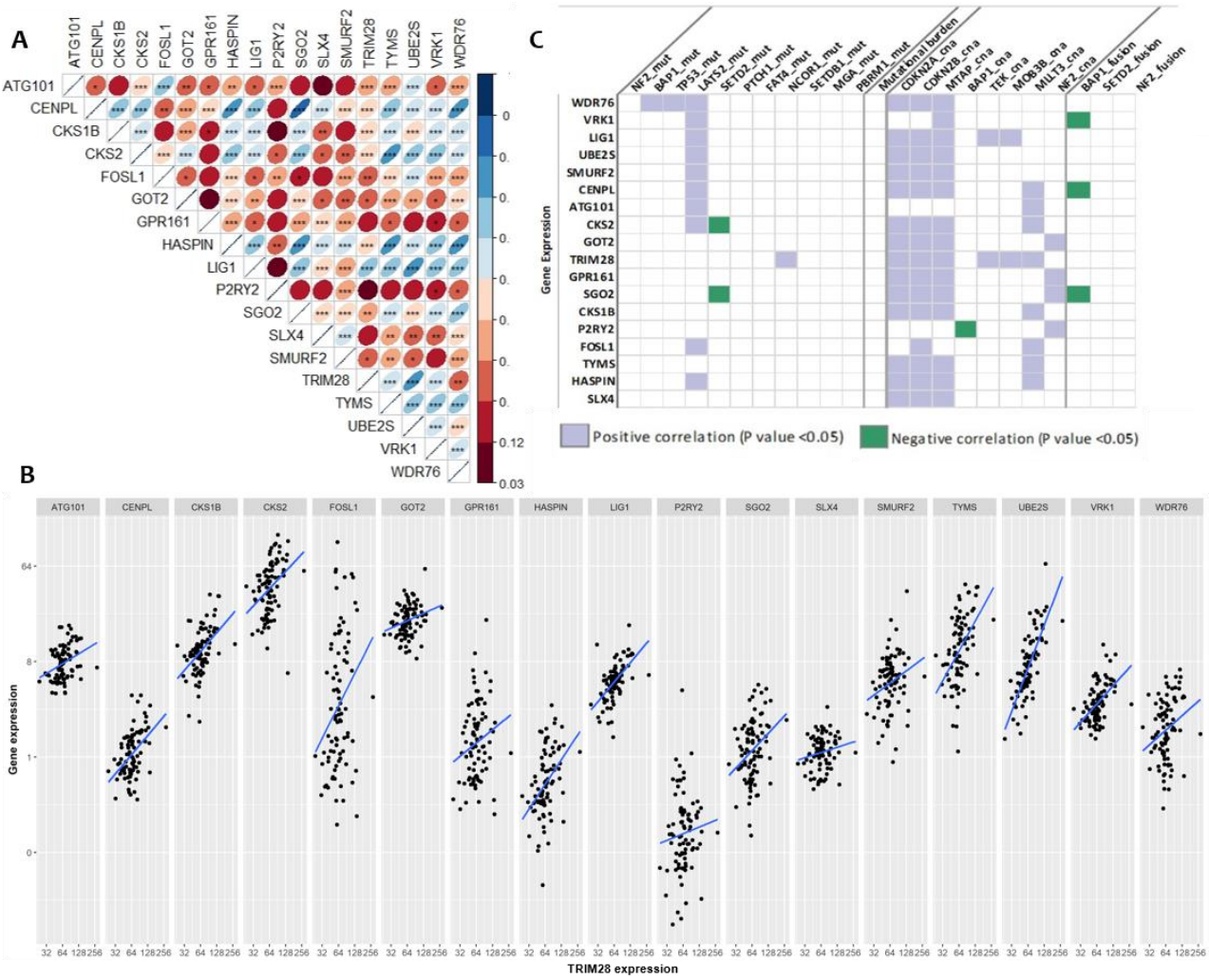

Figure 12. A) Expression correlation matrix (Spearman test) within the 18 chromatin keepers based on TCGA-MESO dataset. *<0.05, **≤0.01, ***≤0.001. **B)** Scatterplot showing correlation of TRIM28 gene expression (X axis) with the other 17 chromatin keepers (Y axis). **C)** Expression correlation of the 18 chromatin keepers with MPM most relevant mutations and mutational burden according to TCGA-MESO data. MPM samples were dichotomized based on the presence of mutations. Differential analysis was conducted to establish whether the expression of the 18 MPM essential epigenetic keepers showed a significantly different distribution in the mutated vs non-mutated group. POS and NEG correlation mean respectively higher or lower gene expression (on Y axis) in presence of mutations (on X axis). Significance was established by adjusted p-value calculation.

Loss of TRIM28 strongly impairs proliferation and induces apoptosis of MPM cells

Considering the strong effect on patients' survival probability and its reported role in genome function, we focused our analysis on TRIM28 with the aim to deepen its role in MPM. Competition assay performed in MSTO-211H/Cas9 cells confirmed that TRIM28 loss

significantly impairs cells' proliferation, coherently with the screening results (Figure 13A-B). Besides, TRIM28 inactivation strongly impairs colony forming ability of MSTO-211H/Cas9 cells (Figure 13C). Coherently, TRIM28 KD by siRNA strongly impaired proliferation of MSTO-211H and NCI-H2052 MPM cell lines (Figure 13D-E, G-H). Moreover, TRIM28 silencing caused a remarkable effect on colony forming ability of both MPM cell lines (Figure 13F, I). MPM cells are strongly affected by cells confluence to properly grow; this could explain the discrepancy between the reduction in cells' proliferation and the stronger effect on colony forming ability upon TRIM28 loss, for which assay the cells are seeded at a low concentration rate.

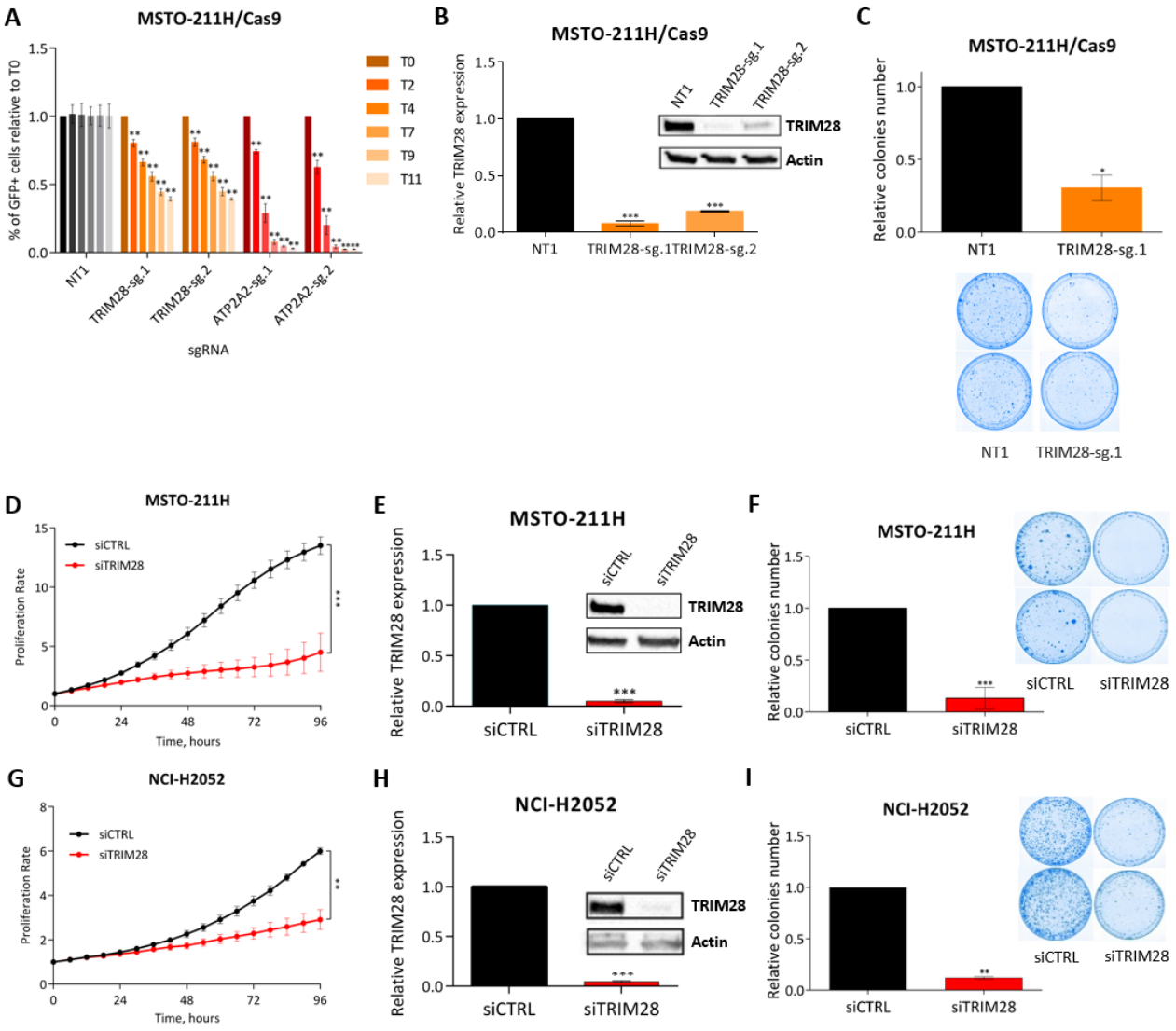

Figure 13. A) Validation assay of the effect of TRIM28 KO using a competition assay. For each time point the ratio between GFP-positive (infected) and GFP-negative (uninfected) cells has been calculated and normalized on T0. Statistical significance has been calculated by comparing the normalized ratio for each sample to T0. Data are mean ± SEM; *≤0.05, **≤0.01, ***≤0.001; N=3. **B)** qRT-PCR (graph) and western blot analysis of TRIM28 expression in NT1 versus TRIM28 KO MSTO-211H/Cas9 cells. Data are represented as mean ± SEM; *≤0.05, **≤0.01, ***≤0.001; N=3. **C)** TRIM28 KO effect on colony forming ability of MSTO-211H/Cas9 cells. On the left is reported the graph showing the number of colonies formed in TRIM28 KO cells

expressed as ratio of NT1. On the right, pictures of cell dishes showing colonies formation in NT1 and TRIM28 KO cells. Data are mean ± SEM; *≤0.05, **≤0.01, ***≤0.001; N=2. **D, G)** Proliferation assays in MSTO-211H (D) and NCI-H2052 (G) cells reported as proliferation rate relative to day 0, measured with Incucyte S3 Live Cell Analysis (Sartorius). Data are represented as mean ± SEM; *≤0.05, **≤0.01, ***≤0.001; N=4. **E, H)** qRT-PCR (graph) and western blot analysis of TRIM28 expression in siCTRL versus siTRIM28 MSTO-211H (E) and NCI-H2052 (H) cells. Data are mean ± SEM; *≤0.05, **≤0.01, ***≤0.001; N=4. **F, I)** TRIM28 KD effect on colony forming ability of MSTO-211H (F) and NCI-H2052 (I) cells. On the left is reported the graph showing the number of colonies formed in siTRIM28 cells expressed as ratio of siCTRL. On the right, pictures of cell dishes showing colonies formation in siCTRL and siTRIM28 cells. Data are mean ± SEM; *≤0.05, **≤0.01, ***≤0.001; N=2.

To explore the biological role of TRIM28 in MPM, after evidence of a dysregulation of the G2/M phases of the cell cycle following TRIM28 silencing (data not shown), we decided to synchronize cells in order to observe this phenomenon in more detail. To this aim, we performed cell cycle analysis on hydroxyurea (HU) synchronized MPM cells upon TRIM28 KD. HU is a ribonucleotide reductase inhibitor that arrests DNA replication, thus blocking and synchronizing the cells in G1/S phase transition. Silencing of TRIM28 caused a marked delay in cycling re-activation in both cell lines; in particular, TRIM28 KD cells difficultly exit from G1 and fail to enter G2/M. In addition, TRIM28 KD caused an accumulation of cells in subG1 (Figure 14A-D). Major mitotic players such as Cyclin B1 (CCNB1), Aurora Kinases A and B (AURKA, AURKB) and phospho-CDK1 (p-CDK1) failed to accumulate in siTRIM28 cells compared to siCTRL, consistent with the difficulty observed for those cells to enter G2/M (Figure 14E, F). CCNB1 and CDK1 are the cyclin and cyclin-dependent kinase respectively, that together control G2/M transition; p-CDK1 is the phosphorylated and active form of CDK1. AURKA and AURKB are cell cycle regulated kinases involved, respectively, in microtubule organization at spindle poles and chromosomes alignment/segregation (Joukov & De Nicolo, 2018). Coherently with the accumulation in subG1, we observed an increase in apoptotic cells upon TRIM28 KD as demonstrated by Annexin V/7AAD staining and increased expression of the pro-apoptotic protein BAX (Figure 14G-J).

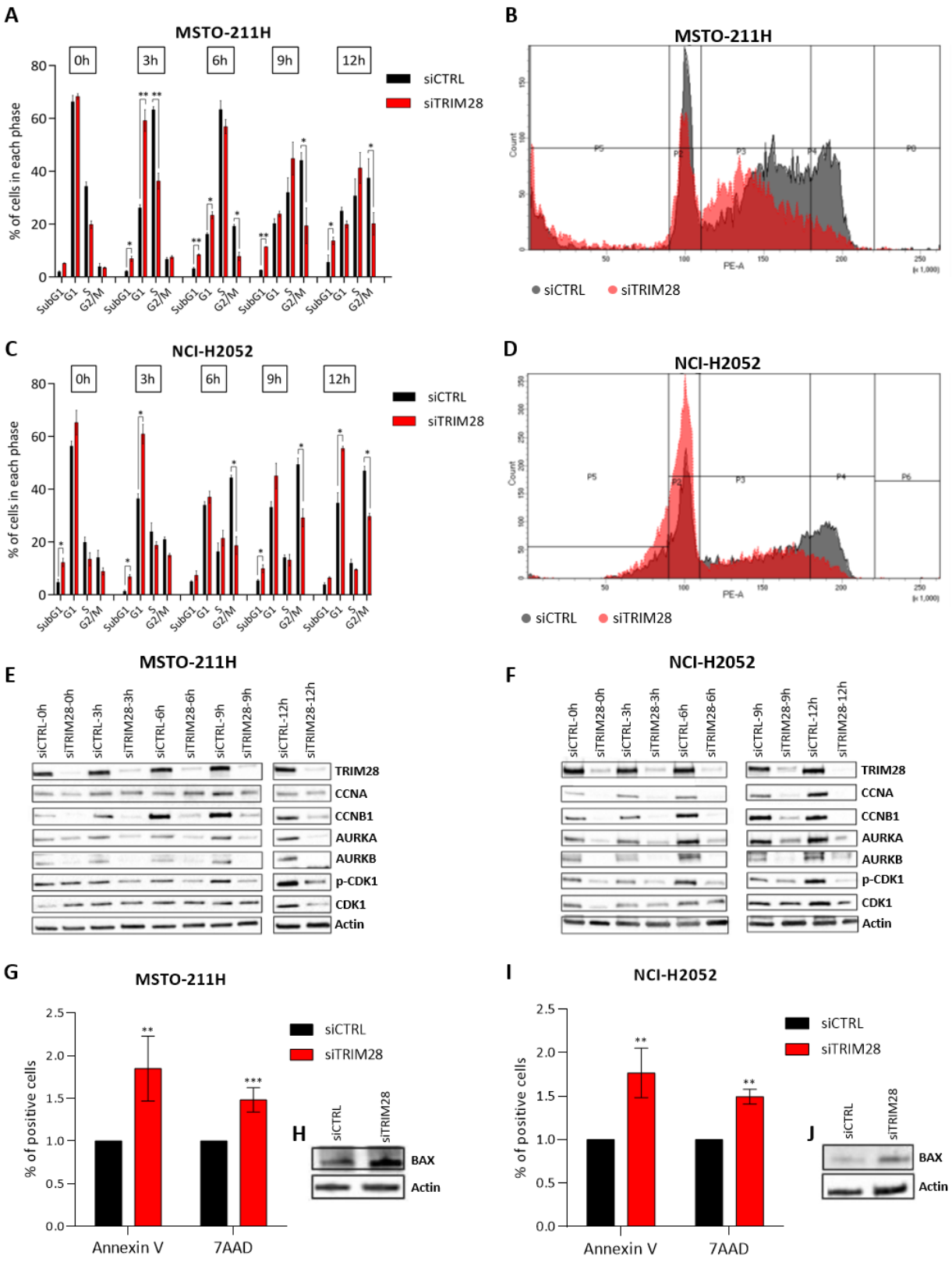

Figure 14. A, C) Cell cycle analysis of MSTO-211H (A) and NCI-H2052 (C) cells upon HU synchronization at the indicated time points after release. Data are mean ± SEM; *≤0.05, **≤0.01, ***≤0.001; N=2. **B, D)** FACS plots of cell cycle analysis of MSTO-211H (B) and NCI-H2052 (D) cells upon HU synchronization at 9h after release. Representative plot of a single time point of a single experiment of the graphs in Figure A and C. **E, F)** Western Blot analysis of TRIM28 and several mitotic markers in siTRIM28 vs siCTRL MSTO-211H (E) and NCI-H2052 (F) cells at the indicated time points after HU release. Data are representative of 2 biological experiments. **G, I)** Apoptosis analysis through Annexin V and 7AAD staining. Cells were collected 72h after

transfection and analyzed with a FACS Canto cytometer. Data are represented as mean ± SEM; *≤0.05, **≤0.01, ***≤0.001; N=3. **H, J)** Western Blot of MSTO-211H (H) and NCI-H2052 (J) cells showing accumulation of the pro-apoptotic protein BAX in TRIM28 KD cells at 72h post transfection.

TRIM28 controls the expression of mitotic genes and is required for correct mitosis execution

In order to deepen the biological role of TRIM28 in MPM, we performed RNA-sequencing (RNA-seq) in MSTO-211H/Cas9 cells infected with two independent sgRNAs targeting TRIM28. 607 genes were significantly deregulated in TRIM28-KO cells compared to cells infected with a non-targeting sgRNA (Figure 15A). Of those, 277 genes (45.6%) were downregulated, while 330 (54.4%) were upregulated, confirming the dual role of TRIM28 in transcription regulation, being able to act as either an activator or a repressor of gene expression. Surprisingly, 32.5% of downregulated genes (N=90) were involved in cell cycle regulation, with a strong enrichment in mitosis control (N=75) (Figure 15A). Coherently, GO analysis performed on the list of TRIM28 downregulated genes highlighted cell cycle regulation and in particular mitosis control as the most represented biological pathways (Figure 15B). Consistently, many mitotic regulators such as *AURKA*, *AURKB*, *BIRC5*, *CDCA8*, *CCNB1* and *CDC20* were significantly downregulated in TRIM28 KO cells compared to control (Figure 15C). Among TRIM28 downregulated genes emerged *TYMS*, *UBE2S*, *CKS1B* and *VRK1* (Figure 15C), identified as part of the 18 genes essential core for MPM survival in our screening (Figure 11A), suggesting that TRIM28 could represent the central element of a program supporting MPM proliferation and survival.

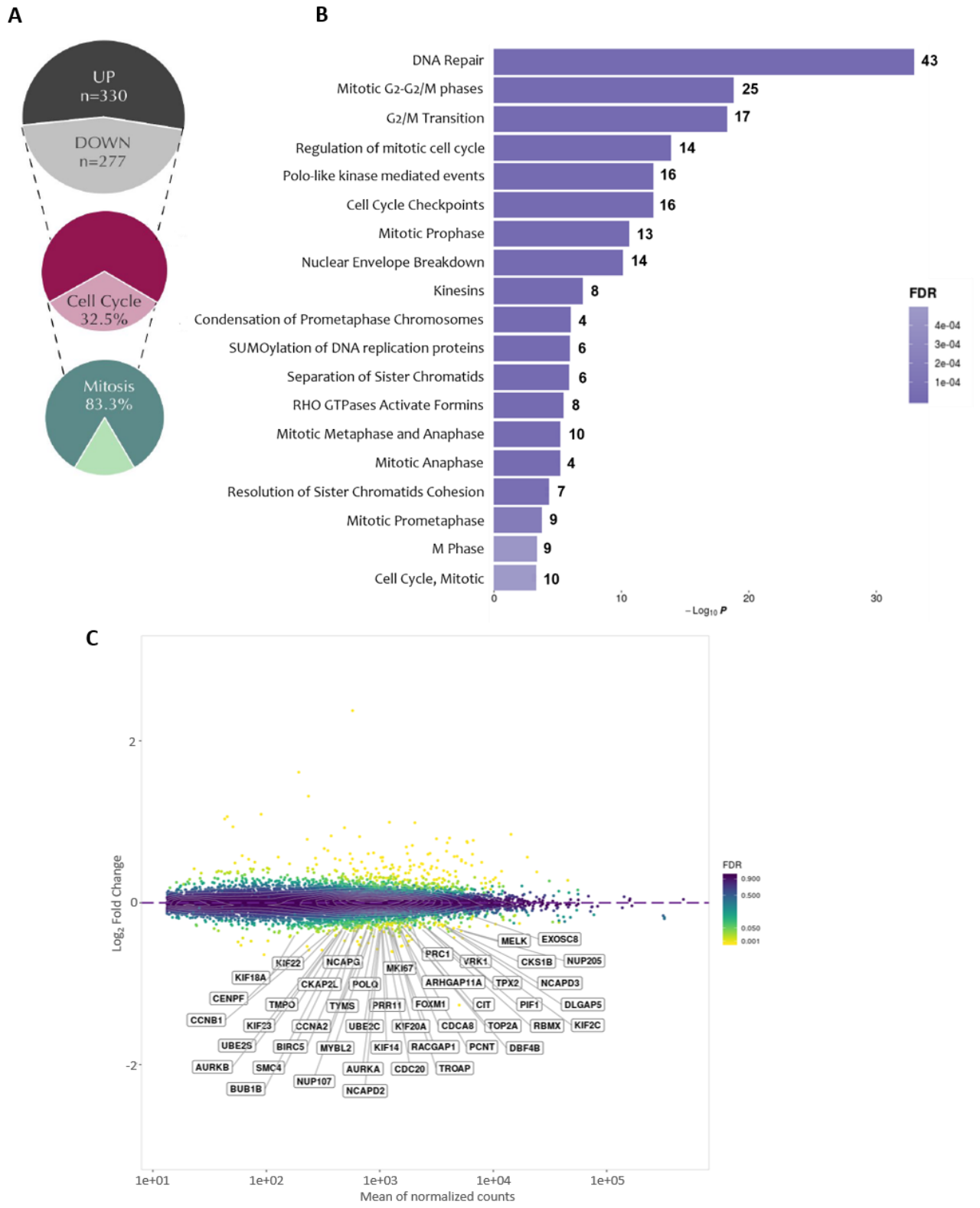

Figure 15. A) RNA-seq deregulated genes and the percentages of cell cycle and mitotic downregulated genes **B)** Barplot of the most significant enriched pathways (FDR<0.05) for genes that are downregulated from RNA-seq. **C)** MA plot visualization of differential expression analysis performed on RNA-seq data. The essential core of downregulated genes is highlighted.

Next, we took advantage of previously published TRIM28 ChIP-sequencing (ChIP-seq) data (McNamara, Guzman, et al., 2016) in order to confirm our results and discriminate between direct and indirect targets. A large fraction of TRIM28 KO downregulated genes (65%; 180/277) showed TRIM28 binding in their regulatory regions (Figure 16A), particularly enriched towards TSS (Figure 16B). Our results suggest that TRIM28 in MPM controls the expression of a gene program involved in mitosis regulation. Cell cycle genes require a well-orchestrated transcriptional and epigenetic control to ensure the precise timing of their activation (Y. Liu et al., 2017). The expression of G2/M genes is dependent on the B-MYB/FOXM1-MuvB complex that, by binding to the “cell-cycle gene homology region” (CHR) that is a peculiarity of mitotic genes, ensure their precise activation once cells are ready to enter mitosis (Müller et al., 2012; Sadasivam et al., 2012). We used a previously published list of 210 genes containing the CHR element and directly regulated by the B-MYB/FOXM1-MuvB complex (Fischer et al., 2016), to identify which TRIM28 targets belonged to this group. Noticeably, 62.8% of CHR genes (132/210) showed TRIM28 binding in their promoter (Figure 16C) and 43 of these (32.5%) were also significantly downregulated by TRIM28 KO according to our RNA-seq results (Figure 16C, D). Noticeably B-MYB and FOXM1, that are known to be them-self regulated through the CHR element, emerged as TRIM28 direct target genes.

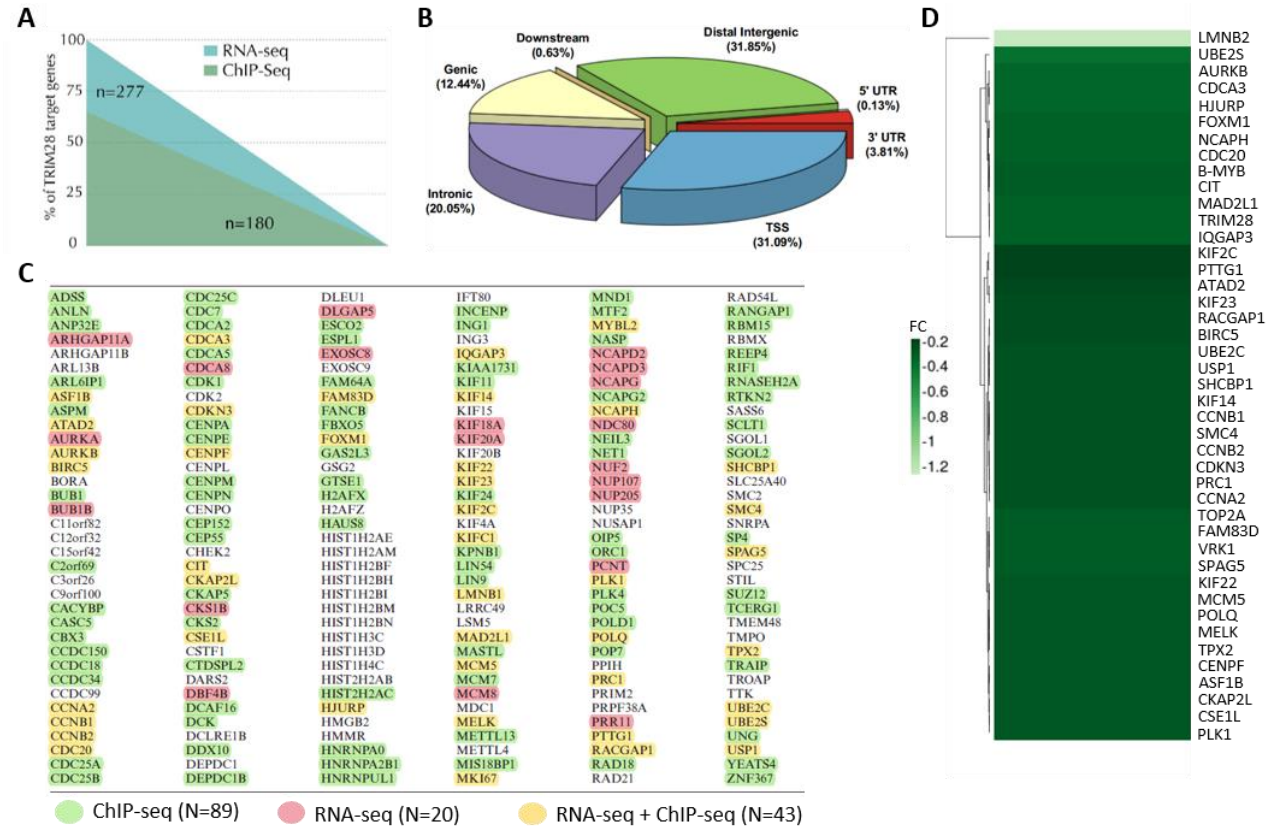

Figure 16. A) Representation of the percentage of RNA-seq downregulated genes that display TRIM28 binding in their promoter by ChIP-Seq data. **B)** Genomic distribution of TRIM28 binding profile associated to downregulated genes in RNA-seq. **C)** List of CHR genes that are direct (ChIP-seq, green and yellow) or indirect (RNA-seq, red) targets of TRIM28. The list of CHR genes was published in Fischer et al., 2016. **D)** Heatmap of the 43 CHR genes significantly downregulated in RNA-seq and presenting TRIM28 binding in their promoter. Green color bar shows fold difference on Log2 scale.

We validated several TRIM28 direct target genes by qRT-PCR and western blot analysis in both MSTO-211H and NCI-H2052 cells and in MSTO-211H/Cas9 cells, confirming that TRIM28 controls the expression of G2/M genes (Figures 17A-F). Coherently, MSTO-211H cells showed a wide spectrum of defects throughout mitosis upon TRIM28 KD in chromosome condensation, mitotic spindle organization and chromosome segregation (Figure 18A-E). TRIM28 KD cells showed decreased levels of condensed chromosomes and, consequently, of H3-pSer10 positive nuclei and of mitotic cells; besides, the number of apoptotic nuclei is enormously increased upon TRIM28 silencing (Figure 18A). In particular, TRIM28 KD cells showed abnormal distribution of chromosomes, defects in chromosomes' segregation, monopolar spindle and loss of midbody (Figures 18C-E). These mitotic defects are likely to be the spontaneous consequence of the imbalanced expression of crucial mitotic players that, ultimately, leads to cell death.

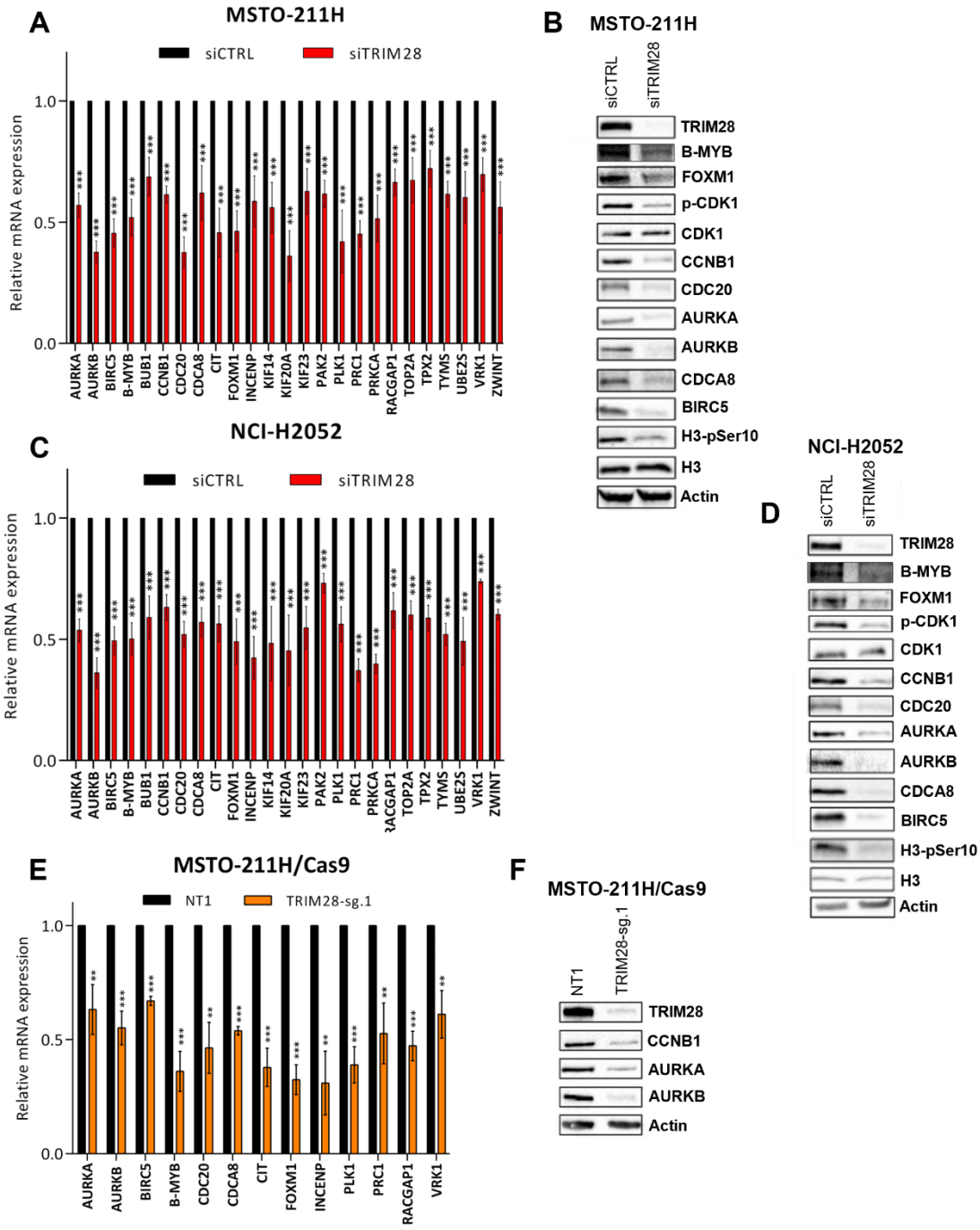

Figure 17. A, C, E) qRT-PCR of a panel of TRIM28 direct target genes. Data are represented as mean ± SEM; *≤0.05, **≤0.01, ***≤0.001; N=4. **B, D, F)** Western blot showing the protein expression levels of several TRIM28 direct targets upon TRIM28 loss compared to Ctrl. Actin is the loading control.

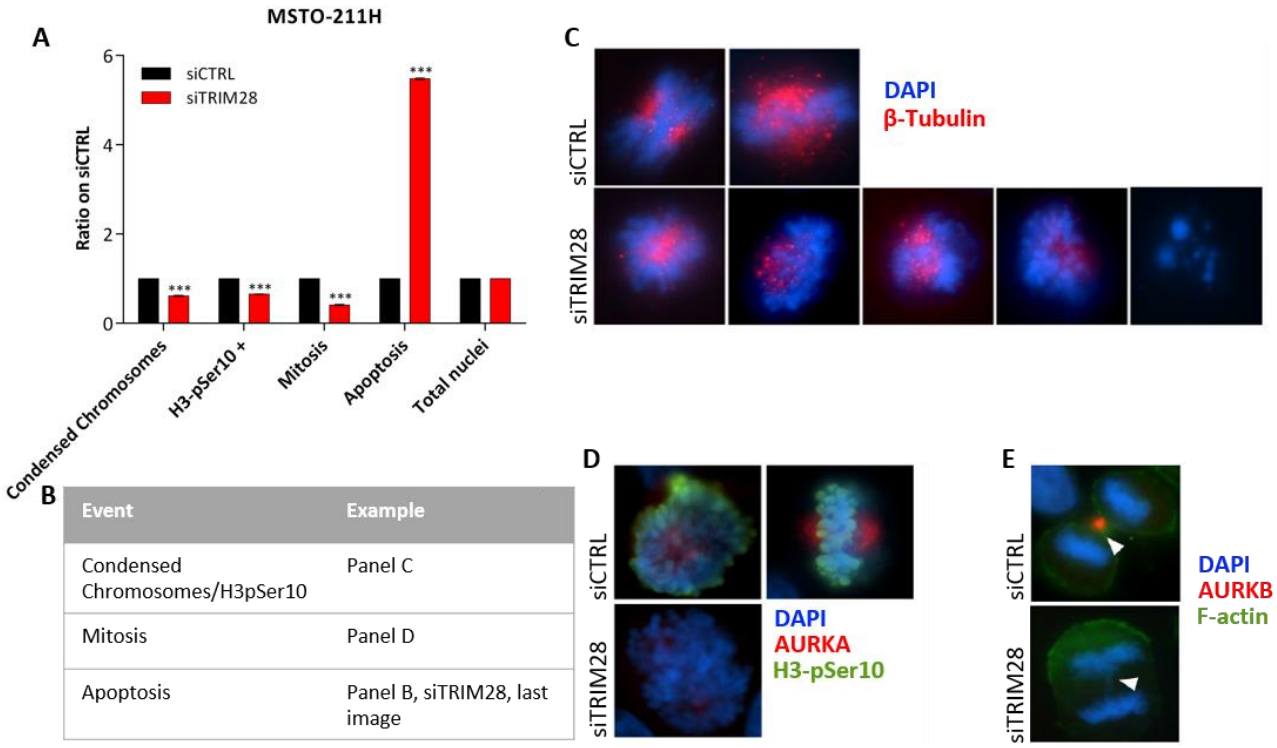

Figure 18. A) Graph representing the distribution of mitotic morphological features in siTRIM28 vs siCTRL MSTO-211H cells analyzed by immunofluorescence staining. *≤0.05, **≤0.01, ***≤0.001. **B)** Table reporting examples of each event analyzed in the graph of the panel A. **C)** Immunofluorescence showing B-tubulin (red) in MSTO-211H siCTRL and siTRIM28 cells. B-tubulin was used to visualize mitotic spindles. siCTRL cells show normal mitotic spindle with regular chromosomes alignment; siTRIM28 cells instead show formation of monopolar/multipolar spindles and many apoptotic nuclei. **D)** Immunofluorescence showing AURKA (red) and H3-pSer10 (green) in MSTO-211H siCTRL and siTRIM28 cells. H3-pSer10 marks condensed chromosomes. siTRIM28 cells show a strong reduction in H3pSer10 positive nuclei, as well as decrease in AURKA levels compared to Ctrl cells. **E)** Immunofluorescence showing AURKB (red) and F-actin (green) in MSTO-211H siCTRL and siTRIM28 cells. siTRIM28 cells show undetectable levels of AURKB and is visible the presence of a lagging chromosome (arrow), while siCTRL cells show AURKB properly positioned in the midbody (arrow) and correct chromosomes segregation.

TRIM28 cooperates with the B-MYB/FOXM1-MuvB complex to mediate CDK9-dependent RNA-PolII proficient transcription of mitotic genes

As transcriptional activator, TRIM28 has been shown to cooperate with context specific TFs and CDK9 to recruit and activate RNA-PolII on pathway-specific target genes promoters (Bacon et al., 2020; McNamara et al., 2016). Thus, in order to define the molecular mechanism by which TRIM28 takes part to the transcriptional activation of mitotic genes, we analyzed TRIM28 ChIP-seq tracks. Coherently with the reported mechanism by Bacon and colleagues (Bacon et al., 2020), TRIM28 was found at the Transcriptional Starting Site (TSS) of mitotic genes together with pSer2-RNA-PolII and CDK9 (Figure 19A). We performed Co-IP experiments to evaluate the physical interaction between TRIM28 and the transcriptional players involved in G2/M genes activation. As expected, we found that TRIM28 interacts

with both phosphorylated and active forms of RNA-PolII (pSer2- and pSer5- RNA-PolII) (Figure 19B), with the subunit of the MuvB complex RBBP4 (Figure 19D) and with CDK9 and FOXM1 (Figure 19C) in MSTO-211H cells. These results suggest that TRIM28 is part of the transcriptional complex that specifically activates the transcription of mitotic genes. To confirm that TRIM28 binds to the TSS of G2/M genes in our model, we performed ChIP-qPCRs in MSTO-211H cells for TRIM28. We confirmed TRIM28 binding to the TSS of *AURKA, AURKB, BIRC5, CCNB1, CDCA8, CDC20, FOXM1* and *PLK1* (Figure 19E) in MPM cells. Then we explored the effect of TRIM28 silencing on RNA-PolII recruitment at the TSS of mitotic genes. TRIM28 KD displaced RNA-PolII from a subset of its mitotic target promoters in MSTO-211H cells (Figure 19F), demonstrating that TRIM28 is required for the active transcription of mitotic genes. These results suggest that TRIM28 not only is required to orchestrate the interactions between RNA-PolII, CDK9 and the B-MYB/FOXM1-MuvB complex, but also to directly recruit RNA-PolII at the TSS of its target genes. Moreover, TRIM28 loss dramatically decreased the levels of the actively elongating form of RNA-PolII, phosphorylated on S2 (pSer2_RNA-PolII), along the gene-body of AURKB (Figure 19G). The reported effects were not observed for CD69, used as a negative control (Figure 19F-G). These results suggest that TRIM28 is required not only for the recruitment of RNA-PolII at the TSS of its target genes, but also for its CDK9-mediated activation into proficient transcription. Collectively, we described a previously unknown function of TRIM28 in G2/M gene expression timing.

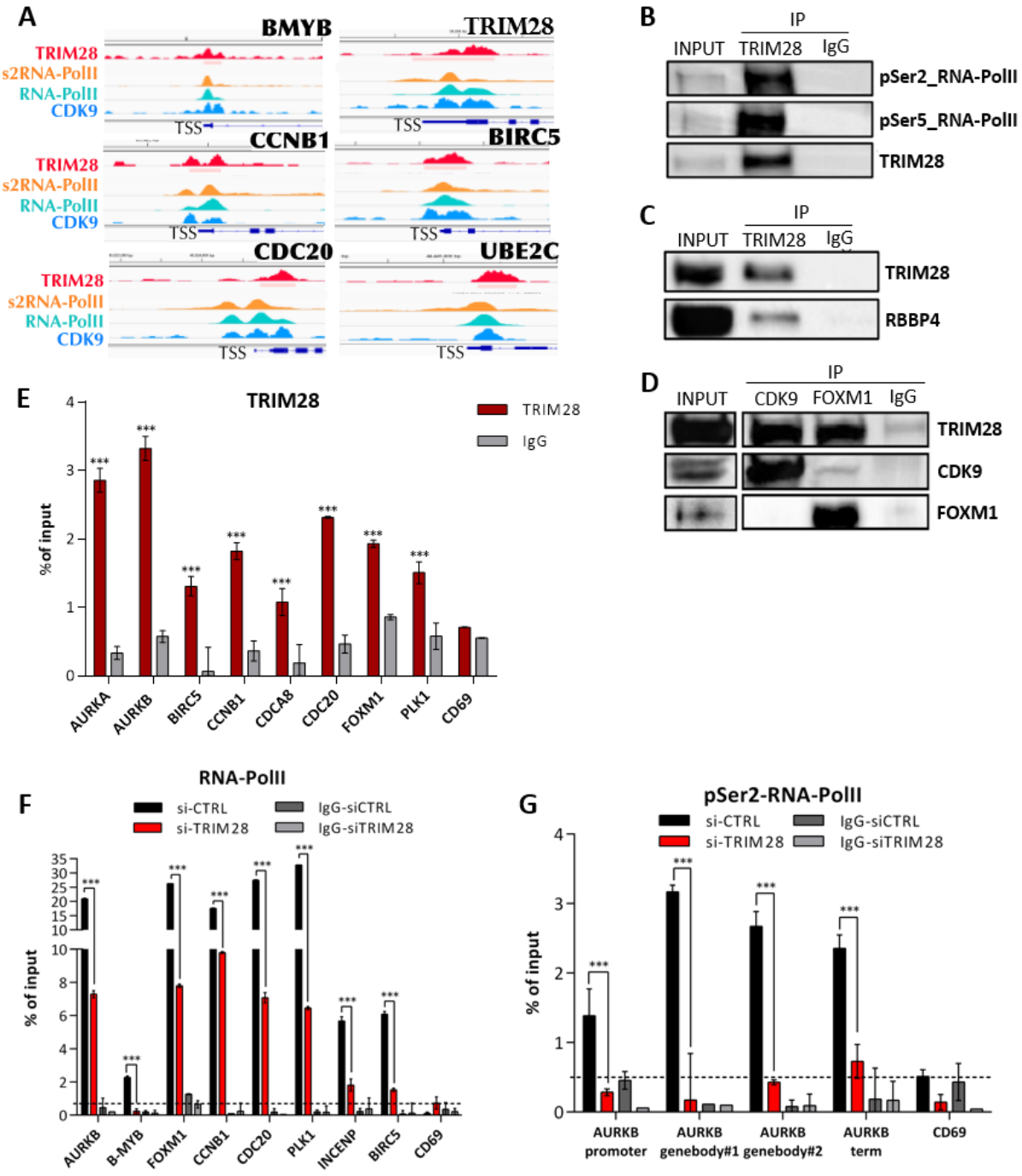

Figure 19. A) Visualization of TRIM28, CDK9, RNA-PolII and pSer2-RNA-PolII binding profiles on selected TRIM28 target genes with Integrative Genome Viewer (IGV). **B, C, D)** Co-IP experiments in MSTO-211H cells. IP and WB were conducted with the indicated antibodies. **E)** ChIP-qPCR validation analysis of TRIM28 occupancy of mitotic target genes' promoters in MSTO-211H cells. CD69 is the negative control. Values are represented as a percentage of input. Data are expressed as mean ± SD and one representative experiment is reported. *≤0.05, **≤0.01, ***≤0.001. N=2. **F)** ChIP analysis of RNA-PolII binding on promoters of several TRIM28 mitotic target genes in siCTRL and siTRIM28 MSTO-211H cells; CD69 is the negative control and the line is setted over it. Values are represented as a percentage of input. Data are expressed as mean ± SD and one representative experiment is reported. *≤0.05, **≤0.01, ***≤0.001. N=3. **G)** ChIP showing S2-RNA-PolII binding alongside the gene-body of AURKB in siCTRL and siTRIM28 MSTO-211H cells; CD69 is the negative control and the line is setted over it. Values are represented as a percentage of input. Data are expressed as mean ± SD and one representative experiment is reported. *≤0.05, **≤0.01, ***≤0.001. N=3.

Then, to further support our results that TRIM28 cooperates with the TFs B-MYB and FOXM1, we investigated the effect of their KD in both MPM cell lines. Coherently with their reported function in cell cycle regulation (Down et al., 2012; Sadasivam et al., 2012) and in line with a potential functional interplay with TRIM28, KD of B-MYB and FOXM1 restrains MPM cells' proliferation by partially (FOXM1) or completely (B-MYB) mimicking the TRIM28 KD effect observed on these cells (Figure 20A-B). As expected, B-MYB and FOXM1 KD significantly affects the expression of G2/M genes, even if TRIM28 KD seem to have a stronger effect (Figure 20C, E). The same results are obtained for the relative protein levels (Figure 20D, F).

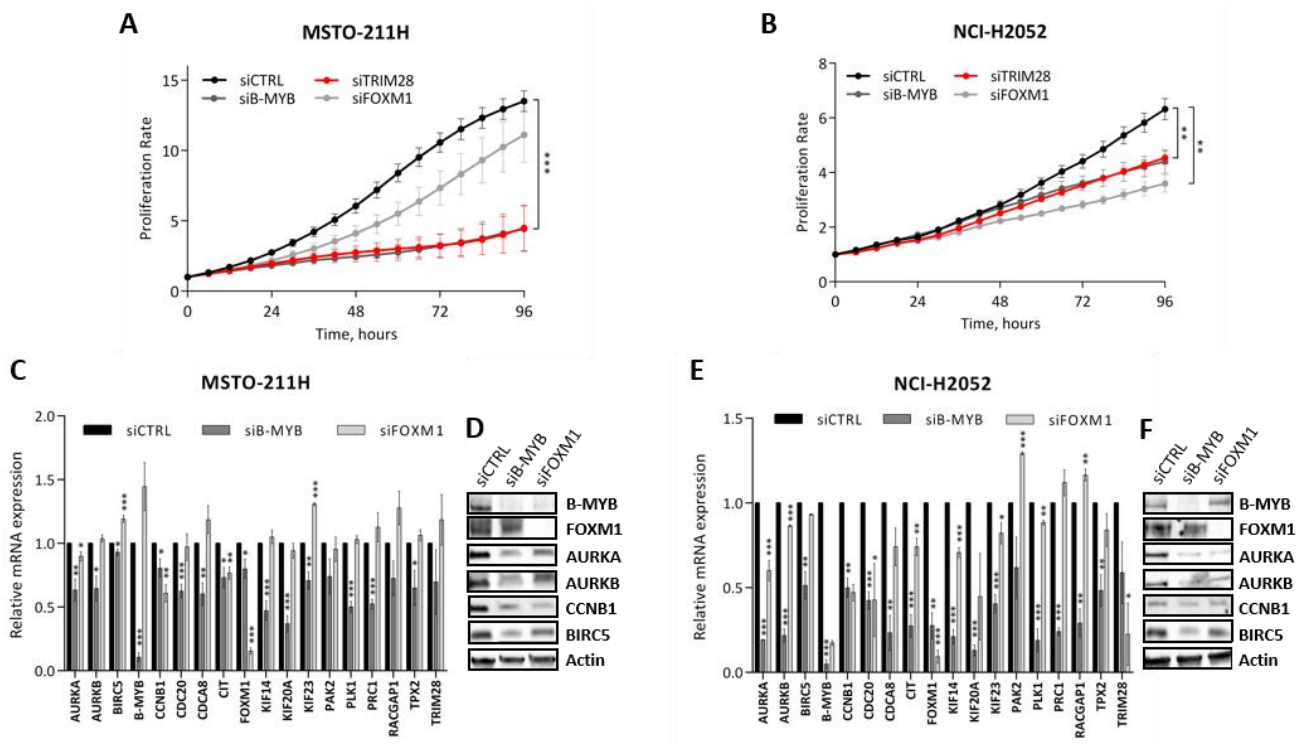

Figure 20. A, B) Proliferation assays reported as proliferation rate relative to day 0, measured with Incucyte S3 Live Cell Analysis (Sartorius) in the indicated cell lines. Data are expressed as mean ± SEM; *≤0.05, **≤0.01, ***≤0.001; N=3. **C, E)** qRT-PCR of a panel of TRIM28 direct target genes. Data are expressed as mean ± SEM; *≤0.05, **≤0.01, ***≤0.001; N=3. **D, F)** Western blot of siCTRL vs siB-MYB and siFOXM1 in MSTO-211H (D) and NCI-H2052 (F) cells. Actin is the loading control.

The CDK9 inhibitor AZD4573 mimics TRIM28 KD effects in MPM cells

Being TRIM28 role in MPM strongly associated to CDK9-dependent RNA-PolII recruitment and activation, we tested CDK9 inhibitors on MPM cell lines as an indirect strategy to hit TRIM28 function. We treated both MSTO-211H and NCI-H2052 cell lines with the pan-CDK inhibitor AT7519 (Santo et al., 2010) and the CDK9 specific inhibitor AZD4573 (Cidado et al., 2020). Both drugs showed a dramatic effect on cells' proliferation, being AZD4573 massively toxic for MPM cell lines even at very low concentrations (MSTO-211H_EC50 =

23 nM; H2052_EC50 = 22.9 nM) (Figures 21A-D). Treatment of MPM cells with sub-lethal doses of AZD4573 strongly impairs their proliferation in a dose-dependent manner in comparison to DMSO treated cells (Figures 21E-F). Finally, we evaluated the effect of AZD4573 on transcription of TRIM28 mitotic target genes. Noticeably, CDK9i strongly impairs the expression of TRIM28 mitotic target genes in both MSTO-211H and NCI-H2052 cells (Figures 22A-B) mimicking TRIM28 KD effects. Moreover, both MSTO-211H and NCI-H2052 cells treated with AZD4573 showed a strong decrease in condensed chromosomes and mitotic cells, while apoptotic nuclei were significantly increased compared to DMSO treated cells (Figures 22C-E). These results suggest that the lethal effects of AZD4573 in MPM acts primarily through the inhibition of TRIM28 transcriptional program, suggesting a functional interplay between TRIM28 and CDK9 in MPM.

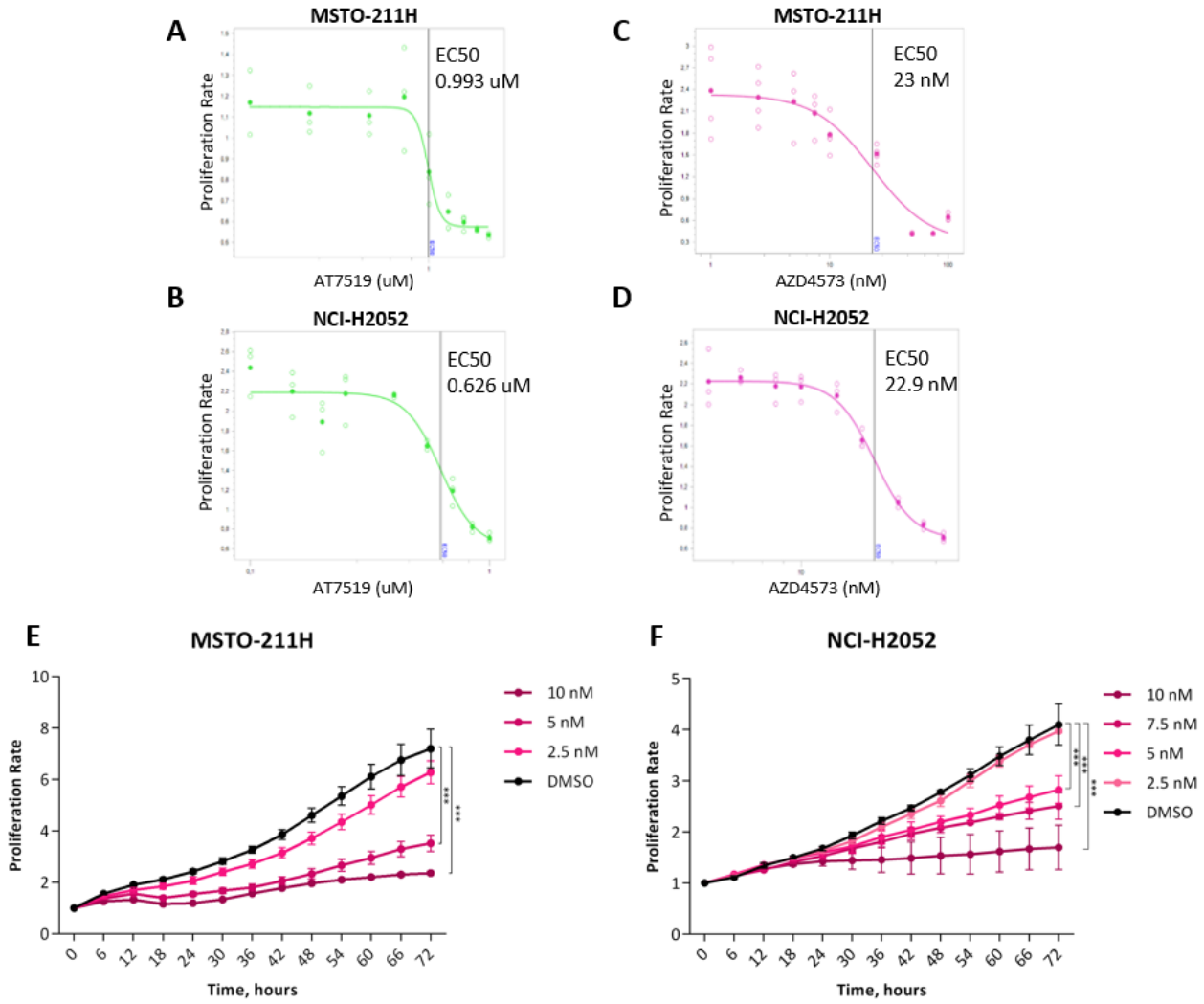

Figure 21. A-D) EC50 analysis in MSTO-211H and NCI-H2052 cells for pan-CDKi AT7519 and CDK9i AZD4573, calculated with Incucyte S3 Live Cell Analysis (Sartorius) at 48h after treatment. **E, F)** Proliferation assays showing the effect of the CDK9i AZD4573 at sub-lethal doses in MSTO-211H (E) and NCI-H2052 (F)

cell lines, measured with Incucyte S3 Live Cell Analysis (Sartorius). Data are expressed as mean ± SD and one representative experiment is reported. *≤0.05, **≤0.01, ***≤0.001. N=3.

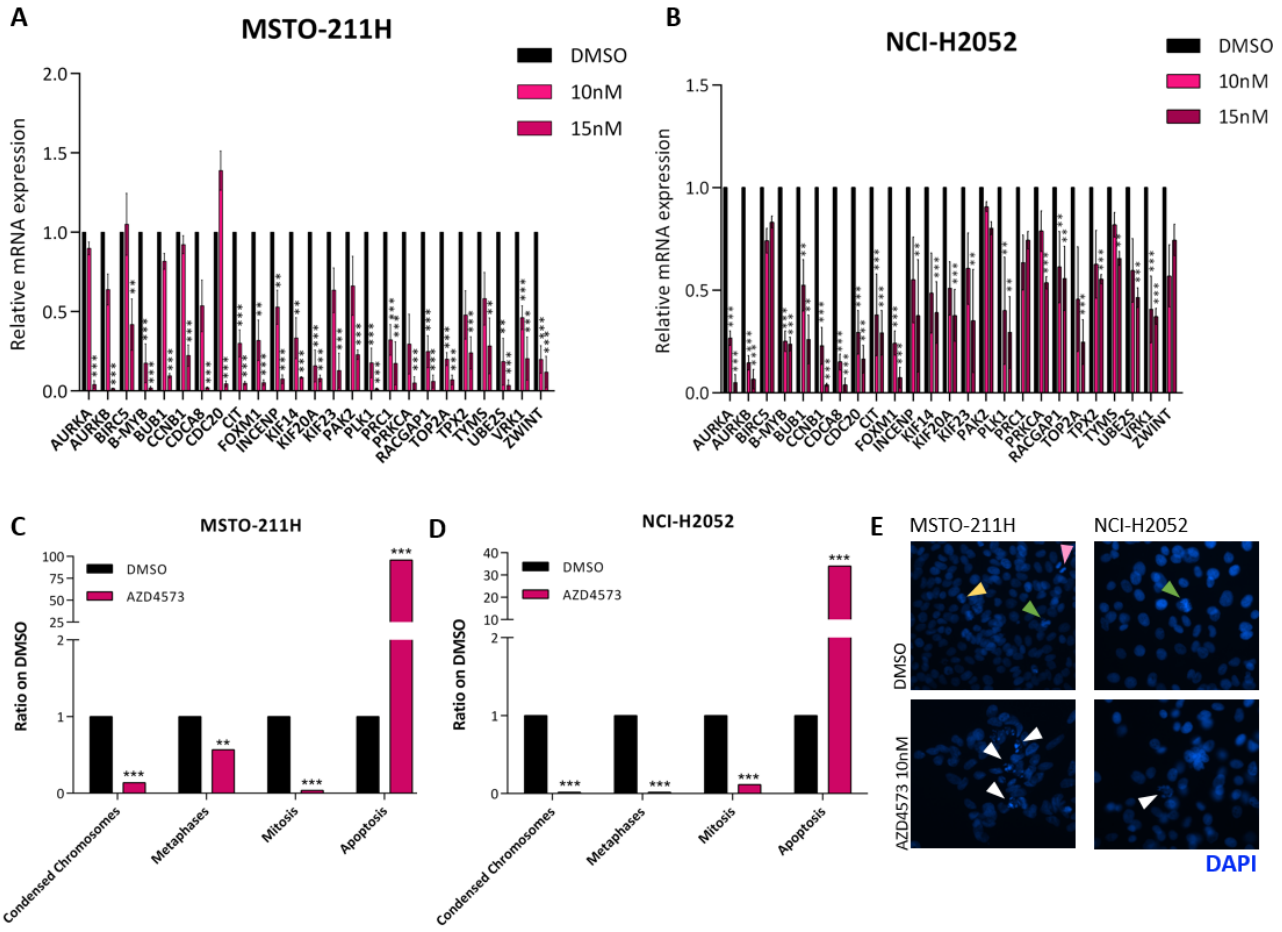

Figure 22. A, B) qRT-PCR analysis of a subset of TRIM28 direct target genes in MPM cell lines treated with DMSO or sub-lethal doses of AZD4573. Data are expressed as mean ± SEM; *≤0.05, **≤0.01, ***≤0.001; N=3. **C, D)** Distribution of mitotic morphological features in 10nM AZD4573 vs DMSO treated MSTO-211H (C) and NCI-H2052 (D) cells analyzed by immunofluorescence staining. **E)** Immunofluorescence showing DAPI staining in 10nM AZD4573 vs DMSO treated MSTO-211H (left boxes) and NCI-H2052 (right boxes) cells. Examples of each event reported in the graphs are indicated by the arrows: white – apoptotic nuclei; yellow – condensed chromosomes; green – metaphases; pink – mitosis.

Model validation in a separate cohort of MPM patients

To validate our results *in vivo*, we retrieved a retrospective cohort of 97 MPM patients that underwent surgical resection in our Institution in the past 10 years (MPM-RE). Besides, we took advantage of the TCGA-MESO cohort (MPM-TCGA) that we already used for survival correlations described above. Clinical data for the patients of the MPM-RE cohort are provided in Table 1. Figure 23A shows the flowchart of the analyses carried out. From the MPM-TCGA dataset, we removed 15 patients due to the lack of follow up, while the remaining 71 had expression profile eligible for the analysis. In the MPM-RE cohort, we investigated the expression of TRIM28 and its G2/M target genes by digital profiling using a custom panel. We performed controls to check the quality of RNAs and after data

normalization, 86 RNA samples provided gene expression profile (GEP) eligible for further analyses (Figure 23A). All tested genes were expressed in the investigated samples. The expression of TRIM28 and its target genes discriminated long- and short- term survivors (long-OS and short-OS) in both patients' cohorts, as revealed by Principal Component Analysis (PCA) (Figure 23B-C). TRIM28 showed a significant positive correlation with all its target genes investigated in MPM patients in both patients' cohorts, confirming our *in vitro* observations (Figure 23D-E). Then, we correlated the expression of TRIM28 and its target genes with patients' OS, finding that the expression of TRIM28 and the majority of its targets was significantly higher in short-OS compared to long-OS in both the MPM-TCGA (Figure 23F) and MPM-RE (Figure 23G) cohorts, confirming their association with aggressiveness of MPM. Coherently, TRIM28 and its targets were significantly associated to a reduced survival probability of MPM patients, as demonstrated by survival analysis. Specifically, we confirmed 97.3% and 86.5% of the investigated genes as negative prognostic factors in the MPM-TCGA (Figure 23H) and MPM-RE (Figure 23I) cohorts, respectively. Among them, TRIM28 showed a negative prognostic value in both cohorts. Finally, we evaluated the association of the remaining 17 essential genes (chromatin keeper) identified by the genome-wide CRISPR/Cas9 screening with patients' survival. All of them were upregulated in high vs low OS, and 15 out of 17 genes significantly decreased survival probability (Figures 24A-B). Overall, these data confirmed that TRIM28 and its related gene program are associated to clinical aggressiveness of MPM *in vivo*. Moreover, the genes constituting the core of 18 chromatin keepers identified as essential in our screening were confirmed as negatively associated with patients' survival probability.

	Total (N=86)
Sex	
F	21 (24.4%)
M	65 (75.6%)
Age	
<=65	25 (29%)
>65	61 (71%)
Histology	
Biphasic	36 (41.8%)
Epithelioid	44 (51.2%)
sarcomatoid	6 (7%)

Status	
Alive	11 (12.8%)
deceased	75 (87.2%)
Stage	
1	45 (52.3%)
2	6 (7%)
3	10 (11.6%)
4	23 (26.8%)
Missing	2 (2.3%)
Type of surgery	
biopsy	43 (50%)
pleurectomy	43 (50%)
Asbestos exposure	
Domestic	8 (9.3%)
professional	67 (77.9%)
NO	7 (8.1%)
Missing	4 (4.7%)
Smoking	
NO	27 (31.4%)
YES	28 (32.6%)
Missing	31 (36%)
Chemotherapy Treatment	
NO	21 (24.4%)
YES	63 (73.3%)
Missing	2 (2.3%)
Response to chemotherapy	
NO	34 (39.5%)
YES	22 (25.6%)
Missing	30 (34.9%)

Table 1. Clinical features of the MPM cohort used in the validation analysis.

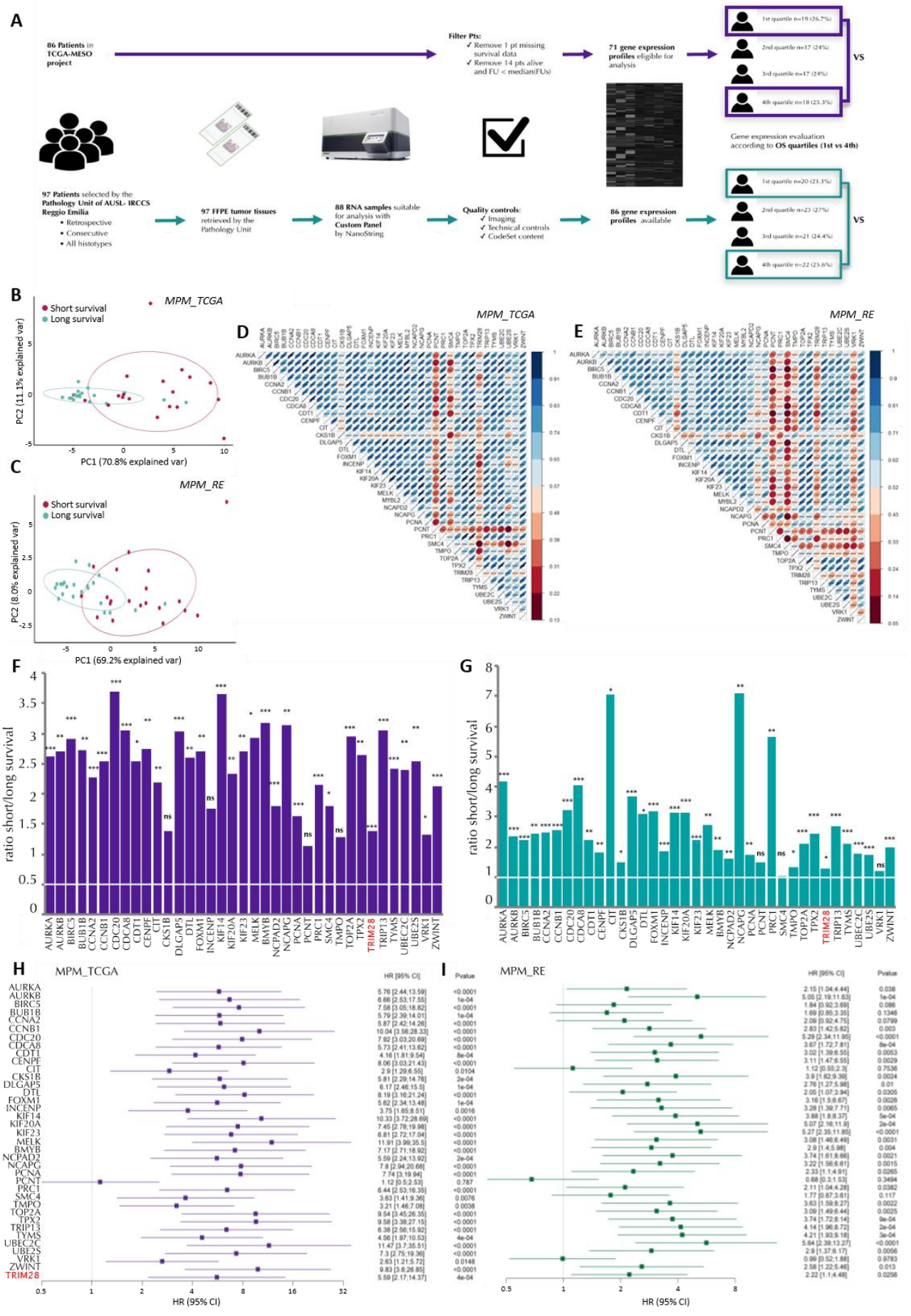
A
86 Patients in TCGA-MESO project
Filter Pts:
✓ Remove 1 pt missing survival data
✓ Remove 14 pts alive and FU < median(FUs)
71 gene expression profiles eligible for analysis
1st quartile n=19 (26.7%)
2nd quartile n=17 (24%)
3rd quartile n=17 (24%)
4th quartile n=18 (25.3%)
VS
Gene expression evaluation according to OS quartiles (1st vs 4th)
97 Patients selected by the Pathology Unit of AUSL- IRCCS Reggio Emilia
• Retrospective
• Consecutive
• All histotypes
97 FFPE tumor tissues retrieved by the Pathology Unit
88 RNA samples suitable for analysis with Custom Panel by NanoString
Quality controls:
✓ Imaging
✓ Technical controls
✓ CodeSet content
86 gene expression profiles available
1st quartile n=20 (23.3%)
2nd quartile n=23 (27%)
3rd quartile n=21 (24.4%)
4th quartile n=22 (25.6%)
VS
B
MPM_TCGA
Short survival
Long survival
PC2 (11.1% explained var)
PC1 (70.8% explained var)
C
MPM_RE
Short survival
Long survival
PC2 (8.0% explained var)
PC1 (69.2% explained var)
D
MPM_TCGA
E
MPM_RE
F
ratio short/long survival
G
ratio short/long survival
H
MPM_TCGA
HR [95% CI]
Pvalue
HR (95% CI)
I
MPM_RE
HR [95% CI]
Pvalue
HR (95% CI)

Figure 23. A) Flowchart of the validation analysis in the MPM-TCGA and MPM-RE cohorts. FU: Follow Up. **B-C)** PCA analysis of the distribution of long and short survivors (I and IV quartile) based on the expression of TRIM28 and its target genes in both cohorts (FDR<0.05). **D-E)** Expression correlation matrix (Spearman test) within TRIM28 and its target genes in the MPM-TCGA **(D)** and MPM-RE **(E)** cohorts. *≤0.05, **≤0.01, ***≤0.001. **F-G)** Histogram representing the ratio of expression of the indicated genes in short vs long survivors (I and IV quartile). *≤0.05, **≤0.01, ***≤0.001. **H-I)** Forest-plot displaying the correlation of TRIM28 and its target genes with reduced survival probability of MPM patients in MPM-TCGA (H) and MPM-RE (I) cohorts. The analysis in the MPM-RE cohort was corrected for surgery and chemotherapy treatment.

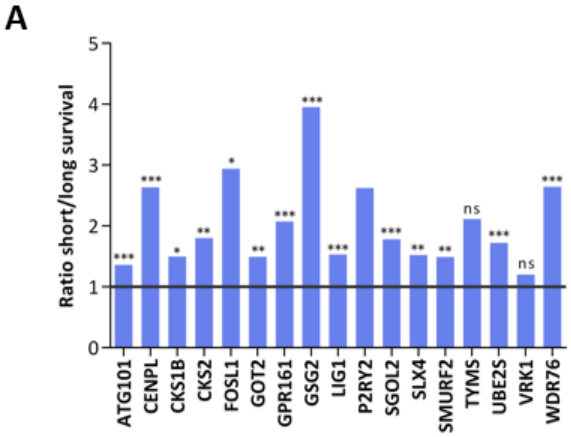

B

Gene	pValue	coeff[95%CI]
ATG101	0.0193	2.66 [1.17 ; 6.02]
CENPL	0.0208	2.75 [1.17 ; 6.49]
CKS1B	0.7536	1.12 [0.55 ; 2.3]
CKS2	0.0001	6.03 [2.44 ; 14.86]
FOSL1	0.053	2.01 [0.99 ; 4.06]
GOT2	0.1565	1.65 [0.83 ; 3.28]
GPR161	0.0046	3.07 [1.41 ; 6.68]
GSG2	0.0004	4.23 [1.91 ; 9.38]
LIG1	0.0128	2.36 [1.2 ; 4.64]
P2RY2	0.8509	0.93 [0.46 ; 1.91]
SGOL2	0.0015	3.46 [1.6 ; 7.47]
SLX4	0.0703	2.63 [0.92 ; 7.49]
SMURF2	0.4234	1.39 [0.62 ; 3.09]
TYMS	0.0003	4.21 [1.93 ; 9.18]
UBE2S	0.0056	2.9 [1.37 ; 6.17]
VRK1	0.9783	0.99 [0.52 ; 1.88]
WDR76	0.0163	2.39 [1.17 ; 4.86]

Figure 24. A) Histogram representing the ratio of expression of the indicated genes in short vs long survivors (I and IV quartile). *≤0.05, **≤0.01, ***≤0.001. **B)** Hazard Ratio obtained by a Cox model analysis of the association of gene expression with MPM survival. The analysis was corrected for surgery and chemotherapy treatment. Genes that are TRIM28 targets are written in blue.

TRIM28 controls Innate Immune Response

TRIM28 was firstly described as a transcriptional corepressor for KRAB-ZFPs, helping their repressive activity by inducing heterochromatin formation. In this context, TRIM28 has been shown to keep endogenous retroviruses quiet.

To explore its role in MPM as a corepressor, we also investigated upregulated genes that emerged from RNA-seq analysis performed in MSTO-211H cells upon TRIM28 KO. Protein network analysis of the 330 upregulated genes revealed that they are functionally related (data not shown). Surprisingly, GO analysis performed on this list showed that these genes are involved in innate immunity and in particular in Interferon I (IFN-I)-mediated immune response and RIG-I/MDA5 signaling (Figure 25A). Indeed, 46/330 genes (14%) are specifically involved in innate immune response and within this list we found all four members of the 2'-5'-Oligoadenylate Synthetase (OAS) family and all four Interferon Induced proteins with Tetratricopeptide repeats (IFIT) proteins. Moreover, we identified *AIM2* and *DDX58 (RIG-I)* among TRIM28 upregulated genes (Figure 25B). These factors are core viral DNA and RNA sensors, respectively, and directly participate to the innate immune response (Ori et al., 2017). We correlated the expression of these 46 genes with

patients' survival probability within the MPM-TCGA dataset (N=87) and found that 9 of them (19,6%) significantly increased patients' OS (Figure 25B), suggesting a protective and anti-tumorigenic role for these genes.

However, validation analysis in a separate internal cohort of MPM patients (MPM-RE) did not confirm these results, and none of the investigated genes showed a significant association with improved survival of MPM patients. This could be due, at least in part, by the fact that samples in the MPM-RE cohort are paraffin-fixed that could alter the tumor purity, particularly relevant when looking into ISG signature.

Induction of innate immunity response, by the activation of IFN pathway is a well established side effect of transcriptional reactivation of ERE. Thus, we hypothesize that the observed upregulation of these genes upon TRIM28 KO is an indirect effect of the epigenetic unmasking of ERE along the genome. Further analyses are currently ongoing to confirm this hypothesis and establish the actual link of TRIM28 and IFN mediated immune response.

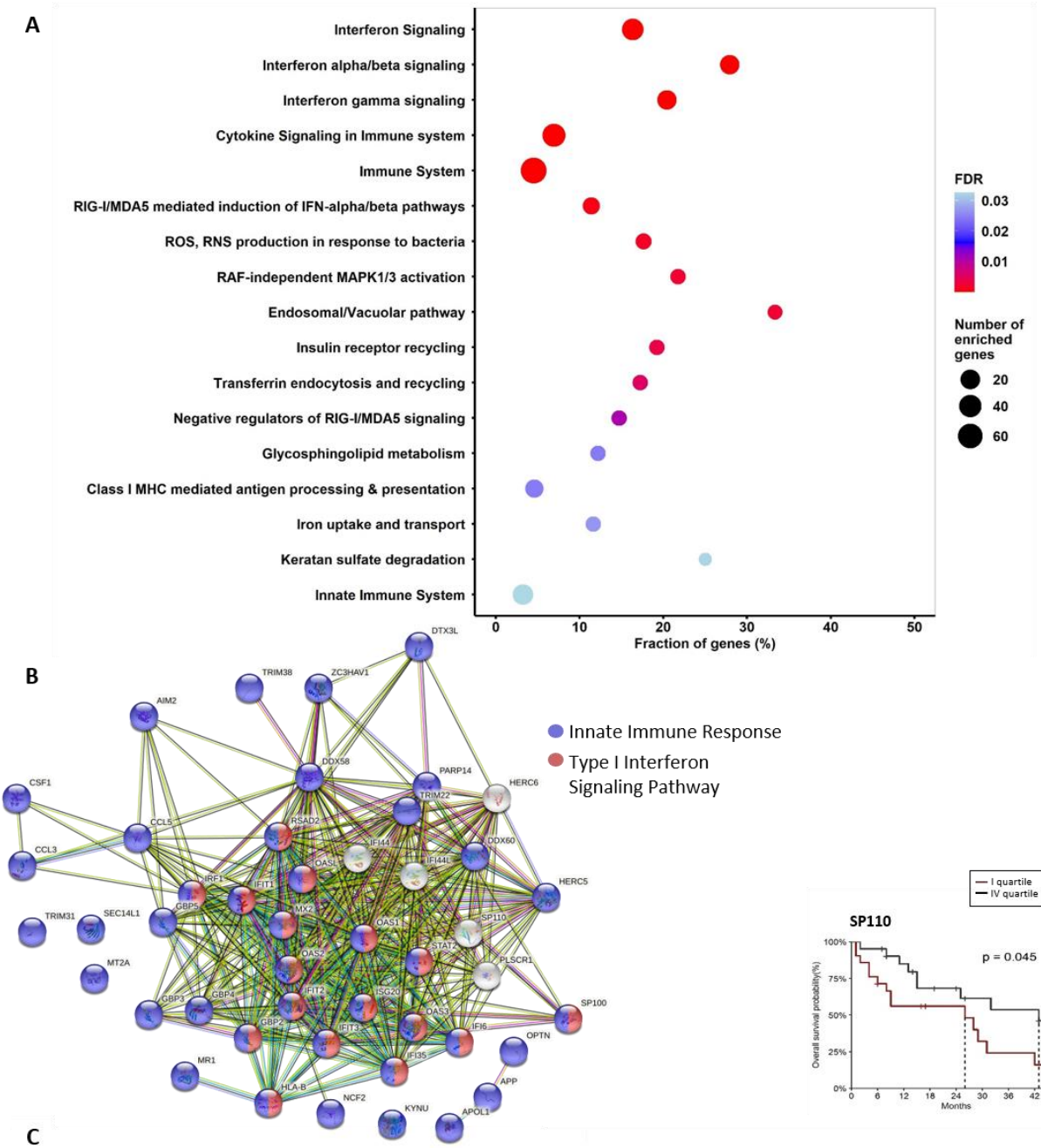
A
Interferon Signaling
Interferon alpha/beta signaling
Interferon gamma signaling
Cytokine Signaling in Immune system
Immune System
RIG-I/MDA5 mediated induction of IFN-alpha/beta pathways
ROS, RNS production in response to bacteria
RAF-independent MAPK1/3 activation
Endosomal/Vacuolar pathway
Insulin receptor recycling
Transferrin endocytosis and recycling
Negative regulators of RIG-I/MDA5 signaling
Glycosphingolipid metabolism
Class I MHC mediated antigen processing & presentation
Iron uptake and transport
Keratan sulfate degradation
Innate Immune System
0
10
20
30
40
50
Fraction of genes (%)
FDR
0.03
0.02
0.01
Number of enriched genes
20
40
60
B
Innate Immune Response
Type I Interferon Signaling Pathway
DTX3L
TRIM38
ZC3HAV1
AIM2
DDX58
PARP14
HERC6
CSF1
TRIM22
CCL5
RSAD2
IFI44
DDX60
CCL3
IFI44L
OASL
IRF1
IFIT1
HERC5
GBP5
MX2
TRIM31
SEC14L1
OAS1
SP110
STAT2
OAS2
PLSCR1
MT2A
IFIT2
ISG20
SP100
GBP3
GBP4
OAS3
GBP2
IFIT3
IFI6
OPTN
IFI35
MR1
APP
HLA-B
NCF2
KYNU
APOL1
I quartile
IV quartile
SP110
p = 0.045
Overall survival probability(%)
Months
C
IFIT1
p = 0.009
IFIT2
p = 0.016
IFIT3
p = 0.04
OAS1
p = 0.007
SP100
p = 0.015
MR1
p = 0.002
TRIM38
p = 0.003
GBP3
p = 0.039

Figure 25. A) Gene ontology enrichment of biological processes upregulated in RNA-seq of TRIM28 KO vs NT1 MSTO-211H/Cas9 cells. **B)** Protein-protein interaction network of the innate immunity genes upregulated upon TRIM28 KO by STRING (v11). **C)** Kaplan Meyer plots showing correlation of ISGs genes with MPM patients' survival based on MESO-TCGA data (N=87). Patients were divided in quartiles of gene expression and compared between 1st (red, low expression) and 4th (black, high expression) quartiles.

Analysis of TCGA clinical data revealed several lncRNAs associated with MPM patients' survival

In recent years, insights into the functional organization of the genome brought to light the relevance of non-coding transcripts in tumorigenesis. Thus, in this section we set to explore the potential contribution of ncRNAs and in particular lncRNAs to MPM progression.

To this end, we took advantage of the transcriptomic profiles and clinical data of the MESO dataset from the TCGA project (N=87). Using two different approaches, we established correlation between gene expression and patients' survival probability (Figure 26A). We obtained a final list of 423 genes showing strong association with patients' outcome. Of these, 121 (29%) were positively associated with improved survival representing genes with a protective role against MPM, while 302 (71%) were negatively associated with survival. The latest are genes that likely confer aggressiveness and lethality to MPM (Figure 26A). 92% of these transcripts were protein coding genes (Figure 26B). GO analysis showed that genes associated with a reduced survival probability were strongly enriched within pathways linked to mitosis, cell growth and cell cycle regulation (Figure 26C). By contrast, genes that were associated to an improved survival probability were partially enriched in immune response associated pathways (Figure 26D). Considering the relevance of the identified pathways in cancer progression, these results support the validity of our analysis. Noticeably, 8% of the survival associated genes were non-coding RNAs (Figure 26B). Of these, 77% encoded for lncRNAs (N=24) (Figure 26E).

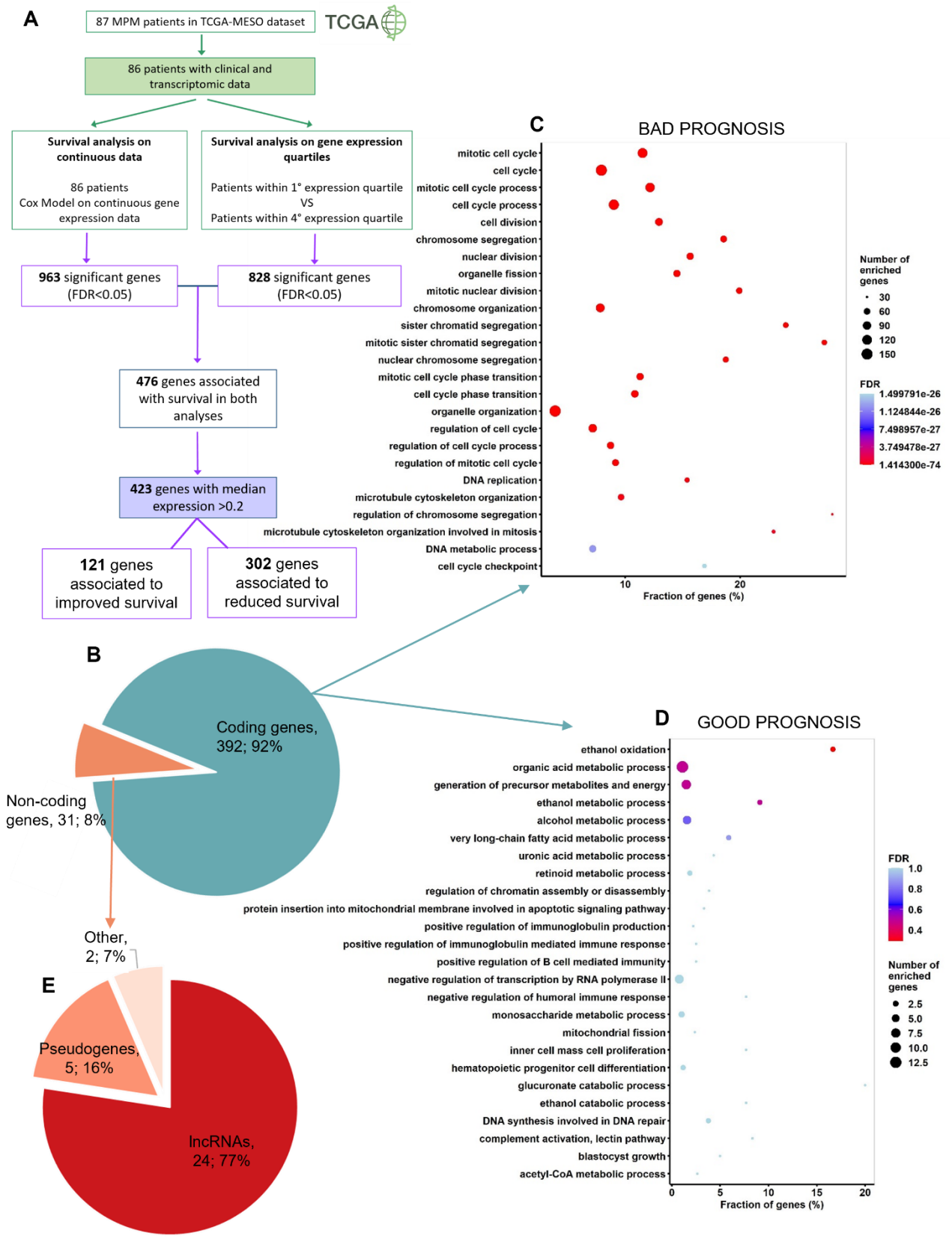

Figure 26. A) Flowchart of overall survival analysis in TCGA-MESO dataset. **B)** Distribution of coding and non-coding genes associated with overall survival. **C-D)** Gene Ontology enrichment of principal biological processes involved in bad **(C)** and good prognosis **(D)**. **E)** Distribution of non-coding genes types associated with overall survival.

Forest plot analysis of the 24 survival-associated lncRNAs showed that 8 of them were strongly associated with reduced survival probability (Figure 27A), while the remaining 16 were related to a better outcome. In particular, LINC00941, that we have already reported as mediator of aggressiveness in thyroid cancer (Gugnoni et al., 2021), showed the strongest correlation (HR 13.5) (Figure 27B). Patients with high LINC00941 expression had a median OS of 9 months versus 55 months of patients with low LINC00941 expression. We confirmed these data in a retrospective cohort of 97 MPM patients from our institution using Nanostring technology as previously described (Figure 23A), focusing on the 8 lncRNAs with negative prognostic features. 5 out of 8 were confirmed as associated to negative survival in our cohort, and their expression is significantly higher in short-OS compared to long-OS (Figure 27C). Of the remaining, one did not significantly associate with reduced survival probability and two were expressed below the threshold. LINC00941 showed the strongest effect on survival probability also in this cohort (HR 4.42). Patients with high LINC00941 expression had a median OS of 8.5 months, whereas patients with low LINC00941 expression had a median OS of 18.5 months (Figure 27D). Using data from the MESO-TCGA dataset, we correlated the expression of LINC00941 with clinical features of MPM and we found a significant positive association with the most aggressive sarcomatoid histotype (Figure 27E). We then correlated its expression with MPM most relevant mutations and mutational burden, finding an increased expression of LINC00941 in *LATS2* WT versus mutated tumors (Figure 27F).

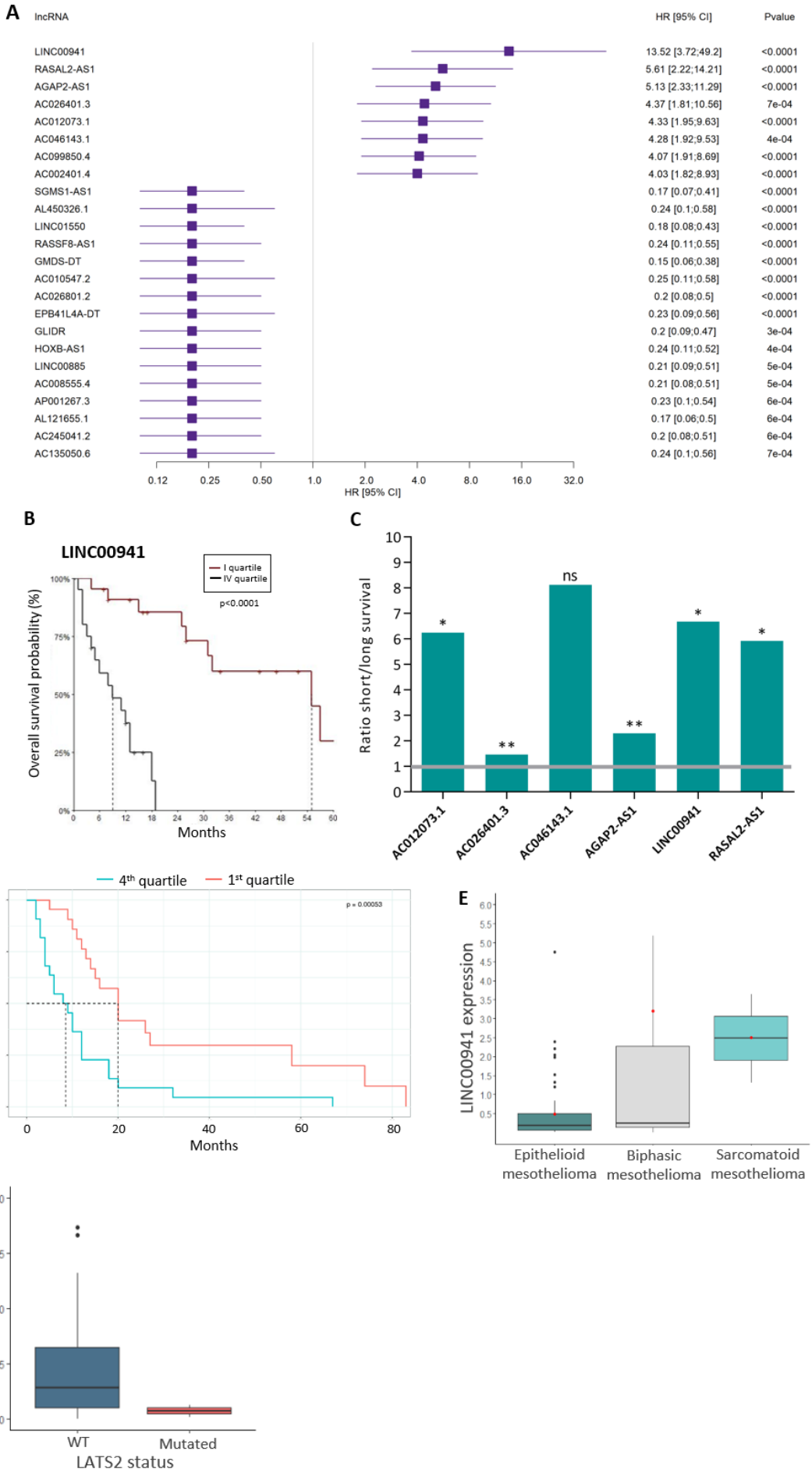
A
lncRNA
HR [95% CI]
Pvalue
LINC00941 13.52 [3.72;49.2] <0.0001
RASAL2-AS1 5.61 [2.22;14.21] <0.0001
AGAP2-AS1 5.13 [2.33;11.29] <0.0001
AC026401.3 4.37 [1.81;10.56] 7e-04
AC012073.1 4.33 [1.95;9.63] <0.0001
AC046143.1 4.28 [1.92;9.53] 4e-04
AC099850.4 4.07 [1.91;8.69] <0.0001
AC002401.4 4.03 [1.82;8.93] <0.0001
SGMS1-AS1 0.17 [0.07;0.41] <0.0001
AL450326.1 0.24 [0.1;0.58] <0.0001
LINC01550 0.18 [0.08;0.43] <0.0001
RASSF8-AS1 0.24 [0.11;0.55] <0.0001
GMDS-DT 0.15 [0.06;0.38] <0.0001
AC010547.2 0.25 [0.11;0.58] <0.0001
AC026801.2 0.2 [0.08;0.5] <0.0001
EPB41L4A-DT 0.23 [0.09;0.56] <0.0001
GLIDR 0.2 [0.09;0.47] 3e-04
HOXB-AS1 0.24 [0.11;0.52] 4e-04
LINC00885 0.21 [0.09;0.51] 5e-04
AC008555.4 0.21 [0.08;0.51] 5e-04
AP001267.3 0.23 [0.1;0.54] 6e-04
AL121655.1 0.17 [0.06;0.5] 6e-04
AC245041.2 0.2 [0.08;0.51] 6e-04
AC135050.6 0.24 [0.1;0.56] 7e-04
0.12 0.25 0.50 1.0 2.0 4.0 8.0 16.0 32.0
HR [95% CI]
B
LINC00941
I quartile
IV quartile
p<0.0001
Overall survival probability (%)
Months
C
Ratio short/long survival
ns
AC012073.1
AC026401.3
AC046143.1
AGAP2-AS1
LINC00941
RASAL2-AS1
D
4th quartile
1st quartile
p = 0.00053
Overall Survival
Months
E
LINC00941 expression
Epithelioid mesothelioma
Biphasic mesothelioma
Sarcomatoid mesothelioma
F
LINC00941 expression
WT
Mutated
LATS2 status

Figure 27. A) Forest plot displaying the correlation of the 24 long non-coding RNAs with overall survival. **B)** Kaplan Meier curves of MPM-TCGA cohort patients within I and IV quartile of LINC00941 expression. **C)** Histogram representing the ratio of expression of the indicated genes in short vs long survivors (I and IV quartile) in the MPM-RE cohort. *≤0.05, **≤0.01, ***≤0.001. **D)** Kaplan Meier curves of MPM-RE cohort patients within I and IV quartile of LINC00941 expression. **E)** Boxplot representation of LINC00941 expression in different MPM histotypes (MPM-TCGA cohort). **F)** Boxplot representation of LINC00941 expression in patients with different LATS2 mutational status (MPM-TCGA cohort).

LINC00941 promotes proliferation, migration and invasion of MPM cells

To establish a functional relation between LINC00941 expression and aggressiveness of MPM, we explored its biological function using siRNA mediated KD approach in two different MPM cell models. First, we explored changes in the overall transcriptional program by performing a RNA-seq analysis in LINC00941 KD vs Ctrl MSTO-211H cells. 3105 significantly deregulated genes upon LINC00941 KD were detected. Of these, 1304 genes were upregulated and 1801 downregulated (Figure 28A-B). GO analysis of downregulated genes revealed that they were mainly involved in response to hypoxia and regulation of G2/M phases of cell cycle (Figure 28C). Upregulated genes were enriched in morphogenesis of epithelial cells and differentiation, and in immune response pathways (Figure 28D). We previously demonstrated that LINC00941 is located preferentially in the cytoplasm (Gugnoni et al., 2021). Thus, we reasoned that its effect on gene expression went through the regulation of upstream transcriptional controllers. Thus, we interrogated the TRUSTT database using the list of LINC00941 target genes searching for enriched putative LINC00941 functionally related TFs. SREBF1, MYC, NFYA and HIF1α were the top scoring predicted upstream regulators of downregulated genes. Noticeably, HIF1α was among the top scoring downregulated genes upon LINC00941 KD (Figure 28E). By contrast, the Polycomb factor EZH2 emerged as the only putative regulator of upregulated genes (Figure 28F).

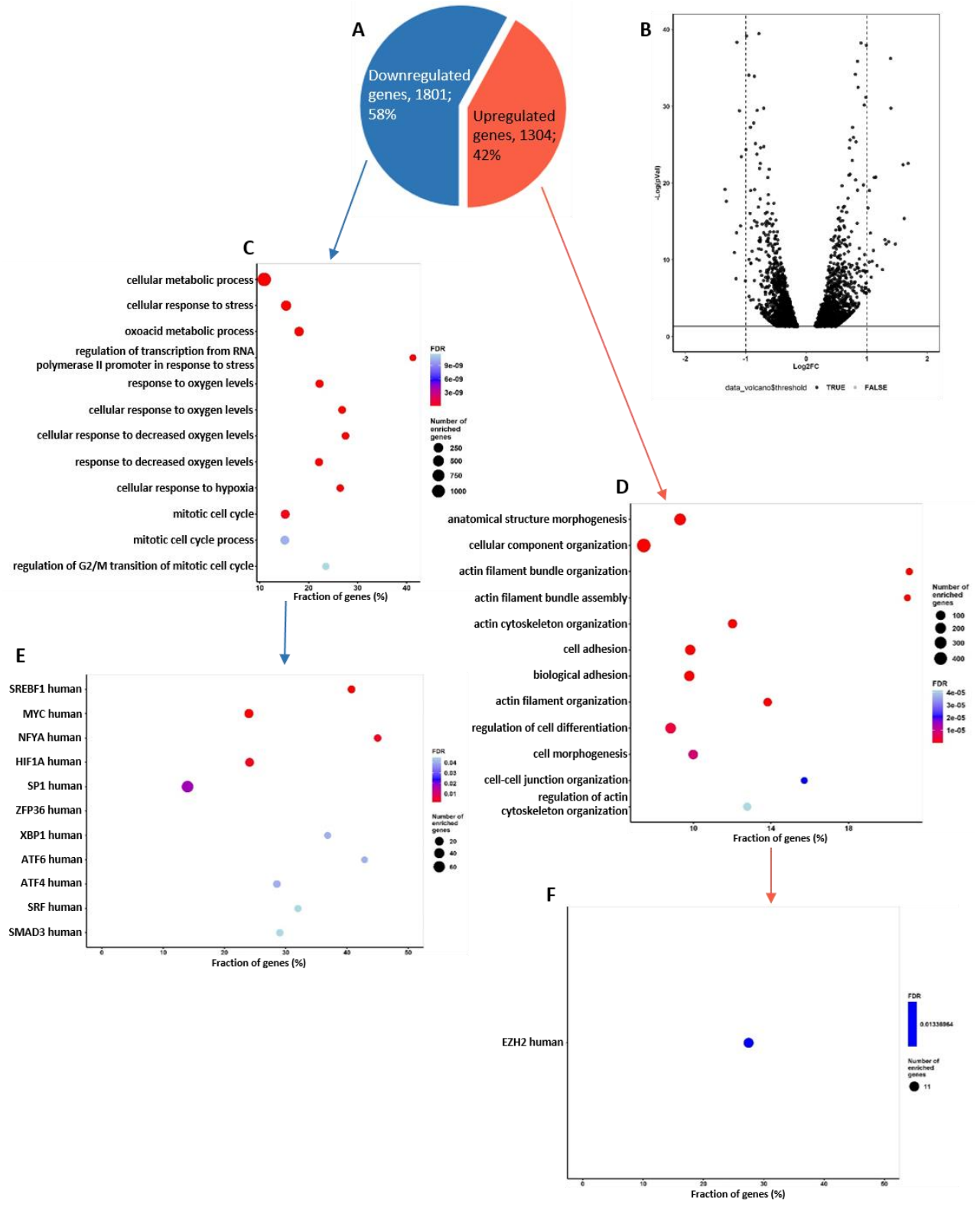

Figure 28. A) Distribution of significant deregulated genes in RNA-seq (siCTRL vs siLINC00941 MSTO-211H cells). **B)** Volcano plot of significantly deregulated genes in RNA-seq. **C)** Gene ontology enrichment of biological processes downregulated in RNA-seq of siLINC00941 vs siCTRL MSTO-211H cells. **D)** Gene ontology enrichment of biological processes upregulated in RNA-seq of siLINC00941 vs siCTRL MSTO-211H cells. **E)** Enrichment of principal transcription factors involved in downregulated processes performed with TRUSTT database. **F)** Enrichment of principal transcription factors involved in upregulated processes performed with TRUSTT database.

Next, we performed in vitro assays to investigate changes in the MPM cell properties upon LINC00941 KD. Noticeably, LINC00941 KD strongly impaired proliferation of both MSTO-211H and NCI-H2052 cells (Figure 29A-D). These results are in agreement with the fact that mitosis regulation emerged among the pathways of downregulated genes by LINC00941. We also performed migration and invasion assays for both MSTO-211H and NCI-H2052 cells and found a significant decrease in migration (Figure 30A-D) and invasion (Figure 31A-B) capability upon LINC00941 KD. These results are consistent with data previously reported in other tumor setting demonstrating that this lincRNA participate to increased motility and invasion (Ai et al., 2020; Chang et al., 2021; J. Wang et al., 2021; Wu et al., 2021).

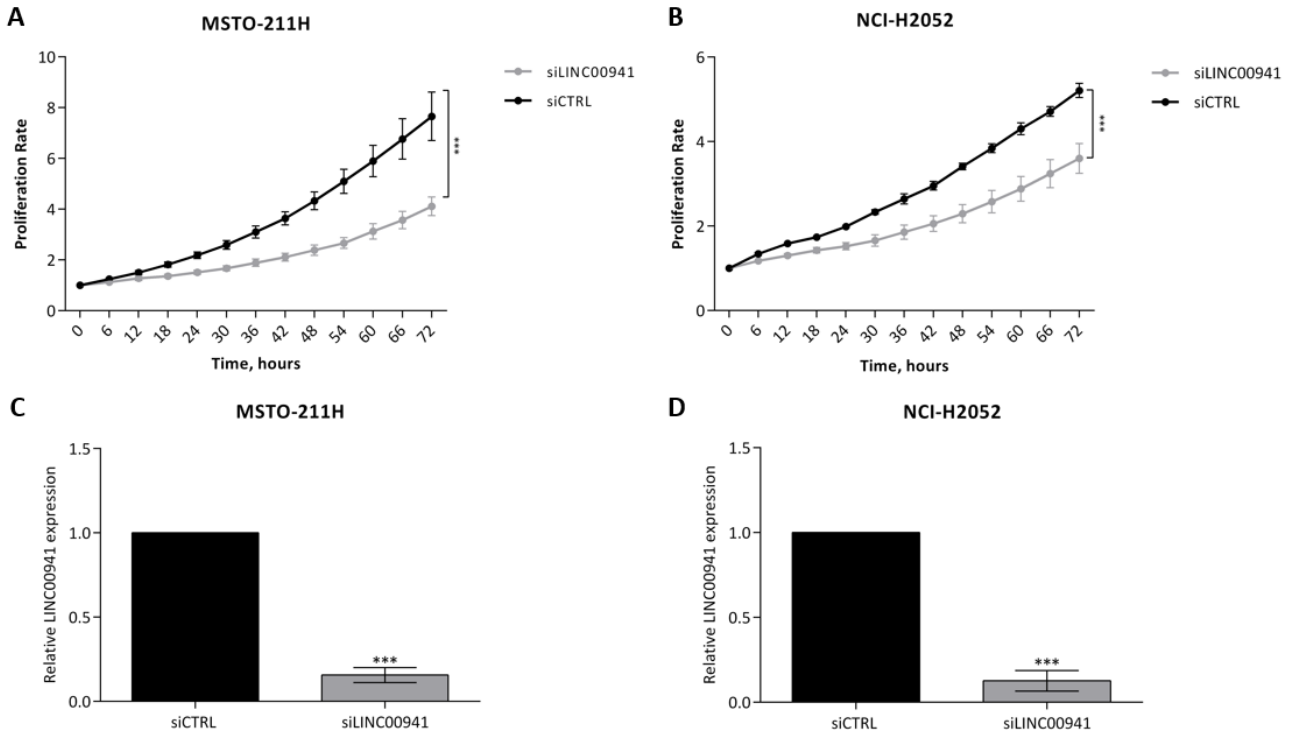

Figure 29. A, B) Proliferation assays in MSTO-211H (A) and NCI-H2052 (B) cells reported as proliferation rate relative to day 0, measured with Incucyte S3 Live Cell Analysis (Sartorius). Data are represented as mean ± SEM; *≤0.05, **≤0.01, ***≤0.001; N=3. **C, D)** qRT-PCR of LINC00941 expression in siCTRL versus siLINC00941 MSTO-211H (C) and NCI-H2052 (D) cells; *≤0.05, **≤0.01, ***≤0.001; N=5.

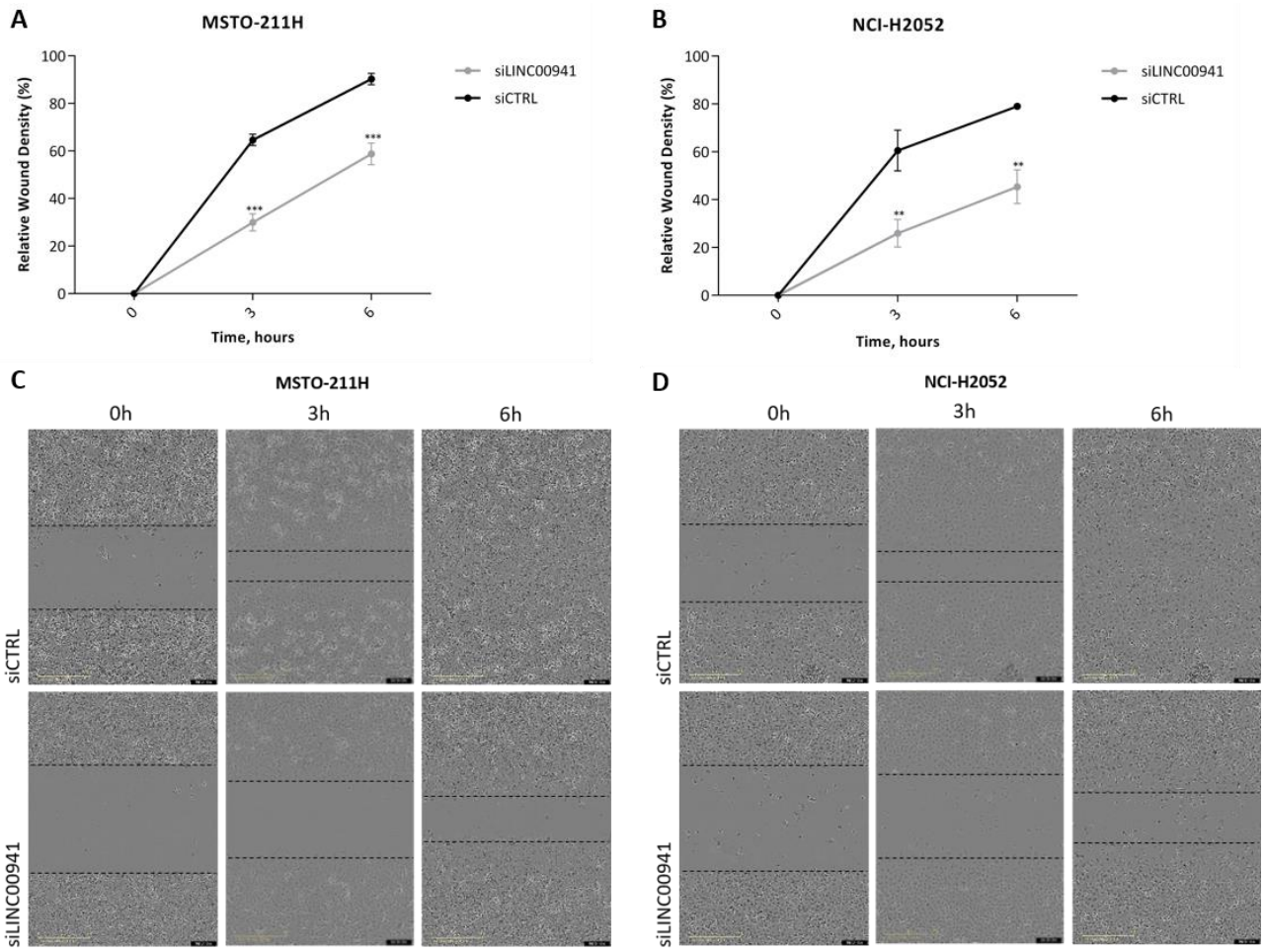

Figure 30. A, B) Graph representing the relative wound density at the indicated time points in MSTO-211H (A) and NCI-H2052 (B) cells transfected with siLINC00941 or siCTRL, measured with Incucyte S3 Live Cell Analysis (Sartorius). Data are represented as mean ± SEM; *≤0.05, **≤0.01, ***≤0.001; N=2. **C, D)** Migration ability of MSTO-211H (C) and NCI-H2052 (D) siCTRL vs siLINC00941 cells.

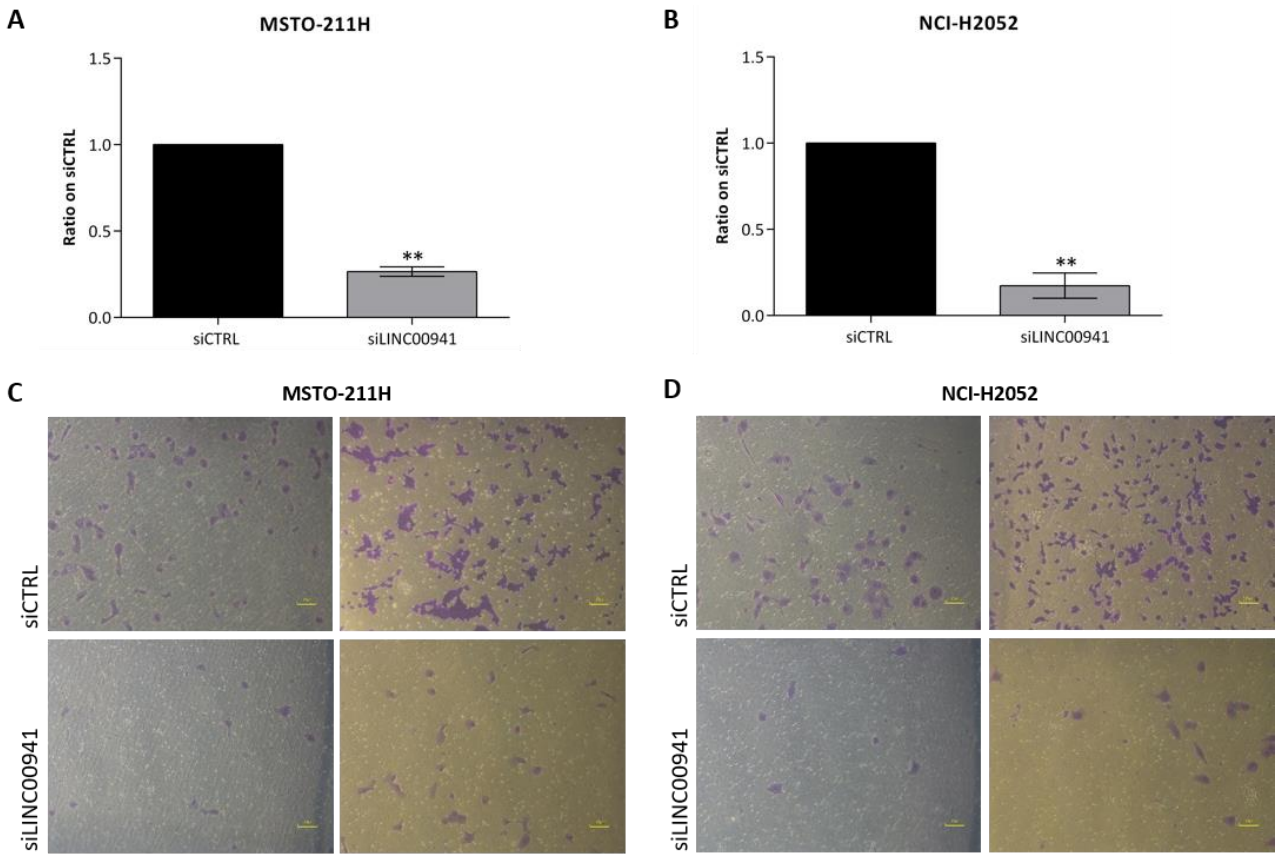

Figure 31. A, B) Graph showing the rate of invasion of MSTO-211H (A) and NCI-H2052 (B) siCTRL vs siLINC00941 cells. Cells were counted using ImageJ software and the number of cells were taken 72h from transfection. **C, D)** Images of invading MSTO-211H (C) and NCI-H2052 (D) siCTRL vs siLINC00941 cells. Images were taken 72h from transfection.

Morphologically, we noticed a striking change in shape and growth properties of LINC00941 KD MSTO-211H cells vs control. While siCTRL MSTO-211H cells showed a small and irregular shape, growing preferentially as separate unites, LINC00941 KD cells presented a drastic tendency to cluster together in three-dimensional organization of tightly connected cells, suggesting a deep reorganization at the level of cell-cell junction properties (Figure 32A). Staining of actin filaments using immunofluorescent-phalloidin confirmed this hypothesis showing that changes in the morphological appearance of the cells was accompanied by a profound reorganization of the cytoskeleton. siLINC00941 cells, differently from siCTRL cells, displayed a rather polygonal phenotype with actin filaments forming highly organized thick fibers running parallel below the cell membrane, as typical of differentiated epithelial cells. In addition, while siCTRL cells were characterized by an elevated number of filopodia and lamellipodia along the entire surface of cell membrane (Figure 32B), LINC00941 KD cells displayed a massive reduction of the structures of movement and an evident restoration of cell-cell contacts, along which actin filaments created bridges of connections to reinforce the strength of cell-cell contacts (Gugnoni et al.,

2017) (Figure 32C). These data are in agreement with the abolished migration and invasiveness observed in KD cells and with the results of RNA-seq showing that LINC00941 KD leads to upregulation of genes enriched in pathways of epithelial polarization and differentiation. Also, these data could explain the clinical observation that LINC00941 expression is preferentially associated with poorly differentiated and sarcomatoid phenotype in patients.

Experiments are undergoing to set the molecular mechanisms trough which LINC00941 could mediate this function.

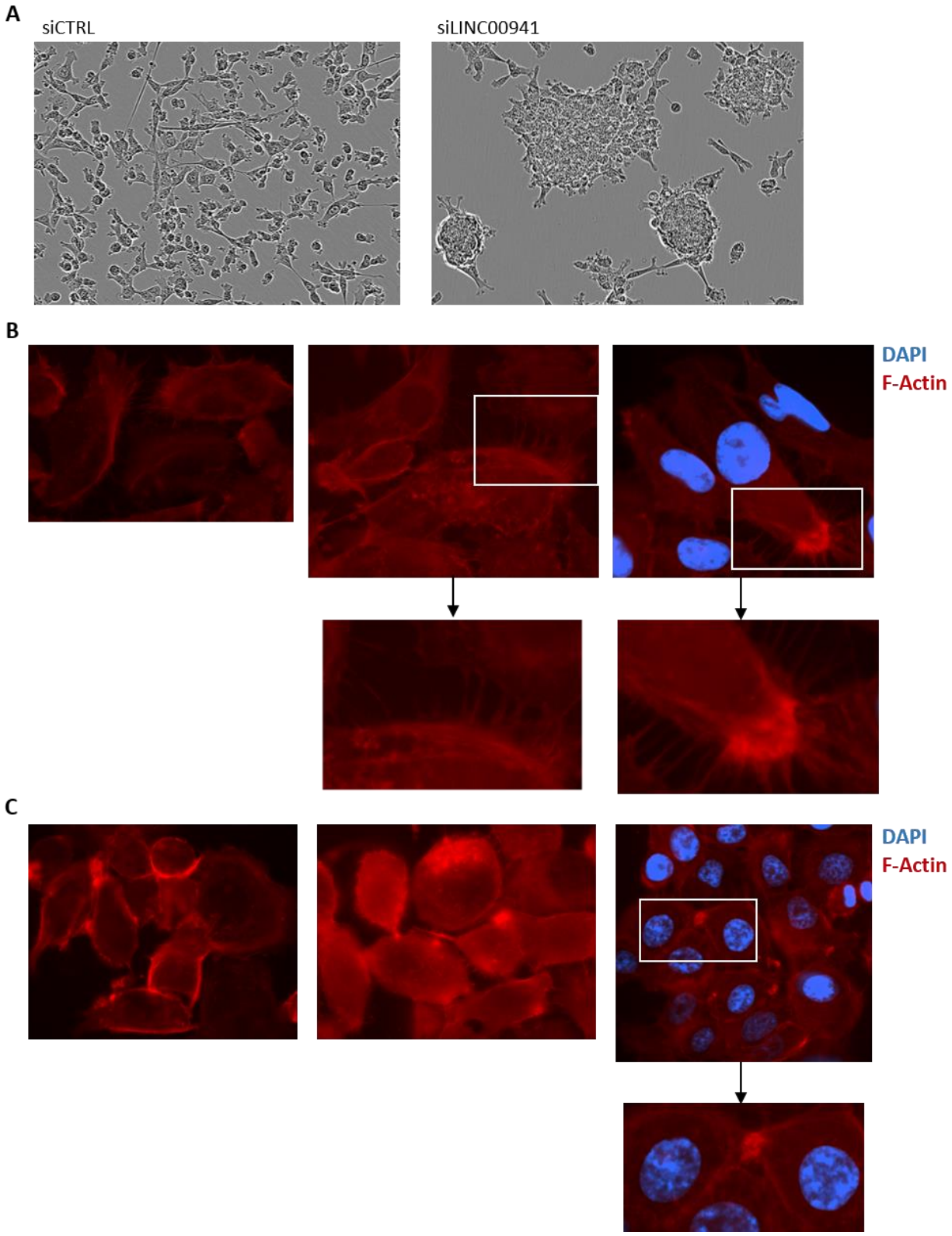

Figure 32. A) Images of MSTO-211H cells transfected with siCTRL (left panel) or siLINC00941 (right panel). The images show the marked change in MSTO-211H cells shape and growth properties upon LINC00941 silencing. Images were taken with Incucyte S3 Live Cell Analysis (Sartorius). **B, C)** Immunofluorescence showing F-actin (red) and DAPI (blue) in MSTO-211H siCTRL (B) and siLINC00941 (C) cells.

LINC00941 mediates HIF1α signalling in MPM cells

Our data indicated that HIF1α is one of the top scoring LINC00941 target genes in MPM and also a putative upstream regulator of LINC00941 associated gene program.

To set the functional relationship between LINC00941 and this TF, we first validated HIF1α and its target genes expression upon LINC00941 KD. In both MPM cell models, HIF1α expression was drastically reduced at the mRNA level, as well as its target genes following the depletion of the lincRNA (Figure 33A-B). Because in normal oxygen conditions HIF1α protein is rapidly degraded, we treated MPM cells with cobalt chloride ($CoCl_2$) that mimics hypoxic conditions and stabilizes HIF1a protein (Figure 33C) (Muñoz-Sánchez & Chánez-Cárdenas, 2019). Noticeably, silencing of LINC00941 completely abolished the induction of HIF1α protein expression observed in siCTRL cells in both cell lines (Figure 33D-E), confirming that loss of LINC00941 impairs the expression of this TF. Coherently, upon $CoCl_2$ treatment and HIF1α activation, we observed an induction of both HIF1α targets and genes induced in response to hypoxic conditions that were downregulated in the RNA-seq. On the contrary, LINC00941 KD cells showed a significant reduction of these genes in hypoxic conditions, consistently with HIF1α inhibition (Figure 33F-G).

Even if preliminary, these results suggest a previously unknown functional relationship between LINC00941 and HIF1α proposing a possible role for this lincRNA in regulating response to low-oxygen conditions, typical of many aggressive cancers.

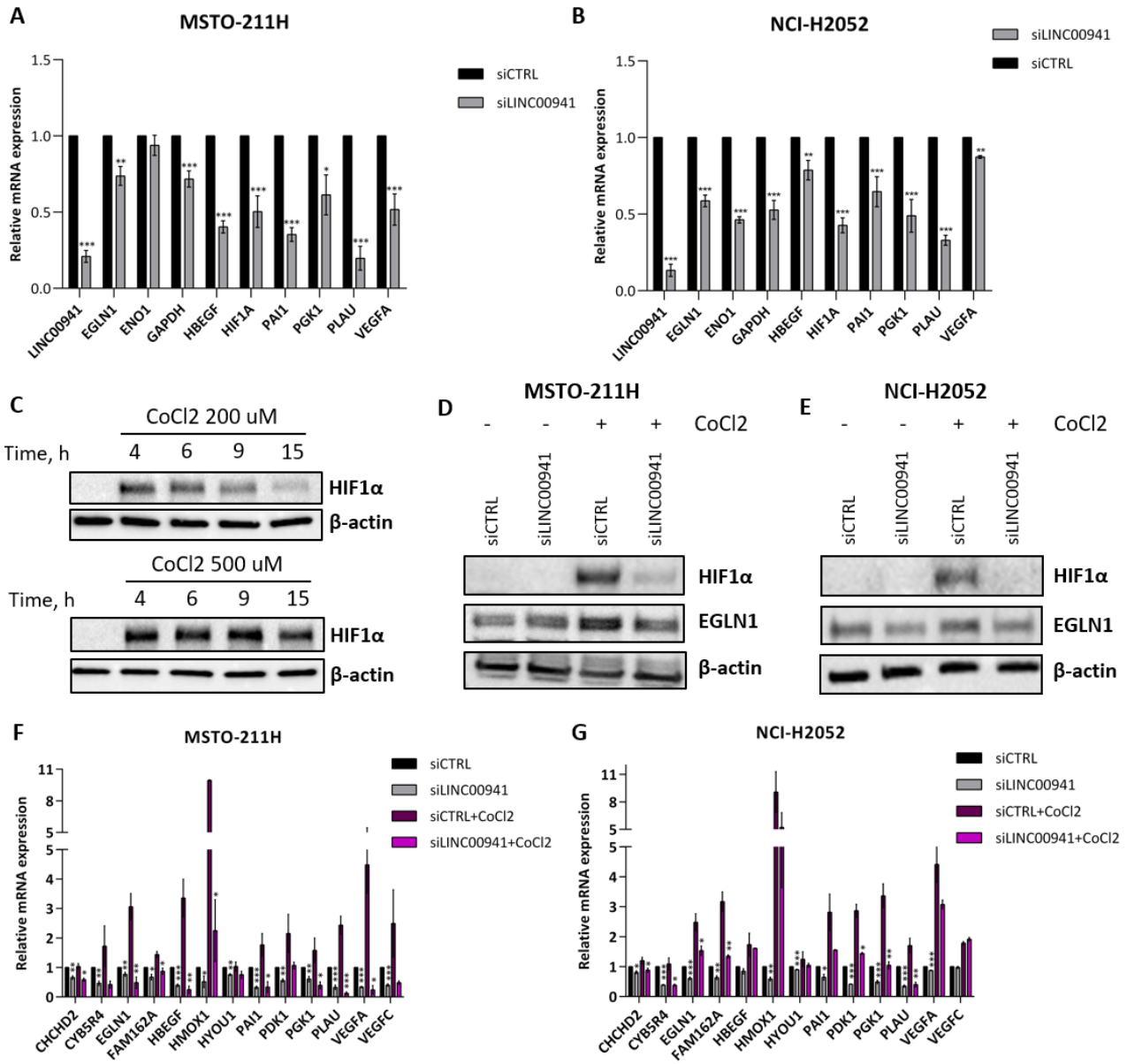

Figure 33. A, B) qRT-PCR of a panel of HIF1α direct target genes in siCTRL vs siLINC00941 MSTO-211H (A) and NCI-H2052 (B) cells. Data are expressed as mean ± SEM; *≤0.05, **≤0.01, ***≤0.001; N=3. **C)** Western Blot analysis of HIF1α protein stabilization in MSTO-211H cells treated with two different doses of $CoCl_2$ for different hours. β-actin is the loading control. **D, E)** Western blot of siCTRL vs siLINC00941 MSTO-211H (D) and NCI-H2052 (E) cells with or without $CoCl_2$ treatment (200 uM for 5h). β-actin is the loading control. **F, G)** qRT-PCR of a panel of HIF1α direct target genes and genes induced in hypoxic conditions in siCTRL vs siLINC00941 MSTO-211H (A) and NCI-H2052 (B) cells upon treatment with 200 uM of $CoCl_2$. Data are expressed as mean ± SEM; *≤0.05, **≤0.01, ***≤0.001; N=3.

DISCUSSION

In the last decade, the development of NGS techniques allowed massive profiling of most tumor types, including MPM (Hylebos et al., 2016; Morganti et al., 2019). These technologies identified many driver mutations in different cancer types, helping to define new therapeutic strategies. However, these high-throughput studies did not improve the treatment of MPM, that still remains a highly lethal cancer (Yap et al., 2017). Several inhibitors of key oncogenic pathways has been tested, such as PI3K/Mtor, HDAC and NFkB, but none of these therapies caused an improvement in MPM patients' outcome (Pasello & Favaretto, 2009). This is due to the purely descriptive nature of profiling studies and to the fact that cancer additions are not only of a genetic nature (Tsherniak et al., 2017). This is particularly true for a disease that, like MPM, escapes to the classical model of cancer evolution. MPM is characterized by a low mutational burden and by a great intra- and inter- patients heterogeneity (Oehl et al., 2018). Thus, despite the efforts made by omics profiling, the molecular events that mark origin and progression of MPM are still not completely clear. Moreover, being MPM a rare disease, researchers have to face the issue of carrying studies with a low number of cases, still hampering the characterization of common events in MPM progression. To date, the therapeutic options for MPM patients are still limited to surgery (rarely) and standard regimens of chemotherapy that delay but do not stop disease progression; more recently immunotherapy has emerged, even if its effects are lower compared to other tumor types (Rijavec et al., 2022; Yap et al., 2017).

To overcome these limitations, here, by employing a systematic genome-wide CRISPR-Cas9 screening integrated with clinical data of MPM patients, we evaluated the effects of single-genes perturbations and their functional consequences *in vivo* to provide new non-genetic vulnerabilities that drive MPM progression. First, we integrated our screening results with the ones available in the DEPMAP database, to overcome the issue of tumor heterogeneity and to find common MPM dependencies. Then, we investigated the association of the identified MPM essential genes with MPM patients' survival across the TCGA-MESO dataset, to explore the functional role of genes that are associated to tumor aggressiveness in real life. This approach, besides confirming the relevance of epigenetic changes in MPM progression, opens the door to the design of new MPM-oriented therapies.

In line with recent evidence that point to epigenome as a primary target of asbestos carcinogenesis (McLoughlin et al., 2017; Sage et al., 2018), we discovered a core of genes involved in chromatin functions as essential for MPM progression. These 18 epigenetic

keepers are associated to a bad prognosis of MPM patients and are essential for MPM cells growth. Among them, we focused on TRIM28 based on its high discrimination of short vs long OS patients. Consistent with its reported role in chromatin dynamics, it is not surprising that TRIM28 is overexpressed in several tumors and is often associated to aggressiveness and poor outcome. Recently, TRIM28 has been described to regulate CDK9-mediated RNA-PolII pause release into productive elongation. Bacon et al. recently demonstrated that TRIM28 by coupling all steps of RNA-PolII cycle is able to sustain oncogenic programs. They showed that TRIM28 binds to the hypo-acetylated tails of histone 4, interacts with RNA-PolII and recruits pathway-specific TFs, promoting CDK9-mediated RNA-PolII pause-release and elongation on pathway specific genes. Cancer cells take advantage of this mechanism to activate oncogenic programs that sustain their survival under specific conditions (Bacon et al., 2020; McNamara, Reeder, et al., 2016).

In the context of MPM, we described a previously uncharacterized function of TRIM28 in taking part to correct mitosis execution by interacting with the transcriptional complex that promotes the activation of mitotic genes. The succession of events that characterize cell cycle need to be finely regulated and requires a well-orchestrated transcriptional and epigenetic control. Progression through the different phases of cell cycle needs that specific classes of genes are activated at precise time points (Y. Liu et al., 2017). The expression of cell cycle dependent genes is regulated by the RB (Retinoblastoma) protein family, the E2F TF family and MuvB (multi-vulva class B) complexes. RB and E2F TFs regulate the activation of early cell cycle genes in G1/S phases, while MuvB complexes are responsible for the transcription of late cell cycle genes in G2/M phases of cell cycle (Fischer et al., 2016; Fischer & Müller, 2017; Y. Liu et al., 2017). The mammalian MuvB core is composed by LIN9, LIN37, LIN52, LIN54 and RBBP4. This complex interacts with different proteins in different phases of the cell cycle that determine its active or inactive state. During S phase, MuvB interacts with B-MYB, forming the B-MYB-MuvB (MMB) complex. This interaction is necessary to recruit FOXM1 in G2 and reach full activation of G2/M genes' expression by FOXM1-MuvB complex (Fischer & Müller, 2017; Sadasivam et al., 2012). G2/M genes share a common sequence in their promoter known as "cell-cycle gene homology region" (CHR). The CHR element is bound by active MuvB complexes that, consequentially, leads to activation of mitotic genes (Fischer et al., 2016).

For the first time, we demonstrated that TRIM28 is recruited to the TSS of mitotic genes at the level of the CHR element. Here, as in the mechanism reported by Bacon and colleagues,

we suppose that TRIM28 stimulates CDK9-mediated activation of RNA-PolII that, by phosphorylating its CTD on Ser2, allows its productive elongation on mitotic genes. We proved that TRIM28 interacts with CDK9 and both active and phosphorylated forms of RNA-PolII, as well with FOXM1 and RBBP4, subunit of the MuvB core, suggesting its functional interplay with MuvB active complexes. We observed that upon TRIM28 loss, RNA-PolII is displaced from the promoters of G2/M genes and its actively elongating form, pSer2-RNA-PolII, is displaced from *AURKB* gene-body. These results suggest that TRIM28, by orchestrating the interactions between RNA-PolII, CDK9 and MuvB active complexes, ensures the timely activation of G2/M genes by keeping RNA-PolII stalled downstream the TSS, ready for prompt activation. Consequentially, the expression of major mitotic players like *CDC20*, *CCNB1*, *AURKA*, *AURKB* and the other components of the Chromosomal Passenger Complex (CPC) (*BIRC5*, *CDCA8* and *INCENP*) is dramatically reduced upon TRIM28 silencing. Therefore, TRIM28 KD cells are unable to carry on mitosis, showing defects in chromosome condensation, alignment and segregation that, finally, result in cell death due to the prolonged G2/M block (Figure 34).

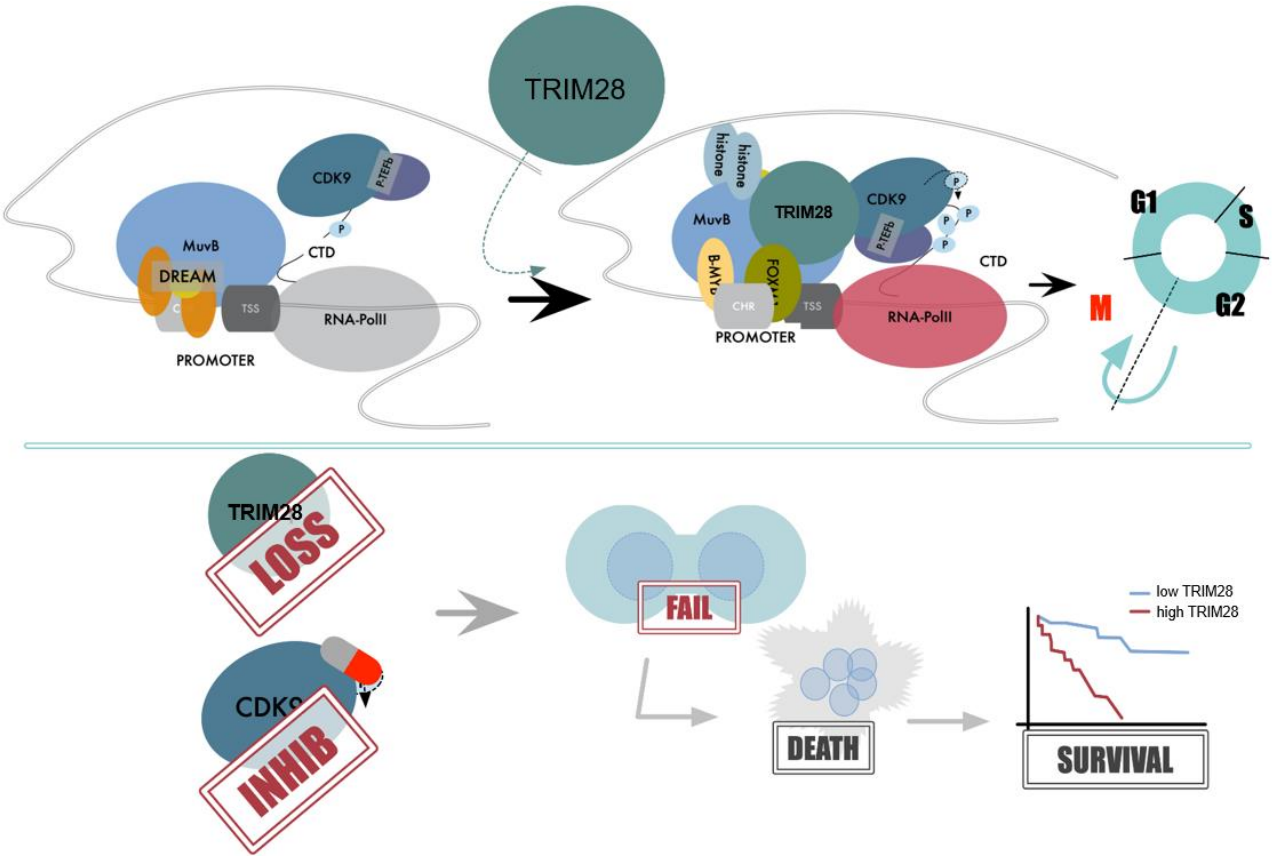

Figure 34. Schematic model representing the mechanism of MPM-dependency from TRIM28 and its clinical implications. TRIM28 binding to the B-MYB/FOXM1-MuvB complex sitting on CHR promoters fosters the recruitment of CDK9 for prompt activation of RNA-PolII into proficient elongation on G2/M genes, thus ensuring

correct mitosis execution. TRIM28 loss, as well as CDK9 inhibitors, leads to mitosis failure that results in cell death. Moreover, TRIM28 high expression is associated to bad survival of MPM patients.

We showed that in MPM TRIM28 contributes to carcinogenesis by keeping the time of mitosis. This function is exerted by the interaction with CDK9 and its mediated RNA-PolII release from pausing. Bacon et al. demonstrated that TRIM28 is necessary for positioning CDK9 on selective target genes promoters, besides CDK9 is indispensable for TRIM28-mediated RNA-PolII activation (Bacon et al., 2020). CDK9 is upregulated in a wide variety of tumors and is often associated to a bad outcome (Anshabo et al., 2021; Franco et al., 2018). Having such a central role in RNA-PolII regulation, CDK9 sustains cancer cells by activating oncogenic gene programs. For these reasons, CDK9 has been regarded as a promising target for the development of new anticancer drugs (Cassandri et al., 2020; Mandal et al., 2021). Consistently, several CDK9 inhibitors as well as pan-CDKs inhibitors have been developed in recent years and tested in several hematological cancers and solid tumors. Given this preamble, we set to hit TRIM28 function in MPM by inhibiting its functional partner CDK9. To this aim we used an highly selective CDK9 inhibitor, AZD4573 (Barlaam et al., 2020; Cidado et al., 2020), and a pan-CDK inhibitor, AT7519 (Santo et al., 2010). Today, AZD4573 is being tested in two phase-I clinical trials against advanced hematological cancers and relapsed/refractory hematological cancers (Alcon et al., 2020; Mandal et al., 2021). We showed that both pan-CDKs and specific-CDK9 inhibitors are highly lethal for MPM cells, even at very low concentrations. Moreover, MPM cells treated with AZD4573 showed an increase in apoptotic nuclei and a decrease in mitotic ones, together with a downregulation of a set of TRIM28 mitotic target genes, mimicking TRIM28 KD effects. These results suggest that the lethal effects of these drugs in MPM act through the inhibition of TRIM28 gene program. Even in preliminary, these results lay the basis for the employment of CDK9 inhibitors in MPM, highlighting the power of functional screening to define new therapeutic approaches.

As a transcriptional corepressor, TRIM28 has been reported to maintain ERVs inactive through the establishment of heterochromatin (Geis & Goff, 2020). Resembling retroviruses and having the ability to move inside the genome, ERVs are harmful elements that mine genomic stability. Thus, their expression needs to be finely regulated to keep the right balance and avoid catastrophic events. ERVs represent a great percentage of non-coding RNAs and their massive reactivation prime Interferon-I mediated immune response (Mu et al., 2016; Tie et al., 2018), contributing to the settlement of a hostile environment for tumor cells. TRIM28, acting as a scaffold platform for the recruitment of heterochromatin inducing

proteins, keep ERVs expression repressed in normal conditions. We observed that TRIM28 KO stimulates the expression of ISGs that are commonly activated upon ERVs expression. We thus hypothesize that ISGs upregulation that we observed upon TRIM28 KO is likely the consequence of the epigenetic unmasking of ERVs along the genome. We also observed that the expression of several ISGs significantly increased patients' survival, suggesting a protective role for these genes, coherently with the activation of the immune response that is hostile to cancer cells. Further analyses are ongoing to establish the link between TRIM28 and IFN-I mediated immune response.

In recent years, the systematic functional annotation of the non-coding genome has revealed that lncRNAs take part to the vast majority of biological processes inside the cells. Being their expression highly specific between cell lines and tissues, it is not surprising that the expression of many lncRNAs is peculiar of cancer cells (Iaccarino & Klapper, 2021; W.-X. Peng et al., 2017; Y. Zhang & Tang, 2018). This finding paved the way for massive characterization of these non-coding transcripts and a mounting interest in identifying cancer specific lncRNAs have emerged in recent years. Given their higher expression specificity than coding transcripts and their easy and non-invasive collection method in patients' tissues and biological fluids, lncRNAs are being extensively studied as possible cancer biomarkers besides to therapeutic targets (Iaccarino & Klapper, 2021).

In this perspective, we analyzed gene expression profiles and clinical data through the TCGA-MESO dataset to explore the contribution of lncRNAs to MPM progression and aggressiveness. We found 5 lncRNAs which expression strongly reduces patients' survival probability across two independent MPM cohorts. LINC00941, that we already identified as mediator of aggressiveness in thyroid cancer (Gugnoni et al., 2021), emerged as the one that better discriminated long vs short OS in both cohorts. The expression of this lincRNA was significantly associated to the most aggressive sarcomatoid histotype. We found that LINC00941 promotes MPM cells' growth, migration and invasion, coherently with its association to tumor aggressiveness, and consistent with evidence in other tumor settings. We found many genes involved in cell morphogenesis and adhesion and in cytoskeleton organization as upregulated by LINC00941 KD. Indeed, upon LINC00941 silencing we observed a striking change in MSTO-211H cells shape, adhesion and growth properties. Moreover, these cells showed a strong reduction of filopodia and lamellipodia, the structures responsible for cell motility. These results are coherent with its association to the aggressive sarcomatoid phenotype and with its reported role in invasion and metastasis of cancer cells.

Our data indicate that LINC00941 may be involved in the regulation of HIF1α signaling. Coherently, we observed a strong downregulation of HIF1α and of its target genes upon LINC00941 KD, both in normoxic and hypoxic conditions. Experiments are undergoing to characterize this functional relationship, However, these data suggest a possible role for LINC00941 in regulating response to low-oxygen conditions, typical of many aggressive cancers.

HIF1α is overexpressed in several cancers, due to either hypoxic tumor microenvironment or genetic alterations. Its high expression is often associated to an increased mortality of patients. This is consistent with its reported role in helping cells to overcome low-oxygen conditions, thus promoting survival of cancer cells (Klabatsa et al., 2006; Tiwari et al., 2020). HIF1α has many direct targets that are characterized by a “Hypoxia-Response Element” (HRE). Among them are many genes involved in angiogenesis, glucose transport, survival and invasion (Slemc & Kunej, 2016). All these mechanisms are advantageous to cancer cells. It is reported that hypoxia enhances cancer cells survival, metastasis and drug resistance in multiple tumor types (Kim et al., 2018; Klabatsa et al., 2006; Tiwari et al., 2020). Thus, it is likely that LINC00941 by regulating HIF1α levels, in particular under hypoxic conditions, may help MPM cells to survive, explaining its association with tumor aggressiveness. Indeed, high HIF1α levels are typical of highly aggressive tumors that, becoming rapidly without blood supply, have to find an alternative way to survive (Kim et al., 2018; Klabatsa et al., 2006).

Through this integrated approach, we discovered TRIM28 and LINC00941 as new non-genetic dependencies of MPM, helping to improve our knowledge on the molecular events that lead to MPM and paving the way for the employment of new drugs in the management of MPM. Besides, we provided clues for the development of new prognostic tools that could help clinicians to tailor patients towards the most appropriate therapeutic option. Collectively, these data highlight the strength of the integration of functional screening with clinical data for the identification of cancer specific dependencies that impact on patients’ real life.

MATERIAL AND METHODS

Cell Culture

MSTO-211H cell line was obtained from Istituto Europeo di Oncologia (IEO, Milan, Italy). NCI-H2052 and HEK293T cell lines were obtained from ATCC (LGC Standards, Sesto San Giovanni, Italy). All cell lines were cultured in RPMI medium added with 10% fetal bovine serum (FBS) and 1% penicillin – streptomycin and grown at 37°C/5% CO_2. Cell lines were routinely tested for Mycoplasma contamination and authenticated by SNP profiling at Multiplexion GmbH (Heidelberg, Germany).

Lentiviral Infection

Lentiviral particles were produced by transfecting HEK-293T cells using Lipofectamine 2000 (Thermo Fisher Scientific, Waltham, Massachussets, USA). 650000 HEK-293T cells were seeded in a 6-well plate in transfection culture medium (complete medium without Penicillin/Streptomicin). The day after, HEK-293T cells were transfected with a mix of the transfer plasmid of interest and the 3rd generation packaging/envelope plasmids: pRSV-Rev, pMDLg/pRRE and pMDG.2 (Addgene plasmids #12253, #12252 and #12259. These plasmids were a gift form Didier Trono). For each transfection we used 2.5ug of total DNA: 625 ng of pRSV-Rev, 625 ng of pMDLg/pRRE, 250 ng of pMDG.2 and 1ug of the plasmid of interest; the plasmid mix was diluted in 150 ul of OptiMEM medium. In parallel, 10 ul of Lipofectamine 2000 (Thermo Fisher Scientific, Waltham, Massachussets, USA) were diluted in 150 ul of OptiMEM medium. The two mix were combined and incubated for 5 minutes at room temperature (RT), then added to HEK-293T cells dropwise. 48h after transfection, viral supernatant was collected and filtered through 0.45 um filters. 500000 MSTO-211H/Cas9-clone G12 cells were seeded in 6-well plates and the day after the viral supernatant was added to the cells together with Polybrene at 4 ug/ml. Cells were centrifuged at 1800 rpm for 45’ at 32°C, then incubated overnight at 37°C. Viral suspension was then removed and replaced with regular culture medium. 24 h after infection, cells were amplified and antibiotic selection started, using Blasticidin (Invivogen, Toulouse, France) at 12 ug/ml for 7 days or Puromycin (Life Technologies, Monza, Italy) at 1 ug/ml for 5 days. Alternatively, cells were amplified and sorted using a FACS Melody (BD Bioscences).

Generation of MSTO-211H clones stably expressing Cas9

MSTO-211H cells were infected with lentiviral particles containing lentiCas9-Blast (Addgene plasmid #52962) as transfer plasmid (Sanjana et al., 2014). LentiCas9-Blast was a gift from

Feng Zhang. After Blasticidin selection, MSTO-211H cells were seeded at one cell/well in a 96-well plate to isolate single clones. We tested MSTO-211H/Cas9 clones by western blotting with anti-Flag antibody (F1804, Sigma-Aldrich). The clones showing the highest Cas9 expression were tested for Cas9 activity by infecting them with the pXPR_011 plasmid (Addgene plasmid #59702), gifted by John Doench and David Root. The plasmid contains an ORF for GFP expression and a sgRNA targeting GFP, thus we analyzed GFP expression with a FACS Canto II Flow Cytometer (BD Bioscences). The clone showing the highest Cas9 activity (lowest GFP residual expression) was selected to perform the screening and subsequent experiments. We selected Clone G12 for subsequent experiments.

Genome-wide screening

Human GeCKOv2 CRISPR knockout pooled library in lentiGuide-Puro plasmid was a gift from Feng Zhang (Addgene #1000000049). The GecKOv2 library is composed by two semi-libraries, A and B, each of which contains 3 sgRNAs targeting each gene. We used the semi-library A to infect MSTO-211H/Cas9 cells in two independent experiments. For each replicate, we infected 180 x 10^6 cells with a multiplicity of infection (MOI) of 0.3, aiming at 600x coverage. After 3 days of puromycin selection, 120 million cells were harvested to sequence T0 time point. The remaining cells were kept in culture and 120 million cells were collected both at 16 and 23 days after T0. Libraries preparation, samples sequencing and bioinformatic analysis have been performed as already described (Gobbi et al. 2019). Library composition was assessed by Next Generation Sequencing (NGS) and single-guide RNAs (sgRNAs) frequencies were compared to day 0, to identify sgRNAs that were depleted and/or enriched over cell growth, using the MAGeCK algorithm (W. Li et al., 2014). For both essential and suppressor genes, we considered only genes that were consistently detected in both experimental bio-replicates (A1 and A2) and at both time-points (T16, T23). From the resulting gene lists, we excluded genes coding for miRNAs (163 for essentials and 10 for suppressors). We also excluded “common essential genes” (608), being vital genes for all cell lines, using the list “Achilles_common_essential” from the “DEPMAP” database (https://depmap.org/portal/). Then, to validate our results, we interrogated the “DEPMAP” database (Tsherniak et al., 2017), in which CRISPR-Cas9 genome-wide data are available for 7 MPM cell lines (MSTO-211H, NCI-H2052, ACC-MESO-1, IST-MES2, NCI-H28, NCI-H2452, MPP89). Only genes showing the same trend in at least 6/7 MPM cell lines were considered. 51% and 26% of essential and suppressor genes were confirmed respectively

by this approach, obtaining a final list of 233 MPM essential genes and 45 MPM suppressor genes.

TCGA Data Analysis

Survival data and gene expression profile on MPM patients were obtained from The Cancer Genome Atlas (TCGA) dataset using the R TCGA biolinks package to download and analyze RNAseq data (workflow.type “HTSeq - FPKM”). Gene expression values were correlated using R Corrplot package. For survival analysis, performed with R Survival package, gene expression values were considered in continuous and also used to dichotomize patients on the basis of 1st and 4th quartile of expression. Genetic variations in MPM were selected among the most altered genes in MPM using cBioPortal (http://www.cbioportal.org) based on TCGA datasets. Differential expression analysis for the 18 core genes was conducted according to mutational status. Significant associations were evaluated by Kruskall-Wallis test.

Knockout cell lines generation and Competition Assays

Two sgRNAs for each target gene were selected from the GeCKOv2 library and cloned into the pLKO5.sgRNA.EFS.GFP into BsmBI cloning site. pLKO5.sgRNA.EFS.GFP was a gift from Benjamin Ebert (Addgene plasmid #57822). sgRNAs sequences are listed in Table 2. MSTO-211H/Cas9 cells have been infected as described above and knockout efficiency was assessed by T7 endonuclease I cleavage assay (ALT-R Kit, Integrated DNA Technologies, Skokie, Illinois, USA) following the instructions described in the next paragraph. Infection efficiency was assessed by GFP detection with a FACS Canto II Flow Cytometer. Cells showing less than 90% GFP positive cells were sorted using a FACS Melody (BD Bioscences). Protein and gene expression analysis were performed both at 5 and 7 days after infection.

For competition assays, cells were infected with a MOI of 0.6- 0.7 and grown for 15 days. Thus, we obtained a co-culture of infected (GFP+) and non-infected (GFP-) cells. We recorded the percentage of GFP+ cells over time with a FACS-Canto II Flow Cytometer at the specified time points, in order to monitor the competition between the two populations.T0 was collected 4 days after infection. A non-targeting sgRNA was used as a negative control, while two sgRNAs targeting ATP2A2 were used as positive controls.

sgRNA	Sequence	Code
NT1	CTGAAAAAGGAAGGAGTTGA	
SMURF2-sg.1	AGAATACGCTTGATCCAAAG	Gecko_A45848
SMURF2-sg.2	TCTTCACAGTATCTGTAGAA	Gecko_B45794
CKS2-sg.1	CCACAAGCAGATCTACTACT	Gecko_B09782
CKS2-sg.2	CCGAGTAGTAGATCTGCTTG	Gecko_A09790
VRK1-sg.1	TTTAAGGAACCCAGTGACAA	Gecko_A53825
VRK1-sg.2	AACTTTAATTCAGTAAAAAG	Gecko_B53759
HASPIN-sg.1	GTCAGGATCGTCGGACTGCG	Gecko_A20424
HASPIN-sg.2	TGACTACACCCTGTCGCGCT	Gecko_A20425
ATP2A2-sg.1	CTCAATCACAAGTTCCAGCA	Gecko_A03607
ATP2A2-sg.2	ACAGAGTTACCGGCTGAAGA	Gecko_A03609
TRIM28-sg.1	TACCAGTAGAGCGCACAGTA	Gecko_A51449
TRIM28-sg.2	GACGCACCTGGTTCGCATCC	Gecko_A51450

Table 2. sgRNAs sequences

Alt-R Genome Editing Detection Kit

Infected cells were collected 1 week after the infection, washed with PBS and lysed with 50ul of QuickExtract DNA Extraction Solution (Lucigen, Wisconsin, USA). The lysate was incubated for 10 minutes at 65°C, then for 5 minutes at 98°C. Total lysed cells were diluted in 100ul of Nuclease-Free Water. PCR mixes were prepared with 4ul of genomic DNA, 300nM of specific primer pairs (see Table 3), 0.3mM of dNTPs (Promega, Milan, Italy), 0.3ul of Phusion High-Fidelity DNA Polymerase (Thermo Fisher Scientific, Waltham, Massachussets, USA), 5ul of 5x Phusion Polymerase HF Buffer (Thermo Fisher Scientific, Waltham, Massachussets, USA) and Nuclease-Free Water to a final volume of 25ul. The PCR reactions were performed on a Thermal Cycler (BioRad, Segrate, Italy) with the following protocol: 95°C for 3 minutes, 95°C for 30 seconds, 68°C for 30 seconds, 72°C for 1 minute. The last three steps were repeated decreasing the temperature from 68°C to 58°C. Then we performed 28 cycles as reported: 95°C for 30 seconds, 58°C for 30 seconds, 72°C for 1 minute. Finally, we formed homo/heteroduplexes in 18ul of final volume using 10ul of PCR sample, 6ul of Nuclease-Free Water and 2ul of 10x T7E1 Reaction Buffer. We used the following protocol: 95°C for 10 minutes, from 95°C to 85°C decreasing 2°C/second, from 85°C to 25°C decreasing 0.3°C/second. The homo/heteroduplexes were digested with 2ul of T7 Endonuclease 1 (1U/ul) for 1h at 37°C. The digestion products were analysed on a 1% agarose gel and visualized with BioRad GelDoc EZ Imaging System.

Target	Forward Primer	Reverse Primer
SMURF2	AAAGAAGCCTATTCAGTGCAA	TTCATGACCCCATTCCTCGG
VRK1	GGAAAGGAATGGGATTTTGGCA	TGGCTCTCTACCTTGATATCCTG
HASPIN-sg.2	ACGCTGTGAGAAGATTGGGG	CCCAGCGGTTGTTATTCTCCT
ATP2A2	AAGGCCTCTGACCGTTCTTG	TCTAAGACCATGCCACACTCTG

Table 3. Alt-R Primers

siRNA Transfections

For RNA Interference transfections we used Silencer Select siRNA oligos (Thermo Fisher Scientific, Waltham, Massachusetts, USA) targeting TRIM28, B-MYB, and FOXM1; a Silencer siRNA was used to silence LINC00941; a non-targeting Silencer Select siRNA was used as control (Table 4). Transfections were performed with the Lipofectamine RNAiMAX reagent (Thermo Fisher Scientific, Waltham, Massachusetts, USA). We used a reverse transfection protocol using 15 nM of each siRNA. A mix containing 7.5 ul of RNAiMAX and 15 nM of siRNA in 300 ul of OptiMEM was prepared for each 6-well reaction and incubated for 20 minutes at RT. Meantime cells were trypsinized and counted. The reaction mix was placed in the wells followed by the cells, we used 500000 MSTO-211H or 400000 NCI-H2052 cells/well. The cells were harvested either 48 or 72 h after transfection for qRT-PCRs, Western Blot, apoptosis and cell cycle analyses. For proliferation, scratch wound-healing and invasion assays and immunofluorescence, cells were harvested and seeded in the respective culture plates 24h after transfection.

Gene Target	Manufacturer	Code	Sequence/siRNA ID
Negative control	Silencer Select siRNA (Thermo Fisher Scientific)	4390847	
TRIM28	Silencer Select siRNA (Thermo Fisher Scientific)	4390824	S19778
B-MYB	Silencer Select siRNA (Thermo Fisher Scientific)	4392420	s9117
FOXM1	Silencer Select siRNA (Thermo Fisher Scientific)	4392420	s5248
LINC00941	Silencer siRNA (Thermo Fisher Scientific)	AM16708	268339

Table 4. siRNAs

Proliferation and Colony Forming Assays

For proliferation assays, MSTO-211H and NCI-H2052 cells were seeded 24h post transfection at a density of 2500 cells/well in a 96-well plate. Images were recorded every 6 hours for 96 hours by the Incucyte ® S3 Live-Cell Analysis System (Sartorius). Growth curves were obtained by confluence ratio relative to 0h.

For colony forming assays, cells were seeded 24h post transfection in 10 cm culture dishes at density of 10000 cells (MSTO-211H) or 2500 cells (NCI-H2052) per dish. Fresh medium was replaced every 2 days for 10 days. The dishes were washed with 1X PBS and fixed with methanol. Colonies were then stained with Crystal Violet solution (0,5% in H_2O) and counted using the ImageJ software.

RNA Extraction, Reverse Transcription and quantitative real-time PCR (qRT-PCR)

Total RNA was extracted from transfected or infected cells with Maxwell® RSC simplyRNA Cells (Promega, Madison, Wisconsin, USA) and quantified with Nanodrop 2000/2000c Spectophotometer (Thermo Fisher Scientific, Waltham, Massachusetts, USA). 500/1000 ng of RNA was retrotranscribed with iScript cDNA kit (Biorad, Hercules, California, USA). Total RNA was mixed with 1ul of RT enzyme, 5x iScript Buffer and Nuclease free water to a total volume of 20 ul. The reaction was performed in thermal cycler using the following protocol: 25°C for 5 min (priming), 45°C for 1h (RT reaction) and 95°C for 1 min (RT inactivation). The obtained cDNA was diluted with Nuclease Free Water (we used 10 ng DNA/well for qRT-PCR reactions). Quantitative real-time PCR (qRT-PCR) was performed using Sso Fast EvaGreen Super Mix (Biorad, Hercules, California, USA) in the CFX96 Real Time PCR Detection System (Biorad, Hercules, California, USA). We used the following protocol: 40 cycles of 95°C for 30 sec, 95°C for 5 sec, 59°C for 5 secRelative expression of target genes was calculated using the $2^{-\Delta\Delta Ct}$ method by normalizing to the reference gene expression Cyclophilin A (*CYPA*). qRT-PCR primers are listed in Table 5.

Target Gene	Forward Primer	Reverse Primer
TRIM28	CAAGATTGTGGCAGAGCGTCCT	CATAGCCTTCCTGCACCTCCAT
AURKA	TCCTGAGGAGGAACTGGCATCAAA	TACCCAGAGGGCGACCAATTTCAA
AURKB	ATCAGCTGCGCAGAGAGATCGAAA	CTGCTCGTCAAATGTGCAGCTCTT
BIRC5	CATCTCTACATTCAAGAACTGG	GGTTAATTCTTCAAACTGCTTC
B-MYB	CACCAGAAACGAGCCTGCCTTA	CTCAGGTCACACCAAGCATCAG
BUB1	GCCATCAAGCCCAAGACTGA	ATCTCCCTGGGTAGCTTCGT
CCNB1	TCCATTATTGATCGGTTCATGC	TCAGTCACAAAAGCAAAGTCACC
CDC20	AGTTCGCGTTCGAGAGTGAC	GGAGTGGTCTGAACCTTGGA
CDCA8	CAGTGACTTGCAGAGGCACAGT	CTCATTTGTGGGTCCGTATGCTG
CIT	AGCACAAGGCTGAGATTCTCGC	CTCGTTCAGTCTCCAGCTTCTG
FOXM1	TCTGCCAATGGCAAGGTCTCCT	CTGGATTCGGTCGTTTCTGCTG
INCENP	GACTCCACCGATGATGAGGC	AGGTTCGGTGGGTGGTAGTA
KIF14	GCACTTTCGGAACAAGCAAACCA	ATGTTGCTGGCAGCGGGACTAA
KIF20A	AGTATCCCAGGAGGAGCAAGT	ATCGTCATCGGACAGCAAGC

KIF23	GTAGCAAGACCTGTAGACAAGGC	TTCGCATGACGGCAAAGGTGGA
PAK2	TGAGCAGAGCAAACGCAGTA	AGGGCCATAAGCTTTCCGTG
PLK1	AGAAGACCCTGTGTGGGACT	ACCTCGAAACTGTGCCCTTT
PRC1	ATAGCCAGGAGCAGAGACAAGC	AACCGCACAATCTCAGCATCGTG
PRKCA	GCCTATGGCGTCCTGTTGTATG	GAAACAGCCTCCTTGGACAAGG
RACGAP1	ATGCTGGCAGACTTTGTGTCCC	CAGCCAGAGATCCTATACAGGC
TOP2A	GTGGCAAGGATTCTGCTAGTCC	ACCATTCAGGCTCAACACGCTG
TPX2	TTCAAGGCTCGTCCAAACACCG	GCTCTCTTCTCAGTAGCCAGCT
TYMS	GGTGTTTTGGAGGAGTTGCTGTG	GGAGAATCCCAGGCTGTCCAAA
UBE2S	CGATGGCATCAAGGTCTTTCCC	CAGCAGGAGTTTCATGCGGAAC
VRK1	GTTGGCAGTGATGCACCTTGTG	AGGAACACCCAGGTACTTCAGC
ZWINT	AGGCATCTTGGAACCTGTAGGC	GGAAATCCGCTACCTGAAGCTG
LINC00941	TTTTGTGTCCAAGCCCCAGA	GCCAAGAGTACAAGTCCAGC
CHCHD2	GTGGAGGAAGTAATGCTGAGCC	CACAGAGCTTGATGTCACCCTG
CYB5R4	CTCTTCACACCAGAGCTTGATCG	CCATTGGTGTGAAGCCTGTTCC
EGLN1	TGATACGCCACTGTAACGGG	CCATTGCCCGGATAACAAGC
ENO1	TTGCAGTCGTGTAATTGGCC	TCATGGGTCACTGAGGCTTT
FAM162A	ATTGCCCTGACGGTGGTAGGAT	CTGCTTCCTCTTTCAGACGAGC
GAPDH	ATTGGGCGCCTGGTCAC	AACATGTAAACCATGTAGTTGAGCTCA
HBEGF	GGAAGAAGAGGGACCCATGT	CTCTCCATGGTAACCCGGG
HIF1A	CTGAGGGGACAGGAGGATCA	AAAGGCAAGTCCAGAGGTGG
HMOX1	CCAGGCAGAGAATGCTGAGTTC	AAGACTGGGCTCTCCTTGTTGC
HYOU1	CTTCAACCTGGATGAGAGTGGC	ACAGGCTGGAAATGGTGTTGCC
PAI1	ACAACAGGAGGAGAAACCCA	AGCTCCTTGTACAGATGCCG
PDK1	CATGTCACGCTGGGTAATGAGG	CTCAACACGAGGTCTTGGTGCA
PGK1	ACTCGGGCTAAGCAGATTGT	GTGCTCACATGGCTGACTTT
PLAU	GGCTCTGTCACCTACGTGTG	CTTGAGCGACCCAGGTAGAC
VEGFA	CTACCTCCACCATGCCAAGT	GCAGTAGCTGCGCTGATAGA
VEGFC	GCCAATCACACTTCCTGCCGAT	AGGTCTTGTTCGCTGCCTGACA

Table 5. qRT-PCR primers

Western Blot

Total proteins were extracted with 5x Passive Lysis Buffer (PLB) (Promega, Madison, Wisconsin, USA) diluted to 1x with water and supplemented with Protease Inhibitor Cocktail (Roche) and phosphatase inhibitor cocktail PhosSTOP (Roche). Protein extracts were incubated on ice for 20 minutes and quantified using the Bradford reagent (Biorad, Hercules, California, USA). Equal amounts of protein lysates were resolved by SDS-PAGE using Mini-Protean TGX pre-cast gels (Biorad, Hercules, California, USA). Proteins were transferred to

a nitrocellulose membrane using the Turbo Blot system (Biorad, Hercules, California, USA). The nitrocellulose membrane was stained with 0.5% Ponceau in 5% acetic acid for 5 minutes to check the loading and then washed 5 minutes with a solution containing PBS 1X and Tween 0.01% (Sigma-Aldrich, Milan, Italy). Next, the membrane was incubated in blocking solution (PBS 1X, Tween 0.01% and Milk 5%). Primary and secondary antibodies with their specificities are listed in Table 6. Finally, the protein signal was acquired with ChemiDoc Imaging System (Biorad, Hercules, California, USA).

Name	***Code***	***Manufacturer***	***Dilution***
TRIM28	10484	Abcam	1:1000
TRIM28	22553	Abcam	1:10000
TRIM28 (C42G12)	4124	Cell Signaling Technology	1:1000
β-Actin (AC-15)	A1978	Sigma Aldrich	1:10000
BAX	AB-10230	Immunological Sciences	1:1000
B-MYB clone LX015.1	MABE866	Merck Millipore	1:1000
CDK9 (EPR22956-37)	239364	Abcam	1:1000
FoxM1 (D3F2B)	20459	Cell Signaling Technology	1:1000
p-CDK1 (10A11)	4539	Cell Signaling Technology	1:1000
CDK1	9116	Cell Signaling Technology	1:1000
CCNB1	245	Santa Cruz Biotechnology	1:500
CDC20	13162	Santa Cruz Biotechnology	1:1000
AURKA (D3E4Q)	14475	Cell Signaling Technology	1:1000
AURKB	3094	Cell Signaling Technology	1:1000
CDCA8 (A-5)(Borealin)	376635	Santa Cruz Biotechnology	1:1000
BIRC5 (B-8)(Survivin)	17779	Santa Cruz Biotechnology	1:500
H3-pSer10	06570	Merck Millipore	1:1000
H3	4499	Cell Signaling Technology	1:5000
RNA-PolII (D8L4Y)	14958	Cell Signaling Technology	1:1000
RNA-PolII-Ser2 (E1Z3G)	13499	Cell Signaling Technology	1:1000
RNA-PolII-Ser5 (D9N5I)	13523	Cell Signaling Technology	1:1000
RBBP4 (EPR3411)	79416	Abcam	1:5000
HIF1α	3716S	Cell Signaling Technology	1:1000
EGLN1	NB100-137	Novus Biologicals	1:1000
Anti-Rabbit IgG	NA934	Amersham	1:5000
Anti-Mouse IgG	NXA931	Amersham	1:5000

Table 6. Primary and Secondary Antibodies for Western Blot

Apoptosis Analysis

72h post transfection, 100000 cells were collected, washed and resuspended in 300ul of 1x Annexin Buffer (in water) (BD Bioscences) and stained with 2.5ul of PE Annexin V and 2.5ul of 7-Amino-Actinomycin (7AAD) (BD Bioscences). After 20 minutes of incubation at +4°C and in the dark, cells were centrifuged and resuspended in 300ul of 1x Annexin buffer and analysed using a FACS Canto II Flow Cytometer (BD Bioscences). Data analysis was performed with FACS DIVA Software (BD Bioscences). Graphs report the ratio of positive cells to either 7AAD or Annexin V compared to ctrl cells.

Cell Cycle Analysis

24h after transfection, $2*10^5$ MSTO-211H cells and $1,5*10^5$ NCI-H2052 cells were seeded in 12-well plates previously coated with Matrigel matrix (Corning) 1:100 in culture medium for 2h. 6h after plating, culture medium was removed and replaced with medium containing 0,5 mM of hydroxyurea (HU) (Sigma-Aldrich, St. Louis, Missouri, USA). 16h after treatment, cells were released in fresh medium and time point 0 has been collected. The cells were collected every 3 hours, up to 12h, washed in PBS and resuspended in Nicoletti solution (0.1% sodium citrate, 0.1% Triton X-100, 50 ug/ml Propidium Iodide in water). After 5 min incubation at +4°C, cells were analyzed by FACS Canto II Flow Cytometer (BD Bioscences). Data analysis was performed with FACS DIVA Software (BD Bioscences).

Immunofluorescence

Immunofluorescence was performed by coating 4-chamber slides (Thermo Fisher Scientific, Waltham, Massachusetts, USA) with Matrigel matrix (Corning) 1:100 in culture medium. 2h after incubation, Matrigel was removed and replaced with cells. We seeded $1*10^5$ MSTO-211H or $8*10^4$ NCI-H2052 cells, 24h post transfection. Cells transfected with siLINC00941 were analysed at 72h post transfection. For the analysis of synchronized cells, they were treated with 0.5 mM of HU (Sigma-Aldrich, St. Louis, Missouri, USA) 6h after plating. 16h after treatment, cells were released in fresh medium and analysed 12h post release. For cells treated with CDK9i, 6h after plating they were treated for 24h and analysed.

Cells were washed in PBS 1X and fixed with 4% paraformaldehyde (in PBS 1X) for 15 min at room temperature (RT). Permeabilization was performed with 0.1% of Triton X-100 (in PBS 1X) for 2 minutes. Cells were blocked with 2% BSA in PBS solution, supplemented with 20% of FBS for 45 minutes. Primary antibodies were diluted in 2% BSA/PBS and incubated at RT for 2h. Secondary antibodies were diluted in 2% BSA/PBS and incubated at RT for

1h. The antibodies used are listed in Table 7. Nuclei were stained with DAPI. Images were acquired with a Nikon Eclipse fluorescence microscope. Counts were performed on 3 different slides, counting at least 300 nuclei per slide.

Name	***Code***	***Manufacturer***	***Dilution***
β-Tubulin	23949	Santa Cruz Biotechnology	1:100
AURKA (D3E4Q)	14475	Cell Signaling Technology	1:100
AURKB	3094	Cell Signaling Technology	1:100
H3-pSer10	CMA312	Merck Millipore	1:100
Alexa Fluor 488 Phalloidin	A12379	Thermo Fisher Scientific	1:40
Alexa Fluor 594 Phalloidin	A12381	Thermo Fisher Scientific	1:400
Alexa Fluor 488 goat anti-mouse IgG	A11001	Thermo Fisher Scientific	1:1000
Alexa Fluor 594 goat anti-rabbit IgG	A11012	Thermo Fisher Scientific	1:1000

Table 7. Primary and Secondary Antibodies for Immunofluorescence

RNA-Seq and Bioinformatics Analysis

For TRIM28 KO RNA-seq, RNA was collected 7 days after infection of MSTO-211H/Cas9 cells using two sgRNAs targeting TRIM28 and a non-targeting sgRNA as a control, in two independent experiments. For LINC00941 KD RNA-seq, RNA was collected 72h post transfection, in two independent experiments. RNA was quantified using Nanodrop (Thermo Fisher Scientific, Waltham, Massachusetts, USA) and quality assessment was performed by Bioanalyzer RNA 6000 nano kit (Agilent Technologies, Santa Clara, California, USA). RNAseq libraries were obtained starting from 500ng of total RNA following Illumina TruSeq Stranded Total RNA preparation protocol (Illumina, San Diego, California, USA). Sequencing was performed using Illumina NextSeq 500 platform (Illumina, San Diego, California, USA) on high-output cartridge (2X75). Sequencing quality was assessed using the FastQC v0.11.8 software (www.bioinformatics.babraham.ac.uk/projects/fastqc/). Raw sequences were then aligned to the human reference transcriptome (GRCh38, Gencode release 30) using STAR version 2.7 (Dobin et al., 2013) and gene abundances were estimated with RSEM algorithm (v1.3.1) (B. Li & Dewey, 2011). Differential expression analysis was performed using DESeq2 R package (Love et al., 2014), considering a False Discovery Rate (FDR) of 10% and excluding genes with low read counts. Only genes coherently de-regulated by both sgRNAs were considered. Significant deregulated genes underwent to enrichment analysis, performed on Gene Ontology biological processes, KEGG and Reactome pathways databases via enrichR package (Kuleshov et al., 2016) and ClueGO (Bindea et al., 2009)via Cytoscape for graphical purpose, using a significance

threshold of 0.05 on p-value corrected for multiple testing using Benjamini–Hochberg method. Data for TRIM28 KO RNA-seq are available at ArrayExpress (E-MTAB-10942).

ChIP-seq analysis

KAP1, CDK9, RNA-PolII and S2RNA-PolII ChIP-sequencing data were retrieved from GEO repository (GSE72622) (McNamara, Guzman, et al., 2016). The significance of the binding profiles was assessed (q-value<0.05) and peaks were then annotated using ChIPseeker R package to the nearest genes using a TSS region of ±3kb.

Co-Immunoprecipitation (Co-IP)

For the Co-IP of endogenous TRIM28 and RNA-PolII, 5x15cm plates of MSTO-211H cells were grown to 80% of confluence. The cells were crosslinked with 1% formaldehyde at RT for 15 minutes, gently rocking. The crosslinking was quenched with a final concentration of glycine of 250mM for 5 minutes at RT. After washing the cells three times with cold PBS, the proteins' extracts were obtained with a modified version of the RIPA Buffer (50mM Tris-HCl pH 7.5, 1mM EDTA, 150mM NaCl, 0.5% NP-40, 5% Glycerol, plus protease and phosphatase inhibitors) and incubated in ice for 15 minutes. In combination with the lysis buffer, a dounce homogenization was performed to further facilitate the cells' disruption. The extract was pre-cleared with Protein G-Sepharose (Cytiva) and then incubated overnight with the antibody. The day after, the Protein G-Sepharose were added for two hours, and then the IP was washed three times with a modified version of TBS (50mM Tris-HCl pH 7.5, 250mM NaCl). The endogenous Co-IP of TRIM28, CDK9, FOXM1 and RBBP4, was performed following the same protocol but without crosslinking. The antibodies used are reported in Table 8.

Name	***Code***	***Manufacturer***	***Dilution***
TRIM28	10483	Abcam	1ug/mg
TRIM28	22553	Abcam	2ug/mg
FoxM1 (D3F2B)	20459	Cell Signaling Technology	1:50
CDK9 (EPR22956-37)	239364	Abcam	1ug/mg
Normal Rabbit IgG	2729	Cell Signaling Technology	1ug/mg
Normal Mouse IgG	2025	Santa Cruz Biotechnology	2ug/mg

Table 8. List of Primary and Secondary antibodies used for Co-IP

ChIP-qPCR

To perform ChIP experiments, we used the SympleChIP Enzymatic Chromatin IP Kit with Magnetic Beads protocol (Cell Signaling #9003) and followed the manufacturer instructions. $8x10^6$ cells were used for each IP. For ChIP performed on transfected cells, we performed reverse transfections in T175 by scaling up reagents from the 6-well condition described above. 48h after transfection, the cells were collected, counted, and crosslinked with 1% formaldehyde for 10 minutes at RT. The crosslinking was quenched with 250mM of glycine for 5 minutes at RT. Cells were then centrifuged and washed two times in ice-cold PBS 1X and subsequent steps were performed as described to isolate nuclei. Chromatin fragmentation was obtained by adding 1ul of Micrococcal Nuclease to each IP for 20 min at 37°C with frequent mixing. Digestion was stopped by adding 10ul of EDTA per IP for 2 min on ice. We then sonicated nuclei for 8 cycles (30 sec ON and 30 sec OFF) to break nuclear membranes, using a Bioruptor Pico sonicator (Diagenode, Milan, Italy). Lysates were clarified by 10 minutes of centrifugation. After resuspending the lysates in ChIP buffer, the input sample was taken and stored at -20°C. The remaining samples were divided based on the IP to be performed and incubated with the antibodies overnight at 4°C with rotation. The day after, 30ul of magnetic beads were added to each IP and incubated for 2h at 4°C with rotation. After three low salt and one high salt washes, chromatin was eluted from antibody/magnetic beads complexes with 150ul of Elution Buffer for 30 minutes at 65°C with gentle vortexing. Eluted chromatin was reverse cross-linked with 6ul of 5M NaCl and 2ul of Proteinase K for 2h at 65°C. DNA was then purificated using spin columns. The antibodies used are listed in Table 9. qPCRs were performed using the SsoFast EvaGreen Supermix (Biorad, Hercules, California, USA) following the manufacturer's instructions. Primers sequences are reported in Table 10.

Name	***Code***	***Manufacturer***	***Dilution***
Rpb1 NTD (D8L4Y)	14958	Cell Signaling Technology	1:50
Phospho-Rpb1 CTD (Ser2) (E1Z3G)	13499	Cell Signaling Technology	1:50
Normal Rabbit IgG	2729	Cell Signaling Technology	1:50
TRIM28	10483	Abcam	

Table 9. List of Primary and Secondary antibodies used for ChIP

Primer Name	**Forward Primer**	**Reverse Primer**
AURKB-Promoter	ACAGGACATCGAGCCAATGG	AACAACTGAATCTGCCACGC
AURKB-Genebody#1	CACCTACCCCCAATTCAAAGAGA	ATATGGGACTATGAGCAGAGGCT
AURKB-Genebody#2	TTACCATTGGCCCCTACAGG	GAGCCGAGATTACGCCATTG

AURKB-Terminal	ATGCACTCTCAAAGGGTGGG	CCAGAGATGATTGAGGGGCG
MYBL2-Promoter	CTTTCCCTGGCTGGCTCTC	CTGGCTCACGTGTCAGTCC
FOXM1-Promoter	GACCGCACAGCCTTCGAG	TGTTTGAAATTGGCGCCGG
CCNB1-Promoter	AATAAGGAGGGAGCAGTGCG	ACACCCAGCAGAAACCAACA
CDC20-Promoter	TGCGACGGTTGGATTTTGAA	CCACCACCTCTCACCGTG
PLK1-Promoter	AATTCGGGGAGGAGCGGA	CAGCACTCATGCTCCCGAAG
INCENP-Promoter	GCCTCTTAGTCCCGCAGATT	CAATCCTCGGCAAGTTTGTCC
BIRC5-Promoter	CTTTGAAAGCAGTCGAGGGG	GTGTGCCGGGAGTTGTAGTC
CD69-Promoter	AATCCCACTTTCCTCCTGCT	GCCGCCTACTTGCTTGACTA

Table 10. List of primers used for ChIP-qPCR

Patients Selection and Nanostring Analysis

A retrospective cohort of 97 MPM consecutive patients was retrieved from the Pathology Unit of our Institution between 2010 and 2021. Inclusion criteria were availability of Formalin Fixed Paraffin Embedded (FFPE) tumor tissues and follow up information. The main endpoint of this analysis was the association between gene expression profiles in tumor specimens and patients' survival. The median overall survival was 15 months (IQR 9-25). Histological sections of all samples were revised by two different pathologists. Project was approved by local ethic committees.

Total RNA was extracted by Maxwell® RSC RNA FFPE kit (Promega) starting from 5 slides of 5µm FFPE tissue. RNA quantity and quality were assessed by NanoDrop 2000 (Thermo Fisher Scientific, Waltham, Massachussets, USA). 86 samples reached the RNA quality standard required (A260/A280 ≥ 1.7 and A260/A230 ≥ 1.8) and we evaluated the expression profile by NanoString using a custom panel called MPM_C9073 (NanoString Technologies) following manufacturers' protocol. This panel was specifically designed on this purpose, including 70 genes among which KAP1, 36 genes identified as KAP1's target, 17 genes considered essential for MPM survival and 20 housekeeping genes.

Analysis of detected gene counts was performed by nSolver Analysis Software 4.0 (NanoString Technologies). For samples that passed imaging quality controls, raw genes counts were normalized on technical controls and three housekeeping genes (AMMECR1L, ERCC3, ZNF346) among the ones included in the panel as previously described. The complete matrix of normalized counts is available at GEO repository (accession number: GSE183088). Gene expression values of KAP1 and its target genes were correlated using Spearman method.

Then patients were stratified according to OS and Fold Changes (FCs) were calculated as ratio between the expression profile of short- survival samples (1st quartile- 20/86) and long-survival samples (4th quartile-22/86). For each comparison pValue (as two-tailed Student's t test) and False Discovery Rate (FDR) obtained by Benjamini-Hochberg method, were calculated. For survival analysis, patients were dichotomized on the basis of 1st and 4th quartile of genes expression, and hazard ratio was calculated by Cox Model corrected for chemotherapy treatment. Bioinformatic analyses on GEP was conducted by R Software v4.0.3 using the following R packages: corrplot, ggplot2, ggbiplot (function prcomp) and survival.

CDKs inhibitors

MSTO-211H and NCI-H2052 transfected cells (siCTRL/siTRIM28) were collected 24h post-transfection and seeded on previously coated Matrigel (Corning) wells. For proliferation assays, cells were seeded at 2500 cells/well in 96-well plates. 6 hours later, culture medium was removed and replaced with medium containing the following drugs: AT7519 and AZD4573 (Selleckchem, Munich, Germany) or the respective control. Both drugs were resuspended in DMSO (Sigma-Aldrich, St. Louis, Missouri, USA). Proliferation assays were conducted as described above. EC50 was calculated with Incucyte ® S3 Live-Cell Analysis System (Sartorius). For qPCRs, cells were treated with AZD4573 for 24h and collected at 72h post transfection.

Scratch Wound Healing Assay

24h after transfection, 60000 MSTO-211H or 40000 NCI-H2052 were seeded in 96-well plates previously coated with Matrigel matrix (Corning) 1:100 in culture medium for 2h. Cells were treated with Mytomicin (Sigma Aldrich, Milan, Italy) at the concentration of 10ug/ml for 2h. Then we replaced the medium with normal complete culture medium. Scratches were applied using a pipette tip. Healing areas were captured at 0, 3 and 6 hours after the scratch using Incucyte ® S3 Live-Cell Analysis System (Sartorius).

Invasion Chamber Assay

72h after transfection, $3*10^4$ MSTO-211H or $2*10^4$ NCI-H2052 cells were seeded in a Matrigel Invasion Chamber or control chambers (CT insert) (BD Biosciences, San Jose, California) in serum-free medium, in triplicate. Complete medium containing 10% FBS was used as chemo-attractant. 24h later, invading cells were fixed with methanol and stained

with a 0.5% Crystal Violet solution in water. Pictures were obtained with a Nikon Ti-E inverted microscope. Three fields for each well were captured and invading cells were manually counted. To obtain the graphs, we divided the cells in the Matrigel Invasion Chamber with the cells in the control insert for each condition.

$CoCl_2$ treatment

$CoCl_2$ was resuspended in water freshly before use. For qRT-PCR and western blot analysis, 72h post transfections cells were treated with 200 uM of $CoCl_2$ for 5h and analysed as described above.

Statistical Analysis

Statistical analysis was performed using GraphPad Prism Software (GraphPad Software, San Diego, California, USA). Statistical significance was determined using the Student's *t* test. Each experiment was performed 2 to 6 times. Threshold for significance was considered p-value <0.05.

REFERENCES

Addison, J. B., Koontz, C., Fugett, J. H., Creighton, C. J., Chen, D., Farrugia, M. K., Padon, R. R., Voronkova, M. A., McLaughlin, S. L., Livengood, R. H., Lin, C.-C., Ruppert, J. M., Pugacheva, E. N., & Ivanov, A. V. (2015). KAP1 promotes proliferation and metastatic progression of breast cancer cells. *Cancer Research*, *75*(2), 344–355. https://doi.org/10.1158/0008-5472.CAN-14-1561

Ahmadzada, T., Reid, G., & Kao, S. (2018). Biomarkers in malignant pleural mesothelioma: Current status and future directions. *Journal of Thoracic Disease*, *10*(Suppl 9), S1003–S1007. https://doi.org/10.21037/jtd.2018.04.31

Ai, Y., Wu, S., Zou, C., & Wei, H. (2020). LINC00941 promotes oral squamous cell carcinoma progression via activating CAPRIN2 and canonical WNT/β-catenin signaling pathway. *Journal of Cellular and Molecular Medicine*, *24*(18), 10512–10524. https://doi.org/10.1111/jcmm.15667

Alcon, C., Manzano-Muñoz, A., & Montero, J. (2020). A New CDK9 Inhibitor on the Block to Treat Hematologic Malignancies. *Clinical Cancer Research: An Official Journal of the American Association for Cancer Research*, *26*(4), 761–763. https://doi.org/10.1158/1078-0432.CCR-19-3670

Alexander, R. P., Fang, G., Rozowsky, J., Snyder, M., & Gerstein, M. B. (2010). Annotating non-coding regions of the genome. *Nature Reviews. Genetics*, *11*(8), 559–571. https://doi.org/10.1038/nrg2814

Anshabo, A. T., Milne, R., Wang, S., & Albrecht, H. (2021). CDK9: A Comprehensive Review of Its Biology, and Its Role as a Potential Target for Anti-Cancer Agents. *Frontiers in Oncology*, *11*, 678559. https://doi.org/10.3389/fonc.2021.678559

Bacon, C. W., Challa, A., Hyder, U., Shukla, A., Borkar, A. N., Bayo, J., Liu, J., Wu, S.-Y., Chiang, C.-M., Kutateladze, T. G., & D'Orso, I. (2020). KAP1 Is a Chromatin Reader that Couples Steps of RNA Polymerase II Transcription to Sustain Oncogenic Programs. *Molecular Cell*, *78*(6), 1133-1151.e14. https://doi.org/10.1016/j.molcel.2020.04.024

Barlaam, B., Casella, R., Cidado, J., Cook, C., De Savi, C., Dishington, A., Donald, C. S., Drew, L., Ferguson, A. D., Ferguson, D., Glossop, S., Grebe, T., Gu, C., Hande, S., Hawkins, J., Hird, A. W., Holmes, J., Horstick, J., Jiang, Y., … Yao, T. (2020). Discovery of AZD4573, a Potent and Selective Inhibitor of CDK9 That Enables Short Duration of Target Engagement for the Treatment of Hematological Malignancies. *Journal of Medicinal Chemistry*, *63*(24), 15564–15590. https://doi.org/10.1021/acs.jmedchem.0c01754

Betti, M., Aspesi, A., Biasi, A., Casalone, E., Ferrante, D., Ogliara, P., Gironi, L. C., Giorgione, R., Farinelli, P., Grosso, F., Libener, R., Rosato, S., Turchetti, D., Maffè, A., Casadio, C., Ascoli, V., Dianzani, C., Colombo, E., Piccolini, E., … Dianzani, I. (2016). CDKN2A and BAP1 germline mutations predispose to melanoma and mesothelioma. *Cancer Letters*, *378*(2), 120–130. https://doi.org/10.1016/j.canlet.2016.05.011

Bianchi, A. B., Mitsunaga, S. I., Cheng, J. Q., Klein, W. M., Jhanwar, S. C., Seizinger, B., Kley, N., Klein-Szanto, A. J., & Testa, J. R. (1995). High frequency of inactivating mutations in the neurofibromatosis type 2 gene (NF2) in primary malignant mesotheliomas. *Proceedings of the National Academy of Sciences of the United States of America*, *92*(24), 10854–10858. https://doi.org/10.1073/pnas.92.24.10854

Bianchi, C., & Bianchi, T. (2007). Malignant mesothelioma: Global incidence and relationship with asbestos. *Industrial Health*, *45*(3), 379–387. https://doi.org/10.2486/indhealth.45.379

Bindea, G., Mlecnik, B., Hackl, H., Charoentong, P., Tosolini, M., Kirilovsky, A., Fridman, W.-H., Pagès, F., Trajanoski, Z., & Galon, J. (2009). ClueGO: A Cytoscape plug-in to decipher functionally grouped gene ontology and pathway annotation networks. *Bioinformatics (Oxford, England)*, *25*(8), 1091–1093. https://doi.org/10.1093/bioinformatics/btp101

Brattås, P. L., Jönsson, M. E., Fasching, L., Nelander Wahlestedt, J., Shahsavani, M., Falk, R., Falk, A., Jern, P., Parmar, M., & Jakobsson, J. (2017). TRIM28 Controls a Gene Regulatory Network Based on Endogenous Retroviruses in Human Neural Progenitor Cells. *Cell Reports*, *18*(1), 1–11. https://doi.org/10.1016/j.celrep.2016.12.010

Bridges, M. C., Daulagala, A. C., & Kourtidis, A. (2021). LNCcation: LncRNA localization and function. *The Journal of Cell Biology*, *220*(2), e202009045. https://doi.org/10.1083/jcb.202009045

Bueno, R., Stawiski, E. W., Goldstein, L. D., Durinck, S., De Rienzo, A., Modrusan, Z., Gnad, F., Nguyen, T. T., Jaiswal, B. S., Chirieac, L. R., Sciaranghella, D., Dao, N., Gustafson, C. E., Munir, K. J., Hackney, J. A., Chaudhuri, A., Gupta, R., Guillory, J., Toy, K., … Seshagiri, S. (2016). Comprehensive genomic analysis of malignant pleural mesothelioma identifies recurrent mutations, gene fusions and splicing alterations. *Nature Genetics*, *48*(4), 407–416. https://doi.org/10.1038/ng.3520

Bunch, H., Zheng, X., Burkholder, A., Dillon, S. T., Motola, S., Birrane, G., Ebmeier, C. C., Levine, S., Fargo, D., Hu, G., Taatjes, D. J., & Calderwood, S. K. (2014). TRIM28 regulates RNA polymerase II promoter-proximal pausing and pause release. *Nature Structural & Molecular Biology*, *21*(10), 876–883. https://doi.org/10.1038/nsmb.2878

Cancer Genome Atlas Research Network, Weinstein, J. N., Collisson, E. A., Mills, G. B., Shaw, K. R. M., Ozenberger, B. A., Ellrott, K., Shmulevich, I., Sander, C., & Stuart, J. M. (2013). The Cancer Genome Atlas Pan-Cancer analysis project. *Nature Genetics*, *45*(10), 1113–1120. https://doi.org/10.1038/ng.2764

Carbone, M., Ly, B. H., Dodson, R. F., Pagano, I., Morris, P. T., Dogan, U. A., Gazdar, A. F., Pass, H. I., & Yang, H. (2012). Malignant mesothelioma: Facts, myths, and hypotheses. *Journal of Cellular Physiology*, *227*(1), 44–58. https://doi.org/10.1002/jcp.22724

Cassandri, M., Fioravanti, R., Pomella, S., Valente, S., Rotili, D., Del Baldo, G., De Angelis, B., Rota, R., & Mai, A. (2020). CDK9 as a Valuable Target in Cancer: From Natural Compounds Inhibitors to Current Treatment in Pediatric Soft Tissue Sarcomas. *Frontiers in Pharmacology*, *11*, 1230. https://doi.org/10.3389/fphar.2020.01230

Chandra Gupta, S., & Nandan Tripathi, Y. (2017). Potential of long non-coding RNAs in cancer patients: From biomarkers to therapeutic targets. *International Journal of Cancer*, *140*(9), 1955–1967. https://doi.org/10.1002/ijc.30546

Chang, L., Zhou, D., & Luo, S. (2021). Novel lncRNA LINC00941 Promotes Proliferation and Invasion of Colon Cancer Through Activation of MYC. *OncoTargets and Therapy*, *14*, 1173–1186. https://doi.org/10.2147/OTT.S293519

Chen, L., Chen, D.-T., Kurtyka, C., Rawal, B., Fulp, W. J., Haura, E. B., & Cress, W. D. (2012). Tripartite motif containing 28 (Trim28) can regulate cell proliferation by bridging HDAC1/E2F interactions. *The Journal of Biological Chemistry*, *287*(48), 40106–40118. https://doi.org/10.1074/jbc.M112.380865

Chen, L., Muñoz-Antonia, T., & Cress, W. D. (2014). Trim28 contributes to EMT via regulation of E-cadherin and N-cadherin in lung cancer cell lines. *PloS One*, *9*(7), e101040. https://doi.org/10.1371/journal.pone.0101040

Cheng, K. C., Cahill, D. S., Kasai, H., Nishimura, S., & Loeb, L. A. (1992). 8-Hydroxyguanine, an abundant form of oxidative DNA damage, causes G----T and A----C substitutions. *The Journal of Biological Chemistry*, *267*(1), 166–172.

Cheung, M., Talarchek, J., Schindeler, K., Saraiva, E., Penney, L. S., Ludman, M., & Testa, J. R. (2013). Further evidence for germline BAP1 mutations predisposing to melanoma and malignant mesothelioma. *Cancer Genetics*, *206*(5), 206–210. https://doi.org/10.1016/j.cancergen.2013.05.018

Chew, S. H., & Toyokuni, S. (2015). Malignant mesothelioma as an oxidative stress-induced cancer: An update. *Free Radical Biology & Medicine*, *86*, 166–178. https://doi.org/10.1016/j.freeradbiomed.2015.05.002

Chi, P., Allis, C. D., & Wang, G. G. (2010). Covalent histone modifications—Miswritten, misinterpreted and mis-erased in human cancers. *Nature Reviews. Cancer*, *10*(7), 457–469. https://doi.org/10.1038/nrc2876

Chiappinelli, K. B., Strissel, P. L., Desrichard, A., Li, H., Henke, C., Akman, B., Hein, A., Rote, N. S., Cope, L. M., Snyder, A., Makarov, V., Budhu, S., Buhu, S., Slamon, D. J., Wolchok, J. D., Pardoll, D. M., Beckmann, M. W., Zahnow, C. A., Merghoub, T., … Strick, R. (2015). Inhibiting DNA Methylation Causes an Interferon Response in Cancer via dsRNA Including Endogenous Retroviruses. *Cell*, *162*(5), 974–986. https://doi.org/10.1016/j.cell.2015.07.011

Christensen, B. C., Godleski, J. J., Marsit, C. J., Houseman, E. A., Lopez-Fagundo, C. Y., Longacker, J. L., Bueno, R., Sugarbaker, D. J., Nelson, H. H., & Kelsey, K. T. (2008). Asbestos exposure predicts cell cycle control gene promoter methylation in pleural mesothelioma. *Carcinogenesis*, *29*(8), 1555–1559. https://doi.org/10.1093/carcin/bgn059

Christensen, B. C., Houseman, E. A., Godleski, J. J., Marsit, C. J., Longacker, J. L., Roelofs, C. R., Karagas, M. R., Wrensch, M. R., Yeh, R.-F., Nelson, H. H., Wiemels, J. L., Zheng, S., Wiencke, J. K., Bueno, R., Sugarbaker, D. J., & Kelsey, K. T. (2009). Epigenetic profiles distinguish pleural mesothelioma from normal pleura and predict lung asbestos burden and clinical outcome. *Cancer Research*, *69*(1), 227–234. https://doi.org/10.1158/0008-5472.CAN-08-2586

Christoph, D. C., & Eberhardt, W. E. E. (2014). Systemic treatment of malignant pleural mesothelioma: New agents in clinical trials raise hope of relevant improvements. *Current Opinion in Oncology*, *26*(2), 171–181. https://doi.org/10.1097/CCO.0000000000000053

Cidado, J., Boiko, S., Proia, T., Ferguson, D., Criscione, S. W., San Martin, M., Pop-Damkov, P., Su, N., Roamio Franklin, V. N., Sekhar Reddy Chilamakuri, C., D'Santos, C. S., Shao, W., Saeh, J. C., Koch, R., Weinstock, D. M., Zinda, M., Fawell, S. E., & Drew, L. (2020). AZD4573 Is a Highly Selective CDK9 Inhibitor That Suppresses MCL-1 and Induces Apoptosis in Hematologic Cancer Cells. *Clinical Cancer Research: An Official Journal of the American Association for Cancer Research*, *26*(4), 922–934. https://doi.org/10.1158/1078-0432.CCR-19-1853

Clemson, C. M., Hutchinson, J. N., Sara, S. A., Ensminger, A. W., Fox, A. H., Chess, A., & Lawrence, J. B. (2009). An architectural role for a nuclear noncoding RNA: NEAT1 RNA is essential for the structure of paraspeckles. *Molecular Cell*, *33*(6), 717–726. https://doi.org/10.1016/j.molcel.2009.01.026

Cowley, G. S., Weir, B. A., Vazquez, F., Tamayo, P., Scott, J. A., Rusin, S., East-Seletsky, A., Ali, L. D., Gerath, W. F., Pantel, S. E., Lizotte, P. H., Jiang, G., Hsiao, J., Tsherniak, A., Dwinell, E., Aoyama, S., Okamoto, M., Harrington, W., Gelfand, E., … Hahn, W. C. (2014). Parallel genome-scale loss of function screens in 216 cancer cell lines for the identification of context-specific genetic dependencies. *Scientific Data*, *1*, 140035. https://doi.org/10.1038/sdata.2014.35

Czerwińska, P., Mazurek, S., & Wiznerowicz, M. (2017). The complexity of TRIM28 contribution to cancer. *Journal of Biomedical Science*, *24*(1), 63. https://doi.org/10.1186/s12929-017-0374-4

Dacic, S., Kothmaier, H., Land, S., Shuai, Y., Halbwedl, I., Morbini, P., Murer, B., Comin, C., Galateau-Salle, F., Demirag, F., Zeren, H., Attanoos, R., Gibbs, A., Cagle, P., & Popper, H. (2008). Prognostic significance of p16/cdkn2a loss in pleural malignant mesotheliomas. *Virchows Archiv: An International Journal of Pathology*, *453*(6), 627–635. https://doi.org/10.1007/s00428-008-0689-3

de Koning, A. P. J., Gu, W., Castoe, T. A., Batzer, M. A., & Pollock, D. D. (2011). Repetitive elements may comprise over two-thirds of the human genome. *PLoS Genetics*, *7*(12), e1002384. https://doi.org/10.1371/journal.pgen.1002384

De Rienzo, A., Archer, M. A., Yeap, B. Y., Dao, N., Sciaranghella, D., Sideris, A. C., Zheng, Y., Holman, A. G., Wang, Y. E., Dal Cin, P. S., Fletcher, J. A., Rubio, R., Croft, L., Quackenbush, J., Sugarbaker, P. E., Munir, K. J., Battilana, J. R., Gustafson, C. E., Chirieac, L. R., … Bueno, R. (2016). Gender-Specific Molecular and Clinical Features Underlie Malignant Pleural Mesothelioma. *Cancer Research*, *76*(2), 319–328. https://doi.org/10.1158/0008-5472.CAN-15-0751

Djebali, S., Davis, C. A., Merkel, A., Dobin, A., Lassmann, T., Mortazavi, A., Tanzer, A., Lagarde, J., Lin, W., Schlesinger, F., Xue, C., Marinov, G. K., Khatun, J., Williams, B. A., Zaleski, C., Rozowsky, J., Röder, M., Kokocinski, F., Abdelhamid, R. F., … Gingeras, T. R. (2012). Landscape of transcription in human cells. *Nature*, *489*(7414), 101–108. https://doi.org/10.1038/nature11233

Dobin, A., Davis, C. A., Schlesinger, F., Drenkow, J., Zaleski, C., Jha, S., Batut, P., Chaisson, M., & Gingeras, T. R. (2013). STAR: Ultrafast universal RNA-seq aligner. *Bioinformatics (Oxford, England)*, *29*(1), 15–21. https://doi.org/10.1093/bioinformatics/bts635

Donaldson, K., Murphy, F. A., Duffin, R., & Poland, C. A. (2010). Asbestos, carbon nanotubes and the pleural mesothelium: A review of the hypothesis regarding the role of long fibre retention in the parietal pleura, inflammation and mesothelioma. *Particle and Fibre Toxicology*, *7*, 5. https://doi.org/10.1186/1743-8977-7-5

D'Orso, I. (2016). 7SKiing on chromatin: Move globally, act locally. *RNA Biology*, *13*(6), 545–553. https://doi.org/10.1080/15476286.2016.1181254

Down, C. F., Millour, J., Lam, E. W.-F., & Watson, R. J. (2012). Binding of FoxM1 to G2/M gene promoters is dependent upon B-Myb. *Biochimica Et Biophysica Acta*, *1819*(8), 855–862. https://doi.org/10.1016/j.bbagrm.2012.03.008

Eckschlager, T., Plch, J., Stiborova, M., & Hrabeta, J. (2017). Histone Deacetylase Inhibitors as Anticancer Drugs. *International Journal of Molecular Sciences*, *18*(7), E1414. https://doi.org/10.3390/ijms18071414

Edwards, J. R., Yarychkivska, O., Boulard, M., & Bestor, T. H. (2017). DNA methylation and DNA methyltransferases. *Epigenetics & Chromatin*, *10*, 23. https://doi.org/10.1186/s13072-017-0130-8

ENCODE Project Consortium, Birney, E., Stamatoyannopoulos, J. A., Dutta, A., Guigó, R., Gingeras, T. R., Margulies, E. H., Weng, Z., Snyder, M., Dermitzakis, E. T., Thurman, R. E., Kuehn, M. S., Taylor, C. M., Neph, S., Koch, C. M., Asthana, S., Malhotra, A., Adzhubei, I., Greenbaum, J. A., … de Jong, P. J. (2007). Identification and analysis of functional elements in 1% of the human genome by the ENCODE pilot project. *Nature*, *447*(7146), 799–816. https://doi.org/10.1038/nature05874

Engreitz, J. M., Haines, J. E., Perez, E. M., Munson, G., Chen, J., Kane, M., McDonel, P. E., Guttman, M., & Lander, E. S. (2016). Local regulation of gene expression by lncRNA promoters, transcription and splicing. *Nature*, *539*(7629), 452–455. https://doi.org/10.1038/nature20149

Esteller, M. (2011). Non-coding RNAs in human disease. *Nature Reviews. Genetics*, *12*(12), 861–874. https://doi.org/10.1038/nrg3074

Fischer, M., & Müller, G. A. (2017). Cell cycle transcription control: DREAM/MuvB and RB-E2F complexes. *Critical Reviews in Biochemistry and Molecular Biology*, *52*(6), 638–662. https://doi.org/10.1080/10409238.2017.1360836

Fischer, M., Quaas, M., Steiner, L., & Engeland, K. (2016). The p53-p21-DREAM-CDE/CHR pathway regulates G2/M cell cycle genes. *Nucleic Acids Research*, *44*(1), 164–174. https://doi.org/10.1093/nar/gkv927

Franco, L. C., Morales, F., Boffo, S., & Giordano, A. (2018). CDK9: A key player in cancer and other diseases. *Journal of Cellular Biochemistry*, *119*(2), 1273–1284. https://doi.org/10.1002/jcb.26293

Friedman, J. R., Fredericks, W. J., Jensen, D. E., Speicher, D. W., Huang, X. P., Neilson, E. G., & Rauscher, F. J. (1996). KAP-1, a novel corepressor for the highly conserved KRAB repression domain. *Genes & Development*, *10*(16), 2067–2078. https://doi.org/10.1101/gad.10.16.2067

Fujii, Y., Amatya, V. J., Kushitani, K., Suzuki, R., Kai, Y., Kambara, T., & Takeshima, Y. (2022). Downregulation of lncRNA PVT1 inhibits proliferation and migration of mesothelioma cells by targeting FOXM1. *Oncology Reports*, *47*(2), 27. https://doi.org/10.3892/or.2021.8238

Gautam, P., Yu, T., & Loh, Y.-H. (2017). Regulation of ERVs in pluripotent stem cells and reprogramming. *Current Opinion in Genetics & Development*, *46*, 194–201. https://doi.org/10.1016/j.gde.2017.07.012

Geis, F. K., & Goff, S. P. (2020). Silencing and Transcriptional Regulation of Endogenous Retroviruses: An Overview. *Viruses*, *12*(8), E884. https://doi.org/10.3390/v12080884

Gil, N., & Ulitsky, I. (2020). Regulation of gene expression by cis-acting long non-coding RNAs. *Nature Reviews. Genetics*, *21*(2), 102–117. https://doi.org/10.1038/s41576-019-0184-5

Gomes, N. P., Bjerke, G., Llorente, B., Szostek, S. A., Emerson, B. M., & Espinosa, J. M. (2006). Gene-specific requirement for P-TEFb activity and RNA polymerase II phosphorylation within the p53 transcriptional program. *Genes & Development*, *20*(5), 601–612. https://doi.org/10.1101/gad.1398206

Graham, M., & Adams, J. M. (1986). Chromosome 8 breakpoint far 3' of the c-myc oncogene in a Burkitt's lymphoma 2;8 variant translocation is equivalent to the murine pvt-1 locus. *The EMBO Journal*, *5*(11), 2845–2851.

Green, E. D., Watson, J. D., & Collins, F. S. (2015). Human Genome Project: Twenty-five years of big biology. *Nature*, *526*(7571), 29–31. https://doi.org/10.1038/526029a

Grünberg, S., & Hahn, S. (2013). Structural insights into transcription initiation by RNA polymerase II. *Trends in Biochemical Sciences*, *38*(12), 603–611. https://doi.org/10.1016/j.tibs.2013.09.002

Guan, Y., Kuo, W.-L., Stilwell, J. L., Takano, H., Lapuk, A. V., Fridlyand, J., Mao, J.-H., Yu, M., Miller, M. A., Santos, J. L., Kalloger, S. E., Carlson, J. W., Ginzinger, D. G., Celniker, S. E., Mills, G. B., Huntsman, D. G., & Gray, J. W. (2007). Amplification of PVT1 contributes to the pathophysiology of ovarian and breast cancer. *Clinical Cancer Research: An Official Journal of the American Association for Cancer Research*, *13*(19), 5745–5755. https://doi.org/10.1158/1078-0432.CCR-06-2882

Gugnoni, M., Manicardi, V., Torricelli, F., Sauta, E., Bellazzi, R., Manzotti, G., Vitale, E., de Biase, D., Piana, S., & Ciarrocchi, A. (2021). Linc00941 Is a Novel Transforming Growth Factor β Target

That Primes Papillary Thyroid Cancer Metastatic Behavior by Regulating the Expression of Cadherin 6. *Thyroid: Official Journal of the American Thyroid Association*, *31*(2), 247–263. https://doi.org/10.1089/thy.2020.0001

Gugnoni, M., Sancisi, V., Gandolfi, G., Manzotti, G., Ragazzi, M., Giordano, D., Tamagnini, I., Tigano, M., Frasoldati, A., Piana, S., & Ciarrocchi, A. (2017). Cadherin-6 promotes EMT and cancer metastasis by restraining autophagy. *Oncogene*, *36*(5), 667–677. https://doi.org/10.1038/onc.2016.237

Guo, G., Chmielecki, J., Goparaju, C., Heguy, A., Dolgalev, I., Carbone, M., Seepo, S., Meyerson, M., & Pass, H. I. (2015). Whole-exome sequencing reveals frequent genetic alterations in BAP1, NF2, CDKN2A, and CUL1 in malignant pleural mesothelioma. *Cancer Research*, *75*(2), 264–269. https://doi.org/10.1158/0008-5472.CAN-14-1008

Gupta, R. A., Shah, N., Wang, K. C., Kim, J., Horlings, H. M., Wong, D. J., Tsai, M.-C., Hung, T., Argani, P., Rinn, J. L., Wang, Y., Brzoska, P., Kong, B., Li, R., West, R. B., van de Vijver, M. J., Sukumar, S., & Chang, H. Y. (2010). Long non-coding RNA HOTAIR reprograms chromatin state to promote cancer metastasis. *Nature*, *464*(7291), 1071–1076. https://doi.org/10.1038/nature08975

Haas, A. R., & Sterman, D. H. (2013). Malignant pleural mesothelioma: Update on treatment options with a focus on novel therapies. *Clinics in Chest Medicine*, *34*(1), 99–111. https://doi.org/10.1016/j.ccm.2012.12.005

Harington, J. S., Miller, K., & Macnab, G. (1971). Hemolysis by asbestos. *Environmental Research*, *4*(2), 95–117. https://doi.org/10.1016/0013-9351(71)90038-7

Hassig, C. A., & Schreiber, S. L. (1997). Nuclear histone acetylases and deacetylases and transcriptional regulation: HATs off to HDACs. *Current Opinion in Chemical Biology*, *1*(3), 300–308. https://doi.org/10.1016/s1367-5931(97)80066-x

He, N., Jahchan, N. S., Hong, E., Li, Q., Bayfield, M. A., Maraia, R. J., Luo, K., & Zhou, Q. (2008). A La-related protein modulates 7SK snRNP integrity to suppress P-TEFb-dependent transcriptional elongation and tumorigenesis. *Molecular Cell*, *29*(5), 588–599. https://doi.org/10.1016/j.molcel.2008.01.003

Hmeljak, J., Sanchez-Vega, F., Hoadley, K. A., Shih, J., Stewart, C., Heiman, D., Tarpey, P., Danilova, L., Drill, E., Gibb, E. A., Bowlby, R., Kanchi, R., Osmanbeyoglu, H. U., Sekido, Y., Takeshita, J., Newton, Y., Graim, K., Gupta, M., Gay, C. M., … Ladanyi, M. (2018). Integrative Molecular Characterization of Malignant Pleural Mesothelioma. *Cancer Discovery*, *8*(12), 1548–1565. https://doi.org/10.1158/2159-8290.CD-18-0804

Hu, J., Han, Q., Gu, Y., Ma, J., McGrath, M., Qiao, F., Chen, B., Song, C., & Ge, Z. (2018). Circular RNA PVT1 expression and its roles in acute lymphoblastic leukemia. *Epigenomics*, *10*(6), 723–732. https://doi.org/10.2217/epi-2017-0142

Hu, M., Fu, X., Cui, Y., Xu, S., Xu, Y., Dong, Q., & Sun, L. (2015). Expression of KAP1 in epithelial ovarian cancer and its correlation with drug-resistance. *International Journal of Clinical and Experimental Medicine*, *8*(10), 17308–17320.

Hu, Y., Guo, G., Li, J., Chen, J., & Tan, P. (2020). Screening key lncRNAs with diagnostic and prognostic value for head and neck squamous cell carcinoma based on machine learning and mRNA-lncRNA co-expression network analysis. *Cancer Biomarkers: Section A of Disease Markers*, *27*(2), 195–206. https://doi.org/10.3233/CBM-190694

Huntley, S., Baggott, D. M., Hamilton, A. T., Tran-Gyamfi, M., Yang, S., Kim, J., Gordon, L., Branscomb, E., & Stubbs, L. (2006). A comprehensive catalog of human KRAB-associated zinc

finger genes: Insights into the evolutionary history of a large family of transcriptional repressors. *Genome Research*, *16*(5), 669–677. https://doi.org/10.1101/gr.4842106

Hylebos, M., Van Camp, G., van Meerbeeck, J. P., & Op de Beeck, K. (2016). The Genetic Landscape of Malignant Pleural Mesothelioma: Results from Massively Parallel Sequencing. *Journal of Thoracic Oncology: Official Publication of the International Association for the Study of Lung Cancer*, *11*(10), 1615–1626. https://doi.org/10.1016/j.jtho.2016.05.020

Iaccarino, I., & Klapper, W. (2021). LncRNA as Cancer Biomarkers. *Methods in Molecular Biology (Clifton, N.J.)*, *2348*, 27–41. https://doi.org/10.1007/978-1-0716-1581-2_2

Iadevaia, V., Zhang, Z., Jan, E., & Proud, C. G. (2012). MTOR signaling regulates the processing of pre-rRNA in human cells. *Nucleic Acids Research*, *40*(6), 2527–2539. https://doi.org/10.1093/nar/gkr1040

Imbeault, M., Helleboid, P.-Y., & Trono, D. (2017). KRAB zinc-finger proteins contribute to the evolution of gene regulatory networks. *Nature*, *543*(7646), 550–554. https://doi.org/10.1038/nature21683

Ismail-Khan, R., Robinson, L. A., Williams, C. C., Garrett, C. R., Bepler, G., & Simon, G. R. (2006). Malignant pleural mesothelioma: A comprehensive review. *Cancer Control: Journal of the Moffitt Cancer Center*, *13*(4), 255–263. https://doi.org/10.1177/107327480601300402

Ivanov, A. V., Peng, H., Yurchenko, V., Yap, K. L., Negorev, D. G., Schultz, D. C., Psulkowski, E., Fredericks, W. J., White, D. E., Maul, G. G., Sadofsky, M. J., Zhou, M.-M., & Rauscher, F. J. (2007). PHD domain-mediated E3 ligase activity directs intramolecular sumoylation of an adjacent bromodomain required for gene silencing. *Molecular Cell*, *28*(5), 823–837. https://doi.org/10.1016/j.molcel.2007.11.012

Iyengar, S., & Farnham, P. J. (2011). KAP1 protein: An enigmatic master regulator of the genome. *The Journal of Biological Chemistry*, *286*(30), 26267–26276. https://doi.org/10.1074/jbc.R111.252569

Iyer, M. K., Niknafs, Y. S., Malik, R., Singhal, U., Sahu, A., Hosono, Y., Barrette, T. R., Prensner, J. R., Evans, J. R., Zhao, S., Poliakov, A., Cao, X., Dhanasekaran, S. M., Wu, Y.-M., Robinson, D. R., Beer, D. G., Feng, F. Y., Iyer, H. K., & Chinnaiyan, A. M. (2015). The landscape of long noncoding RNAs in the human transcriptome. *Nature Genetics*, *47*(3), 199–208. https://doi.org/10.1038/ng.3192

Joukov, V., & De Nicolo, A. (2018). Aurora-PLK1 cascades as key signaling modules in the regulation of mitosis. *Science Signaling*, *11*(543), eaar4195. https://doi.org/10.1126/scisignal.aar4195

Kang, H. C., Kim, H. K., Lee, S., Mendez, P., Kim, J. W., Woodard, G., Yoon, J.-H., Jen, K.-Y., Fang, L. T., Jones, K., Jablons, D. M., & Kim, I.-J. (2016). Whole exome and targeted deep sequencing identify genome-wide allelic loss and frequent SETDB1 mutations in malignant pleural mesotheliomas. *Oncotarget*, *7*(7), 8321–8331. https://doi.org/10.18632/oncotarget.7032

Kim, M.-C., Hwang, S.-H., Kim, N.-Y., Lee, H.-S., Ji, S., Yang, Y., & Kim, Y. (2018). Hypoxia promotes acquisition of aggressive phenotypes in human malignant mesothelioma. *BMC Cancer*, *18*(1), 819. https://doi.org/10.1186/s12885-018-4720-z

Klabatsa, A., Sheaff, M. T., Steele, J. P. C., Evans, M. T., Rudd, R. M., & Fennell, D. A. (2006). Expression and prognostic significance of hypoxia-inducible factor 1alpha (HIF-1alpha) in malignant pleural mesothelioma (MPM). *Lung Cancer (Amsterdam, Netherlands)*, *51*(1), 53–59. https://doi.org/10.1016/j.lungcan.2005.07.010

Kondo, Y., Shinjo, K., & Katsushima, K. (2017). Long non-coding RNAs as an epigenetic regulator in human cancers. *Cancer Science*, *108*(10), 1927–1933. https://doi.org/10.1111/cas.13342

Krasinskas, A. M., Bartlett, D. L., Cieply, K., & Dacic, S. (2010). CDKN2A and MTAP deletions in peritoneal mesotheliomas are correlated with loss of p16 protein expression and poor survival. *Modern Pathology: An Official Journal of the United States and Canadian Academy of Pathology, Inc*, *23*(4), 531–538. https://doi.org/10.1038/modpathol.2009.186

Kuleshov, M. V., Jones, M. R., Rouillard, A. D., Fernandez, N. F., Duan, Q., Wang, Z., Koplev, S., Jenkins, S. L., Jagodnik, K. M., Lachmann, A., McDermott, M. G., Monteiro, C. D., Gundersen, G. W., & Ma'ayan, A. (2016). Enrichr: A comprehensive gene set enrichment analysis web server 2016 update. *Nucleic Acids Research*, *44*(W1), W90-97. https://doi.org/10.1093/nar/gkw377

LaFave, L. M., Béguelin, W., Koche, R., Teater, M., Spitzer, B., Chramiec, A., Papalexi, E., Keller, M. D., Hricik, T., Konstantinoff, K., Micol, J.-B., Durham, B., Knutson, S. K., Campbell, J. E., Blum, G., Shi, X., Doud, E. H., Krivtsov, A. V., Chung, Y. R., … Levine, R. L. (2015). Loss of BAP1 function leads to EZH2-dependent transformation. *Nature Medicine*, *21*(11), 1344–1349. https://doi.org/10.1038/nm.3947

Lander, E. S., Linton, L. M., Birren, B., Nusbaum, C., Zody, M. C., Baldwin, J., Devon, K., Dewar, K., Doyle, M., FitzHugh, W., Funke, R., Gage, D., Harris, K., Heaford, A., Howland, J., Kann, L., Lehoczky, J., LeVine, R., McEwan, P., … International Human Genome Sequencing Consortium. (2001). Initial sequencing and analysis of the human genome. *Nature*, *409*(6822), 860–921. https://doi.org/10.1038/35057062

Lechner, M. S., Begg, G. E., Speicher, D. W., & Rauscher, F. J. (2000). Molecular determinants for targeting heterochromatin protein 1-mediated gene silencing: Direct chromoshadow domain-KAP-1 corepressor interaction is essential. *Molecular and Cellular Biology*, *20*(17), 6449–6465. https://doi.org/10.1128/mcb.20.17.6449-6465.2000

Li, B., & Dewey, C. N. (2011). RSEM: Accurate transcript quantification from RNA-Seq data with or without a reference genome. *BMC Bioinformatics*, *12*, 323. https://doi.org/10.1186/1471-2105-12-323

Li, W., Xu, H., Xiao, T., Cong, L., Love, M. I., Zhang, F., Irizarry, R. A., Liu, J. S., Brown, M., & Liu, X. S. (2014). MAGeCK enables robust identification of essential genes from genome-scale CRISPR/Cas9 knockout screens. *Genome Biology*, *15*(12), 554. https://doi.org/10.1186/s13059-014-0554-4

Li, W., You, L., Cooper, J., Schiavon, G., Pepe-Caprio, A., Zhou, L., Ishii, R., Giovannini, M., Hanemann, C. O., Long, S. B., Erdjument-Bromage, H., Zhou, P., Tempst, P., & Giancotti, F. G. (2010). Merlin/NF2 suppresses tumorigenesis by inhibiting the E3 ubiquitin ligase CRL4(DCAF1) in the nucleus. *Cell*, *140*(4), 477–490. https://doi.org/10.1016/j.cell.2010.01.029

Li, X., Lee, Y.-K., Jeng, J.-C., Yen, Y., Schultz, D. C., Shih, H.-M., & Ann, D. K. (2007). Role for KAP1 serine 824 phosphorylation and sumoylation/desumoylation switch in regulating KAP1-mediated transcriptional repression. *The Journal of Biological Chemistry*, *282*(50), 36177–36189. https://doi.org/10.1074/jbc.M706912200

Lin, L.-F., Li, C.-F., Wang, W.-J., Yang, W.-M., Wang, D. D.-H., Chang, W.-C., Lee, W.-H., & Wang, J.-M. (2013). Loss of ZBRK1 contributes to the increase of KAP1 and promotes KAP1-mediated metastasis and invasion in cervical cancer. *PloS One*, *8*(8), e73033. https://doi.org/10.1371/journal.pone.0073033

Liu, H., Wu, N., Zhang, Z., Zhong, X., Zhang, H., Guo, H., Nie, Y., & Liu, Y. (2019). Long Non-coding RNA LINC00941 as a Potential Biomarker Promotes the Proliferation and Metastasis of Gastric Cancer. *Frontiers in Genetics*, *10*, 5. https://doi.org/10.3389/fgene.2019.00005

Liu, Y., Chen, S., Wang, S., Soares, F., Fischer, M., Meng, F., Du, Z., Lin, C., Meyer, C., DeCaprio, J. A., Brown, M., Liu, X. S., & He, H. H. (2017). Transcriptional landscape of the human cell cycle. *Proceedings of the National Academy of Sciences of the United States of America*, *114*(13), 3473–3478. https://doi.org/10.1073/pnas.1617636114

Lorenzini, E., Ciarrocchi, A., & Torricelli, F. (2021). Molecular Fingerprints of Malignant Pleural Mesothelioma: Not Just a Matter of Genetic Alterations. *Journal of Clinical Medicine*, *10*(11), 2470. https://doi.org/10.3390/jcm10112470

Love, M. I., Huber, W., & Anders, S. (2014). Moderated estimation of fold change and dispersion for RNA-seq data with DESeq2. *Genome Biology*, *15*(12), 550. https://doi.org/10.1186/s13059-014-0550-8

Luo, C., Tao, Y., Zhang, Y., Zhu, Y., Minyao, D. N., Haleem, M., Dong, C., Zhang, L., Zhang, X., Zhao, J., & Liao, Q. (2018). Regulatory network analysis of high expressed long non-coding RNA LINC00941 in gastric cancer. *Gene*, *662*, 103–109. https://doi.org/10.1016/j.gene.2018.04.023

Ma, S., Meng, Z., Chen, R., & Guan, K.-L. (2019). The Hippo Pathway: Biology and Pathophysiology. *Annual Review of Biochemistry*, *88*, 577–604. https://doi.org/10.1146/annurev-biochem-013118-111829

Mandal, R., Becker, S., & Strebhardt, K. (2021). Targeting CDK9 for Anti-Cancer Therapeutics. *Cancers*, *13*(9), 2181. https://doi.org/10.3390/cancers13092181

Masclef, L., Ahmed, O., Estavoyer, B., Larrivée, B., Labrecque, N., Nijnik, A., & Affar, E. B. (2021). Roles and mechanisms of BAP1 deubiquitinase in tumor suppression. *Cell Death and Differentiation*, *28*(2), 606–625. https://doi.org/10.1038/s41418-020-00709-4

McLoughlin, K. C., Kaufman, A. S., & Schrump, D. S. (2017). Targeting the epigenome in malignant pleural mesothelioma. *Translational Lung Cancer Research*, *6*(3), 350–365. https://doi.org/10.21037/tlcr.2017.06.06

McNamara, R. P., Guzman, C., Reeder, J. E., & D'Orso, I. (2016). Genome-wide analysis of KAP1, the 7SK snRNP complex, and RNA polymerase II. *Genomics Data*, *7*, 250–255. https://doi.org/10.1016/j.gdata.2016.01.019

McNamara, R. P., Reeder, J. E., McMillan, E. A., Bacon, C. W., McCann, J. L., & D'Orso, I. (2016). KAP1 Recruitment of the 7SK snRNP Complex to Promoters Enables Transcription Elongation by RNA Polymerase II. *Molecular Cell*, *61*(1), 39–53. https://doi.org/10.1016/j.molcel.2015.11.004

Miyanaga, A., Masuda, M., Tsuta, K., Kawasaki, K., Nakamura, Y., Sakuma, T., Asamura, H., Gemma, A., & Yamada, T. (2015). Hippo pathway gene mutations in malignant mesothelioma: Revealed by RNA and targeted exon sequencing. *Journal of Thoracic Oncology: Official Publication of the International Association for the Study of Lung Cancer*, *10*(5), 844–851. https://doi.org/10.1097/JTO.0000000000000493

Morganti, S., Tarantino, P., Ferraro, E., D'Amico, P., Viale, G., Trapani, D., Duso, B. A., & Curigliano, G. (2019). Complexity of genome sequencing and reporting: Next generation sequencing (NGS) technologies and implementation of precision medicine in real life. *Critical Reviews in Oncology/Hematology*, *133*, 171–182. https://doi.org/10.1016/j.critrevonc.2018.11.008

Mossman, B. T., Kamp, D. W., & Weitzman, S. A. (1996). Mechanisms of carcinogenesis and clinical features of asbestos-associated cancers. *Cancer Investigation*, *14*(5), 466–480. https://doi.org/10.3109/07357909609018904

Msiska, Z., Pacurari, M., Mishra, A., Leonard, S. S., Castranova, V., & Vallyathan, V. (2010). DNA double-strand breaks by asbestos, silica, and titanium dioxide: Possible biomarker of carcinogenic potential? *American Journal of Respiratory Cell and Molecular Biology*, *43*(2), 210–219. https://doi.org/10.1165/rcmb.2009-0062OC

Mu, X., Ahmad, S., & Hur, S. (2016). Endogenous Retroelements and the Host Innate Immune Sensors. *Advances in Immunology*, *132*, 47–69. https://doi.org/10.1016/bs.ai.2016.07.001

Müller, G. A., Quaas, M., Schümann, M., Krause, E., Padi, M., Fischer, M., Litovchick, L., DeCaprio, J. A., & Engeland, K. (2012). The CHR promoter element controls cell cycle-dependent gene transcription and binds the DREAM and MMB complexes. *Nucleic Acids Research*, *40*(4), 1561–1578. https://doi.org/10.1093/nar/gkr793

Muñoz-Sánchez, J., & Chánez-Cárdenas, M. E. (2019). The use of cobalt chloride as a chemical hypoxia model. *Journal of Applied Toxicology: JAT*, *39*(4), 556–570. https://doi.org/10.1002/jat.3749

Nakagawa, H., & Fujita, M. (2018). Whole genome sequencing analysis for cancer genomics and precision medicine. *Cancer Science*, *109*(3), 513–522. https://doi.org/10.1111/cas.13505

Oehl, K., Vrugt, B., Opitz, I., & Meerang, M. (2018). Heterogeneity in Malignant Pleural Mesothelioma. *International Journal of Molecular Sciences*, *19*(6), E1603. https://doi.org/10.3390/ijms19061603

Ohar, J. A., Cheung, M., Talarchek, J., Howard, S. E., Howard, T. D., Hesdorffer, M., Peng, H., Rauscher, F. J., & Testa, J. R. (2016). Germline BAP1 Mutational Landscape of Asbestos-Exposed Malignant Mesothelioma Patients with Family History of Cancer. *Cancer Research*, *76*(2), 206–215. https://doi.org/10.1158/0008-5472.CAN-15-0295

Ori, D., Murase, M., & Kawai, T. (2017). Cytosolic nucleic acid sensors and innate immune regulation. *International Reviews of Immunology*, *36*(2), 74–88. https://doi.org/10.1080/08830185.2017.1298749

Ozato, K., Shin, D.-M., Chang, T.-H., & Morse, H. C. (2008). TRIM family proteins and their emerging roles in innate immunity. *Nature Reviews. Immunology*, *8*(11), 849–860. https://doi.org/10.1038/nri2413

Pasello, G., & Favaretto, A. (2009). Molecular targets in malignant pleural mesothelioma treatment. *Current Drug Targets*, *10*(12), 1235–1244. https://doi.org/10.2174/138945009789753200

Peng, H., Feldman, I., & Rauscher, F. J. (2002). Hetero-oligomerization among the TIF family of RBCC/TRIM domain-containing nuclear cofactors: A potential mechanism for regulating the switch between coactivation and corepression. *Journal of Molecular Biology*, *320*(3), 629–644. https://doi.org/10.1016/S0022-2836(02)00477-1

Peng, W.-X., Koirala, P., & Mo, Y.-Y. (2017). LncRNA-mediated regulation of cell signaling in cancer. *Oncogene*, *36*(41), 5661–5667. https://doi.org/10.1038/onc.2017.184

Peterlin, B. M., & Price, D. H. (2006). Controlling the elongation phase of transcription with P-TEFb. *Molecular Cell*, *23*(3), 297–305. https://doi.org/10.1016/j.molcel.2006.06.014

Pfister, S. X., Ahrabi, S., Zalmas, L.-P., Sarkar, S., Aymard, F., Bachrati, C. Z., Helleday, T., Legube, G., La Thangue, N. B., Porter, A. C. G., & Humphrey, T. C. (2014). SETD2-dependent

histone H3K36 trimethylation is required for homologous recombination repair and genome stability. *Cell Reports*, *7*(6), 2006–2018. https://doi.org/10.1016/j.celrep.2014.05.026

Qi, Z.-X., Cai, J.-J., Chen, L.-C., Yue, Q., Gong, Y., Yao, Y., & Mao, Y. (2016). TRIM28 as an independent prognostic marker plays critical roles in glioma progression. *Journal of Neuro-Oncology*, *126*(1), 19–26. https://doi.org/10.1007/s11060-015-1897-8

Quinn, J. J., & Chang, H. Y. (2016). Unique features of long non-coding RNA biogenesis and function. *Nature Reviews. Genetics*, *17*(1), 47–62. https://doi.org/10.1038/nrg.2015.10

Remon, J., Reguart, N., Corral, J., & Lianes, P. (2015). Malignant pleural mesothelioma: New hope in the horizon with novel therapeutic strategies. *Cancer Treatment Reviews*, *41*(1), 27–34. https://doi.org/10.1016/j.ctrv.2014.10.007

Ren, M.-H., Chen, S., Wang, L.-G., Rui, W.-X., & Li, P. (2021). LINC00941 Promotes Progression of Non-Small Cell Lung Cancer by Sponging miR-877-3p to Regulate VEGFA Expression. *Frontiers in Oncology*, *11*, 650037. https://doi.org/10.3389/fonc.2021.650037

Renganathan, A., Kresoja-Rakic, J., Echeverry, N., Ziltener, G., Vrugt, B., Opitz, I., Stahel, R. A., & Felley-Bosco, E. (2014). GAS5 long non-coding RNA in malignant pleural mesothelioma. *Molecular Cancer*, *13*, 119. https://doi.org/10.1186/1476-4598-13-119

Rijavec, E., Biello, F., Barletta, G., Dellepiane, C., & Genova, C. (2022). Novel approaches for the treatment of unresectable malignant pleural mesothelioma: A focus on immunotherapy and target therapy (Review). *Molecular and Clinical Oncology*, *16*(4), 89. https://doi.org/10.3892/mco.2022.2522

Riquelme, E., Suraokar, M. B., Rodriguez, J., Mino, B., Lin, H. Y., Rice, D. C., Tsao, A., & Wistuba, I. I. (2014). Frequent coamplification and cooperation between C-MYC and PVT1 oncogenes promote malignant pleural mesothelioma. *Journal of Thoracic Oncology: Official Publication of the International Association for the Study of Lung Cancer*, *9*(7), 998–1007. https://doi.org/10.1097/JTO.0000000000000202

Roulois, D., Loo Yau, H., Singhania, R., Wang, Y., Danesh, A., Shen, S. Y., Han, H., Liang, G., Jones, P. A., Pugh, T. J., O'Brien, C., & De Carvalho, D. D. (2015). DNA-Demethylating Agents Target Colorectal Cancer Cells by Inducing Viral Mimicry by Endogenous Transcripts. *Cell*, *162*(5), 961–973. https://doi.org/10.1016/j.cell.2015.07.056

Rowe, H. M., Jakobsson, J., Mesnard, D., Rougemont, J., Reynard, S., Aktas, T., Maillard, P. V., Layard-Liesching, H., Verp, S., Marquis, J., Spitz, F., Constam, D. B., & Trono, D. (2010). KAP1 controls endogenous retroviruses in embryonic stem cells. *Nature*, *463*(7278), 237–240. https://doi.org/10.1038/nature08674

Rozengurt, E., Sinnett-Smith, J., & Eibl, G. (2018). Yes-associated protein (YAP) in pancreatic cancer: At the epicenter of a targetable signaling network associated with patient survival. *Signal Transduction and Targeted Therapy*, *3*(1), 1–10. https://doi.org/10.1038/s41392-017-0005-2

Sacco, J. J., Kenyani, J., Butt, Z., Carter, R., Chew, H. Y., Cheeseman, L. P., Darling, S., Denny, M., Urbé, S., Clague, M. J., & Coulson, J. M. (2015). Loss of the deubiquitylase BAP1 alters class I histone deacetylase expression and sensitivity of mesothelioma cells to HDAC inhibitors. *Oncotarget*, *6*(15), 13757–13771. https://doi.org/10.18632/oncotarget.3765

Sadasivam, S., Duan, S., & DeCaprio, J. A. (2012). The MuvB complex sequentially recruits B-Myb and FoxM1 to promote mitotic gene expression. *Genes & Development*, *26*(5), 474–489. https://doi.org/10.1101/gad.181933.111

Sage, A. P., Martinez, V. D., Minatel, B. C., Pewarchuk, M. E., Marshall, E. A., MacAulay, G. M., Hubaux, R., Pearson, D. D., Goodarzi, A. A., Dellaire, G., & Lam, W. L. (2018). Genomics and Epigenetics of Malignant Mesothelioma. *High-Throughput*, *7*(3), E20. https://doi.org/10.3390/ht7030020

Sanjana, N. E., Shalem, O., & Zhang, F. (2014). Improved vectors and genome-wide libraries for CRISPR screening. *Nature Methods*, *11*(8), 783–784. https://doi.org/10.1038/nmeth.3047

Santo, L., Vallet, S., Hideshima, T., Cirstea, D., Ikeda, H., Pozzi, S., Patel, K., Okawa, Y., Gorgun, G., Perrone, G., Calabrese, E., Yule, M., Squires, M., Ladetto, M., Boccadoro, M., Richardson, P. G., Munshi, N. C., Anderson, K. C., & Raje, N. (2010). AT7519, A novel small molecule multi-cyclin-dependent kinase inhibitor, induces apoptosis in multiple myeloma via GSK-3beta activation and RNA polymerase II inhibition. *Oncogene*, *29*(16), 2325–2336. https://doi.org/10.1038/onc.2009.510

Schmidt, L. H., Spieker, T., Koschmieder, S., Schäffers, S., Humberg, J., Jungen, D., Bulk, E., Hascher, A., Wittmer, D., Marra, A., Hillejan, L., Wiebe, K., Berdel, W. E., Wiewrodt, R., & Muller-Tidow, C. (2011). The long noncoding MALAT-1 RNA indicates a poor prognosis in non-small cell lung cancer and induces migration and tumor growth. *Journal of Thoracic Oncology: Official Publication of the International Association for the Study of Lung Cancer*, *6*(12), 1984–1992. https://doi.org/10.1097/JTO.0b013e3182307eac

Schultz, D. C., Friedman, J. R., & Rauscher, F. J. (2001). Targeting histone deacetylase complexes via KRAB-zinc finger proteins: The PHD and bromodomains of KAP-1 form a cooperative unit that recruits a novel isoform of the Mi-2alpha subunit of NuRD. *Genes & Development*, *15*(4), 428–443. https://doi.org/10.1101/gad.869501

Seifarth, W., Frank, O., Zeilfelder, U., Spiess, B., Greenwood, A. D., Hehlmann, R., & Leib-Mösch, C. (2005). Comprehensive analysis of human endogenous retrovirus transcriptional activity in human tissues with a retrovirus-specific microarray. *Journal of Virology*, *79*(1), 341–352. https://doi.org/10.1128/JVI.79.1.341-352.2005

Sekido, Y. (2011). Inactivation of Merlin in malignant mesothelioma cells and the Hippo signaling cascade dysregulation. *Pathology International*, *61*(6), 331–344. https://doi.org/10.1111/j.1440-1827.2011.02666.x

Shalem, O., Sanjana, N. E., Hartenian, E., Shi, X., Scott, D. A., Mikkelson, T., Heckl, D., Ebert, B. L., Root, D. E., Doench, J. G., & Zhang, F. (2014). Genome-scale CRISPR-Cas9 knockout screening in human cells. *Science (New York, N.Y.)*, *343*(6166), 84–87. https://doi.org/10.1126/science.1247005

Shames, D. S., Minna, J. D., & Gazdar, A. F. (2007). DNA methylation in health, disease, and cancer. *Current Molecular Medicine*, *7*(1), 85–102. https://doi.org/10.2174/156652407779940413

Slemc, L., & Kunej, T. (2016). Transcription factor HIF1A: Downstream targets, associated pathways, polymorphic hypoxia response element (HRE) sites, and initiative for standardization of reporting in scientific literature. *Tumour Biology: The Journal of the International Society for Oncodevelopmental Biology and Medicine*, *37*(11), 14851–14861. https://doi.org/10.1007/s13277-016-5331-4

Stoye, J. P. (2012). Studies of endogenous retroviruses reveal a continuing evolutionary saga. *Nature Reviews. Microbiology*, *10*(6), 395–406. https://doi.org/10.1038/nrmicro2783

Strepkos, D., Markouli, M., Klonou, A., Papavassiliou, A. G., & Piperi, C. (2021). Histone Methyltransferase SETDB1: A Common Denominator of Tumorigenesis with Therapeutic Potential. *Cancer Research*, *81*(3), 525–534. https://doi.org/10.1158/0008-5472.CAN-20-2906

Testa, J. R., Cheung, M., Pei, J., Below, J. E., Tan, Y., Sementino, E., Cox, N. J., Dogan, A. U., Pass, H. I., Trusa, S., Hesdorffer, M., Nasu, M., Powers, A., Rivera, Z., Comertpay, S., Tanji, M., Gaudino, G., Yang, H., & Carbone, M. (2011). Germline BAP1 mutations predispose to malignant mesothelioma. *Nature Genetics*, *43*(10), 1022–1025. https://doi.org/10.1038/ng.912

Tie, C. H., Fernandes, L., Conde, L., Robbez-Masson, L., Sumner, R. P., Peacock, T., Rodriguez-Plata, M. T., Mickute, G., Gifford, R., Towers, G. J., Herrero, J., & Rowe, H. M. (2018). KAP1 regulates endogenous retroviruses in adult human cells and contributes to innate immune control. *EMBO Reports*, *19*(10), e45000. https://doi.org/10.15252/embr.201745000

Tiwari, A., Tashiro, K., Dixit, A., Soni, A., Vogel, K., Hall, B., Shafqat, I., Slaughter, J., Param, N., Le, A., Saunders, E., Paithane, U., Garcia, G., Campos, A. R., Zettervall, J., Carlson, M., Starr, T. K., Marahrens, Y., Deshpande, A. J., … Bagchi, A. (2020). Loss of HIF1A From Pancreatic Cancer Cells Increases Expression of PPP1R1B and Degradation of p53 to Promote Invasion and Metastasis. *Gastroenterology*, *159*(5), 1882-1897.e5. https://doi.org/10.1053/j.gastro.2020.07.046

Tranchant, R., Quetel, L., Tallet, A., Meiller, C., Renier, A., de Koning, L., de Reynies, A., Le Pimpec-Barthes, F., Zucman-Rossi, J., Jaurand, M.-C., & Jean, D. (2017). Co-occurring Mutations of Tumor Suppressor Genes, LATS2 and NF2, in Malignant Pleural Mesothelioma. *Clinical Cancer Research: An Official Journal of the American Association for Cancer Research*, *23*(12), 3191–3202. https://doi.org/10.1158/1078-0432.CCR-16-1971

Tsherniak, A., Vazquez, F., Montgomery, P. G., Weir, B. A., Kryukov, G., Cowley, G. S., Gill, S., Harrington, W. F., Pantel, S., Krill-Burger, J. M., Meyers, R. M., Ali, L., Goodale, A., Lee, Y., Jiang, G., Hsiao, J., Gerath, W. F. J., Howell, S., Merkel, E., … Hahn, W. C. (2017). Defining a Cancer Dependency Map. *Cell*, *170*(3), 564-576.e16. https://doi.org/10.1016/j.cell.2017.06.010

Turelli, P., Castro-Diaz, N., Marzetta, F., Kapopoulou, A., Raclot, C., Duc, J., Tieng, V., Quenneville, S., & Trono, D. (2014). Interplay of TRIM28 and DNA methylation in controlling human endogenous retroelements. *Genome Research*, *24*(8), 1260–1270. https://doi.org/10.1101/gr.172833.114

Urrutia, R. (2003). KRAB-containing zinc-finger repressor proteins. *Genome Biology*, *4*(10), 231. https://doi.org/10.1186/gb-2003-4-10-231

Ventii, K. H., Devi, N. S., Friedrich, K. L., Chernova, T. A., Tighiouart, M., Van Meir, E. G., & Wilkinson, K. D. (2008). BRCA1-associated protein-1 is a tumor suppressor that requires deubiquitinating activity and nuclear localization. *Cancer Research*, *68*(17), 6953–6962. https://doi.org/10.1158/0008-5472.CAN-08-0365

Venturini, L., You, J., Stadler, M., Galien, R., Lallemand, V., Koken, M. H., Mattei, M. G., Ganser, A., Chambon, P., Losson, R., & de Thé, H. (1999). TIF1gamma, a novel member of the transcriptional intermediary factor 1 family. *Oncogene*, *18*(5), 1209–1217. https://doi.org/10.1038/sj.onc.1202655

Wagner, J. C., Sleggs, C. A., & Marchand, P. (1960). Diffuse pleural mesothelioma and asbestos exposure in the North Western Cape Province. *British Journal of Industrial Medicine*, *17*, 260–271. https://doi.org/10.1136/oem.17.4.260

Wang, D., & Hu, Y. (2019). Long Non-coding RNA PVT1 Competitively Binds MicroRNA-424-5p to Regulate CARM1 in Radiosensitivity of Non-Small-Cell Lung Cancer. *Molecular Therapy. Nucleic Acids*, *16*, 130–140. https://doi.org/10.1016/j.omtn.2018.12.006

Wang, J., He, Z., Xu, J., Chen, P., & Jiang, J. (2021). Long noncoding RNA LINC00941 promotes pancreatic cancer progression by competitively binding miR-335-5p to regulate ROCK1-mediated

LIMK1/Cofilin-1 signaling. *Cell Death & Disease*, *12*(1), 36. https://doi.org/10.1038/s41419-020-03316-w

Wang, L., Zhao, H., Xu, Y., Li, J., Deng, C., Deng, Y., Bai, J., Li, X., Xiao, Y., & Zhang, Y. (2019). Systematic identification of lincRNA-based prognostic biomarkers by integrating lincRNA expression and copy number variation in lung adenocarcinoma. *International Journal of Cancer*, *144*(7), 1723–1734. https://doi.org/10.1002/ijc.31865

Wang, Y., Jiang, J., Li, Q., Ma, H., Xu, Z., & Gao, Y. (2016). KAP1 is overexpressed in hepatocellular carcinoma and its clinical significance. *International Journal of Clinical Oncology*, *21*(5), 927–933. https://doi.org/10.1007/s10147-016-0979-8

Wei, C., Cheng, J., Zhou, B., Zhu, L., Khan, M. A., He, T., Zhou, S., He, J., Lu, X., Chen, H., Zhang, D., Zhao, Y., & Fu, J. (2016). Tripartite motif containing 28 (TRIM28) promotes breast cancer metastasis by stabilizing TWIST1 protein. *Scientific Reports*, *6*, 29822. https://doi.org/10.1038/srep29822

Wright, C. M., Kirschner, M. B., Cheng, Y. Y., O'Byrne, K. J., Gray, S. G., Schelch, K., Hoda, M. A., Klebe, S., McCaughan, B., van Zandwijk, N., & Reid, G. (2013). Long non coding RNAs (lncRNAs) are dysregulated in Malignant Pleural Mesothelioma (MPM). *PloS One*, *8*(8), e70940. https://doi.org/10.1371/journal.pone.0070940

Wu, N., Jiang, M., Liu, H., Chu, Y., Wang, D., Cao, J., Wang, Z., Xie, X., Han, Y., & Xu, B. (2021). LINC00941 promotes CRC metastasis through preventing SMAD4 protein degradation and activating the TGF-β/SMAD2/3 signaling pathway. *Cell Death and Differentiation*, *28*(1), 219–232. https://doi.org/10.1038/s41418-020-0596-y

Yan, X., Zhang, D., Wu, W., Wu, S., Qian, J., Hao, Y., Yan, F., Zhu, P., Wu, J., Huang, G., Huang, Y., Luo, J., Liu, X., Liu, B., Chen, X., Du, Y., Chen, R., & Fan, Z. (2017). Mesenchymal Stem Cells Promote Hepatocarcinogenesis via lncRNA-MUF Interaction with ANXA2 and miR-34a. *Cancer Research*, *77*(23), 6704–6716. https://doi.org/10.1158/0008-5472.CAN-17-1915

Yang, H., Bocchetta, M., Kroczynska, B., Elmishad, A. G., Chen, Y., Liu, Z., Bubici, C., Mossman, B. T., Pass, H. I., Testa, J. R., Franzoso, G., & Carbone, M. (2006). TNF-alpha inhibits asbestos-induced cytotoxicity via a NF-kappaB-dependent pathway, a possible mechanism for asbestos-induced oncogenesis. *Proceedings of the National Academy of Sciences of the United States of America*, *103*(27), 10397–10402. https://doi.org/10.1073/pnas.0604008103

Yang, H., Rivera, Z., Jube, S., Nasu, M., Bertino, P., Goparaju, C., Franzoso, G., Lotze, M. T., Krausz, T., Pass, H. I., Bianchi, M. E., & Carbone, M. (2010). Programmed necrosis induced by asbestos in human mesothelial cells causes high-mobility group box 1 protein release and resultant inflammation. *Proceedings of the National Academy of Sciences of the United States of America*, *107*(28), 12611–12616. https://doi.org/10.1073/pnas.1006542107

Yap, T. A., Aerts, J. G., Popat, S., & Fennell, D. A. (2017). Novel insights into mesothelioma biology and implications for therapy. *Nature Reviews. Cancer*, *17*(8), 475–488. https://doi.org/10.1038/nrc.2017.42

Yokoe, T., Toiyama, Y., Okugawa, Y., Tanaka, K., Ohi, M., Inoue, Y., Mohri, Y., Miki, C., & Kusunoki, M. (2010). KAP1 is associated with peritoneal carcinomatosis in gastric cancer. *Annals of Surgical Oncology*, *17*(3), 821–828. https://doi.org/10.1245/s10434-009-0795-8

Yoshikawa, Y., Sato, A., Tsujimura, T., Emi, M., Morinaga, T., Fukuoka, K., Yamada, S., Murakami, A., Kondo, N., Matsumoto, S., Okumura, Y., Tanaka, F., Hasegawa, S., Nakano, T., & Hashimoto-Tamaoki, T. (2012). Frequent inactivation of the BAP1 gene in epithelioid-type

malignant mesothelioma. *Cancer Science*, *103*(5), 868–874. https://doi.org/10.1111/j.1349-7006.2012.02223.x

Yu, C., Zhan, L., Jiang, J., Pan, Y., Zhang, H., Li, X., Pen, F., Wang, M., Qin, R., & Sun, C. (2014). KAP-1 is overexpressed and correlates with increased metastatic ability and tumorigenicity in pancreatic cancer. *Medical Oncology (Northwood, London, England)*, *31*(7), 25. https://doi.org/10.1007/s12032-014-0025-5

Zeng, L., Yap, K. L., Ivanov, A. V., Wang, X., Mujtaba, S., Plotnikova, O., Rauscher, F. J., & Zhou, M.-M. (2008). Structural insights into human KAP1 PHD finger-bromodomain and its role in gene silencing. *Nature Structural & Molecular Biology*, *15*(6), 626–633. https://doi.org/10.1038/nsmb.1416

Zeng, L., & Zhou, M. M. (2002). Bromodomain: An acetyl-lysine binding domain. *FEBS Letters*, *513*(1), 124–128. https://doi.org/10.1016/s0014-5793(01)03309-9

Zhang, F., & Lupski, J. R. (2015). Non-coding genetic variants in human disease. *Human Molecular Genetics*, *24*(R1), R102-110. https://doi.org/10.1093/hmg/ddv259

Zhang, L., Lu, Q., & Chang, C. (2020). Epigenetics in Health and Disease. *Advances in Experimental Medicine and Biology*, *1253*, 3–55. https://doi.org/10.1007/978-981-15-3449-2_1

Zhang, Y., & Tang, L. (2018). The Application of lncRNAs in Cancer Treatment and Diagnosis. *Recent Patents on Anti-Cancer Drug Discovery*, *13*(3), 292–301. https://doi.org/10.2174/1574892813666180226121819

Zhou, Q., Li, T., & Price, D. H. (2012). RNA polymerase II elongation control. *Annual Review of Biochemistry*, *81*, 119–143. https://doi.org/10.1146/annurev-biochem-052610-095910

ACKNOWLEDGEMENTS

In this Ph.D experience I would like to thank especially the laboratory coordinator, as well as my tutor, Dr. Alessia Ciarrocchi who allowed me to carry out my research project and with whom I discussed my research activity. I would also like to thank all my colleagues that made me grow professionally and with whom I have exchanged ideas and learnt new methods. In particular, my gratitude goes to Raffaella Zamponi that helped me technically with the experiments, to Dr. Federica Torricelli, Dr. Benedetta Donati, Dr. Elisabetta Sauta and Veronica Manicardi that managed all the bioinformatic analysis of my Ph. D project, and to Dr. Valentina Sancisi that helped me during my first year of Ph.D both technically and in managing the experiments.

I sincerely thank all my family, my parents Lina and Alfio, my sister Francesca and his partner Simone that made me aunt for the first time of the beautiful Cloe, and my brother Alessio. I especially thank my husband Lorenzo and all my dear friends. They always supported me, especially in difficult moments that I went through.

Finally, I would like to thank Prof. Davide Ambrosetti that from my bachelor degree has always been my thesis relator, supporting my work.